Modelling, Inspection, and Post-Processing of Layer-Based Additive Manufacturing surfaces to Maintain Product Quality

By

Amirali Lalehpour

A thesis submitted in partial fulfilment

of the requirement for the degree of

Master of Applied science

In

The Faculty of Engineering and Applied Science

Mechanical Engineering

University of Ontario Institute of Technology

April 2017

ABSTRACT

Today's Additive Manufacturing (AM) is mostly layer-based. Despite AM's great capabilities in fabrication of complex geometries, product's surface roughness is a limiting factor in many industrial applications. Therefore, application of AM parts in industrial services highly relies on appropriate modeling, inspection, and post-processing of the fabricated surfaces. A thorough investigation of surface roughness to improve surface quality of AM products is the focus of this thesis by developing methodologies to complete the three tasks of modelling, inspection, and post-processing of AM surfaces.

A theoretical formulation to model surface roughness of layer based manufactured parts is developed by defining centerline using a Total Least Square (TLS) approach and the model is validated experimentally. The developed model is also used for surface topography of AM parts as a new metrology approach. Optical scanning data point cloud of Fused Deposition Modeling (FDM) parts are used to conduct inspection based on the developed methodology. 3D topography of the surfaces are reconstructed when a good agreement with the corresponding 2D profilometer inspection is observed. Acetone vapour bath smoothing is used for post-processing of FDM parts. The number of smoothing cycles, and the duration of each cycle are considered as the main smoothing parameters. Effect of geometric complexity and smoothing parameters are studied and the best smoothing settings are proposed for a desired level of smoothing requirement. The developed experimental models allow engineers to plan the smoothing process based on the build orientation and geometric complexity of the product.

Keywords: Additive Manufacturing, Layer-based Manufacturing, Surface Roughness, Surface Quality, Surface Topography, Laser Scanning, Point Claud, Fused Deposition Modeling, Total Least Square Fitting, Acetone Vapour Bath Smoothing

ACKNOWLEDGMENT

I would like to express my gratitude to my supervisor Dr. Ahmad Barari that without his great support and understanding, I would not be able to accomplish my academic goals.

TABLE OF CONTENTS

LIST OF FIGURES

LIST OF TABLES

NOMENCLATURE

Symbol	Description
A	Area
a	Line parameter
b	Layer depression and Line parameter
c	Line parameter
E	Deviation from centerline
h	Vertical intersection of centerline
L	Length
m	Centerline slope
n	Number of points
P	Height of peaks
R_a	Average profile roughness
R_{da}	Mean slope of a surface with centerline
R_{dq}	Root mean square slope of a surface with centerline
R_{ku}	Kurtosisness of a surface
R_{max}	Peak valley height
R_q	Root mean Ssquare roughness
RMS	Root Mean Square roughness
RS_m	Mean Width of Profile Elements

R_{sk}	Skewness of a surface
R_t	Peak valley height
R_z	Mean Roughness Depth
R_{ZJIS}	Mean Roughness Depth in JIS
S	Profile features spacing
S_a	Average Surface roughness.
S_{ds}	Density of summits of the surface
S_p	Highest peak.
S_q	Root mean square Surface roughness.
S_{sk}	Skewness of the surface.
S_{td}	Texture direction of the surface
S_{tr}	Texture aspect ratio of the surface
S_v	Lowest valley.
S_z	Ten point height of the surface.
t	Layer thickness
V	Depth of valleys
W	Step width
Z	Surface points distance from centerline
α	Centerline angle or build orientation
θ	Surface slope, build orientation
φ	Surface profile angle from vertical axis

ABBREVIATIONS

Abbreviation	Description
AA	Arithmetic Average
ABS	Acrylonitrile Butadiene Styrene
AFB	Abrasive Fluidized Bed
AFM	Atomic Force Microscopy
AFM	Abrasive Flow Machining
AJD	Abrasive Jet Deburring
ALM	Additive Laser Manufacturing
AM	Additive manufacturing
APS	Atmospheric Plasma Spraying
BF	Barrel Finishing
CAD	Computer Aided Design
CLA	Center Line Average
CNC	Computer Numerical Control
DMLA	Direct Metal Laser Additive
DMLS	Direct Metal Laser Sintering
FDM	Fused Deposition Modeling
GPS	Geometrical Product Specifications
HCM	Hot Cutter Machining

ISO	International Standard Organization
JIS	Japanese Institute of Standards
LM	Layer Manufacturing
MEMS	Micro Electro Mechanical Systems
MMP	Micro Machining Process
PBF	Powder Bed Fusion
PGI	Phase Grating Interferometric
RRP	Roughness Reduction Percentage
SEM	Scanning Electron Microscopy
SL	Stereo Lithography
SLA	Selective Laser Additive
SRS	Surface Roughness Sensitivity
STL	STereoLithography
TET	Total Exposure Time
TLS	Total Least Square
XCT	X-Ray Computed Tomography

1. INTRODUCTION

Additive manufacturing (AM) is getting more attention as a manufacturing rather than a prototyping process for various applications today. Since its emergence and development into a manufacturing process, AM made it possible to manufacture lots of complicated designs and geometries, which where almost unfeasible by the traditional methods. An interesting fact about AM is that there is not a direct relationship between the cost and complexity of the product as it is for traditional processes. The concern in AM is the size of the part, not its complexity. Am does not require many expensive and time consuming lateral processes such as jig and fixture, die and tool design. The final product can be manufactured by AM. However, the product may require a post processing, which is negligible compared to the lateral processes in traditional methods. In addition, the optimum designs, specifically the topologically optimized designs, are very expensive to manufacture by the traditional methods or even unfeasible. In this respect, AM obviates many problems in the way of innovation and manufacturing of optimum structures. The designer can think in a broader context without much concern about complexity and manufacturability of the design.

1.1. MOTIVATION: POOR SURFACE INTEGRITY OF AM PARTS

AM processes have many advantages over the traditional methods in manufacturing complex geometries and its phenomenal capabilities. Therefore, it is important to conduct research works to obviate its downfalls and improve it toward a process capable of manufacturing functional final products. Similar to every other manufacturing process, AM also has its own deficiencies that need to be reduced or eliminated. The rough surface of AM part is its main drawback. The need for a specific surface quality is due to design requirements such as surface integrity, assembly fitting, aesthetic requirements, surface functionality or the requirements of any other downstream manufacturing process.

The poor surface roughness is mainly a result of the layer by layer deposition of material, which creates the staircase effect for all inclined surfaces. For the horizontal and vertical surfaces the ridge pattern is the main part of the surface roughness. The staircase effect is directly influenced by layer thickness. Thinner layer thickness results in less staircase effect and so better surface quality. The process parameters, such as layer thickness, define the ridges that cause the surface roughness. AM surfaces include textures that are strongly related to the filling pattern or the trajectories followed by the solidifying mechanisms such as the laser beam or polymer injection head, etc.

1.2. OBJECTIVE: IMPROVING THE SURFACE INTEGRITY OF AM PARTS

In order to improve the surface integrity in AM family of manufacturing processes, our approach is categorized into three main stages. The three stages are modeling the surface roughness, inspection of the manufactured surface and finally the post processing stage.

The first two steps are general for all AM processes since the layer-based nature of them. However, the post processing stage needs to be considered for each AM process separately as there are material and process differences. The three stages are discussed in the following paragraphs.

1.2.1. Analytical modeling of the surface profile

An acceptable surface roughness on a manufactured surface is so important in industrial applications. Therefore, an analytical approach to predict the final surface roughness is of substantial importance. An accurate model for surface roughness can be employed for actively controlling the manufacturing parameters to achieve the desired surface roughness or to plan for the proper selection of the required post-processing. The two main process parameters affecting the surface roughness are the layer thickness and build orientation. The analytical model developed in this research, utilizes the Total Least Square (TLS) method for defining the centerline used to calculate the surface roughness. In the research works conducted so far, it is presumed that the centerline used in calculating the surface roughness passes through the mid point of the surface profile. However, based on the definition of centerline, the sum of the distance of all points on the surface from the centerline must be minimum. This assumption casts doubt on the validity of the fact that the distance of all points from the line passing through the mid point of the surface profile is minimum. Therefore, in developing the centerline in this research, this assumption is not made and the centerline is found based on procedures taken to minimize the sum of the distances. Thus, the line found using the developed procedure is considered as the centerline.

1.2.2. Inspection of the surfaces manufactured by AM methods

Inspection of the surfaces manufactured by AM processes is a challenging task as the surfaces mostly contain rough textures and patterns. The layer-based nature of AM surfaces necessitates a comprehensive research to stablish a methodology for measuring AM surfaces. The surface measurement devices commercially available are laser based machines, optical microscopes for surface topography and the mechanical roughness measuring devices. The surface being inspected defines the most appropriate method to measure the surface. The layer-based nature of AM surfaces creates a very repetitive and fine-featured pattern that makes it difficult for inspection devices to measure them. All three types of surface measuring devices are utilized in this research to select the best option for each surface topography specification.

Larger layer thicknesses tend to create more sensible features and larger values of surface roughness. The combined effect of layer thickness and build orientation defines the maximum surface roughness that the measuring device can measure. In the case of laser-based devices, the reflection of the laser beam from the surface is so important. On very smooth surfaces with very fine patterns, the laser-based devices such as Faro Arm have trouble in identifying the patterns. The optical microscope shows the 3D surface topography and gives valuable information about the surface under inspection. This device was used to study the effect of post-processing stage compared to the surface before finishing. After the post processing, a mechanical roughness device was used to measure the surface roughness after post processing.

1.2.3. Post processing of the parts

Considering all efforts made to improve the process parameters to get a better surface roughness, the AM processes still suffer from a poor surface quality. Application of AM parts in industrial services highly relies on an appropriate post-processing stage to improve the surface roughness of the products. Since each AM process uses a certain type of material, the post processing stage must be studied for the specific AM process. In this research, Fused Deposition Modeling (FDM) method is considered as the manufacturing method and efforts has been made to improve its surface roughness. The main sources of roughness for AM processes can be divided into three main categories based on their importance: first, the inherent layer by layer characteristics of these methods. Second, the slicing and chordal errors and third, the fabrication parameters. The first category of the roughness sources of AM parts can be improved by optimizing the third category (fabrication parameters). FDM process has many process parameters such as, layer thickness, part orientation, raster angle, road width, air gap between roads and model temperature making this process more crucial from surface roughness aspect. The first logical procedure is to optimize all the pre-processing and processing factors. Optimizing the layer thickness based on the features complexity, and the triangulation step are the pre-processing steps to be considered. Post-processing is the only option to further enhance the surface roughness of FDM parts. Therefore, after optimizing all the pre-processing and process parameters for objective functions such as mechanical properties, build time and etc., the next step is to do the optimization with an eye on minimizing the required post-processing as the objective function. The post-processing can be categorized into two groups: mechanical and chemical processes. The main disadvantages of mechanical

approach are inaccessibility of some sections, the need for clamping the work piece, delicate features on AM parts, and details of the mechanical tool used. Considering all the cons and pros of the mechanical finishing processes, yet they cannot fulfill the requirements of a functional and efficient finishing process for FDM parts. An efficient method should be able to improve the surface roughness while keeping the mechanical and geometrical properties constant, improving the surface roughness all over the surface without limitation, and without requiring clamping and extra costly operations.

Chemical finishing improves the surface roughness significantly without the limitations pointed out for mechanical approaches. However, it has material restrictions that makes it not applicable for all parts. It can be used for parts made of Acrylonitrile Butadiene Styrene (ABS). Acetone vapour bath smoothing is used for the post-processing stage. Smoothing parameters are divided into the number of smoothing cycles and the duration of each cycle. Effect of design and smoothing parameters are studied and the best smoothing setting is proposed for each set of design parameters. An experimental model is developed to enable the engineers to predict the final surface roughness based on the build orientation and define the required post-processing steps to achieve it.

The structure of this thesis is as follows: After the introduction section, chapter 2 discusses the background and literature review in surface roughness of layer-based manufacturing parts including modeling, inspection and post processing. In chapter 3, the proposed methodologies are presented and chapter 4 includes the results and discussions. In chapter 5, the concluding points are provided and suggestions for future research are presented.

2. LITERATURE REVIEW AND BACKGROUND

2.1. INTRODUCTION

The literature review is divided into three sections: first, analytical modeling of the surface roughness. Second, the surface inspection methods, terminologies and devices. Finally, the post processing stage to improve the surface integrity. In order to understand the surface roughness and how the surface texture can be modeled for layer-based manufacturing parts, a literature review of modeling the surface roughness is presented first and then surface topography inspection and roughness terminologies are discussed. At the end, the research works about post processing of layer-based manufacturing parts are presented.

2.2. ANALYTICAL MODELING OF SURFACE ROUGHNESS

Additive manufacturing is a layer-based process and the final part is made by layer by layer depositing the material. As a result, staircase effect will be present on all inclined surfaces (Figure 2-1). There is no staircase effect on horizontal and vertical surfaces so the dominating factor in surface texture will be the ridge pattern. Staircase effect is one of the main characteristics of all AM manufactured parts. The portion of surface pattern related

to staircase effect is dominating over the ridge pattern. Therefore, staircase effect, if present, is the main factor affecting the surface roughness and requires more attention. The influence of staircase effect and ridge pattern on the surface texture of AM parts can be considered at macro and micro levels, respectively. Additive manufacturing methods can be divided into two primary categories: trajectory and non-trajectory. The trajectory AM processes, such as Fused Deposition Modeling (FDM), require a solidifying head move over the surface and deposit the material as beads. The surface pattern of these methods includes the ridge patterns. The Selective Laser Sintering methods are also trajectory processes but the layers are manufactured by sintering the powder particles and there are no beads. In the non-trajectory AM processes, the entire layer is manufactured at once, such as Stereolithography or SLA.

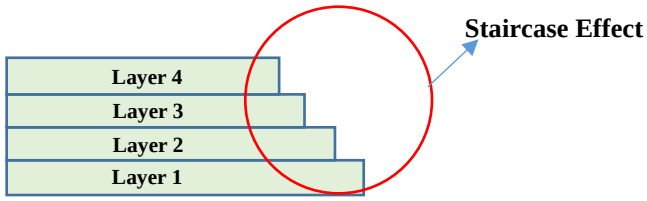

Figure 2-1 Schematic representation of staircase effect in layer based manufacturing.

The two main characteristics of a surface manufactured by layer-based methods, such as Fused Deposition Modeling (FDM), are the staircase effect and ridge patterns. The former causes the profile cusps and the latter is created by the beads deposited adjacent to each other. The ridge pattern significantly affects the surface roughness of the horizontal surfaces and the cusps are the dominating factor affecting the surface roughness of every inclined surface from the horizontal plane [1]. The process parameters such as layer thickness and filling pattern, define the ridges that cause the surface roughness. The effects

of the process parameters on the structural quality of parts manufactured by FDM are studied in the literature [2].

Regarding the importance of an appropriate surface roughness on a manufactured surface, an analytical approach to estimate the final surface roughness is of substantial importance. Developing an accurate model to predict the resulting surface roughness based on the manufacturing parameters can be employed for actively controlling the manufacturing parameters to achieve the desired surface roughness or to plan for the proper selection of required post-processing setups. The two main process parameters affecting the surface roughness are the layer thickness and build orientation. One of the commonly adopted approaches to calculate the surface roughness in layer-based parts is derived from trigonometry of the cusp geometries caused by the staircase effect [3 and 4]. In their initial model, the surface was considered as stair-steps with square corners. Later, in a more general form, the surface profile was modelled by sharp triangular shape with angle φ from the vertical line. A schematic representation of the model is presented in Figure 2-2. Build orientation or surface angle plays a crucial role on the final surface roughness. The proposed trigonometric formula to calculate surface roughness with square corners and sharp triangular corners are presented in Equations (2-1 and 2-2), respectively.

$$R_a = \frac{t}{4}\cos(\theta) \tag{2-1}$$

$$R_a = \frac{\sum A^n}{L^n} = \frac{t(tan\varphi\ sin\theta + cos\theta)}{4} + \mathrm{K} \tag{2-2}$$

where R_a is the surface roughness, t is the layer thickness, φ is the angle counter clockwise from the vertical line and θ is the surface angle or built orientation.

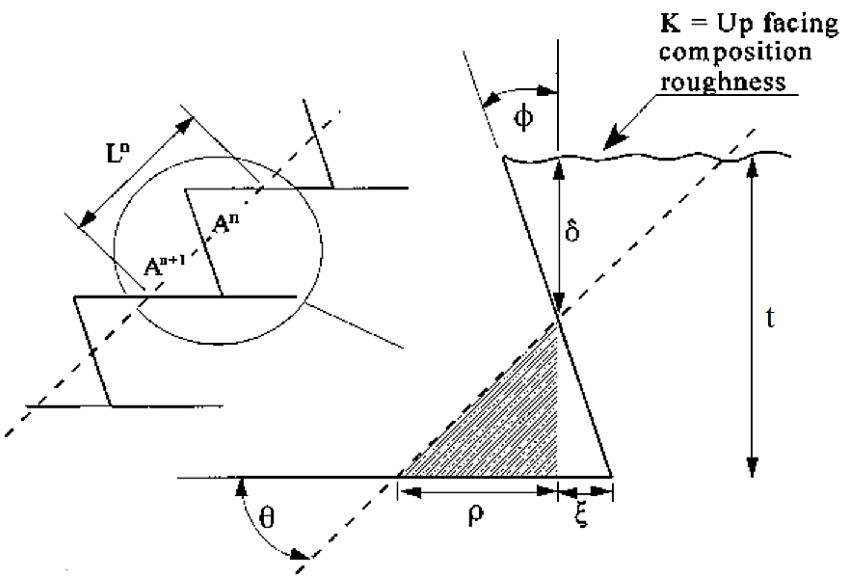

Figure 2-2 Schematic of the trigonometric model [3 and 4].

R.I. Campbell et al. [5] used the experimental measurement data to visually represent the predicted surface roughness of a given CAD model. The designed specimen had surface angles from 0° to 180° with increments of 2°. The surface roughness was measured using a mechanical roughness measurement device. They also compared their experimental results with the trigonometric model presented by Reeves et al. [3 and 4]. They noted that in some cases there is not a satisfactory conformance between them. This finding and the other similar observations encouraged the researchers to look for other parameters such as the details of the cusp corners to develop a better model for the surface roughness.

The simple formula in Equation (2-1) is referenced in Campbell et al. [5] as: $R_a = tsin\theta/4tan\theta$ which has misled some researchers [6 and 7] to the end that they have used the formula as: $R_a = tsin(\frac{\theta}{4})\tan(\theta)$.

Ahn et al. [8 and 9] considered the edge profile as an inclined line with φ angle from the vertical line (Figure 2-3). Their research was aimed at finding the optimum build orientation to minimize the required post-processing. In developing the model, the same trigonometry process was used and the proposed formula is as follows:

$$R_a = \frac{A}{w} = \frac{L}{2}\left|\frac{\cos(\theta - \emptyset)}{cos\emptyset}\right| \tag{2-3}$$

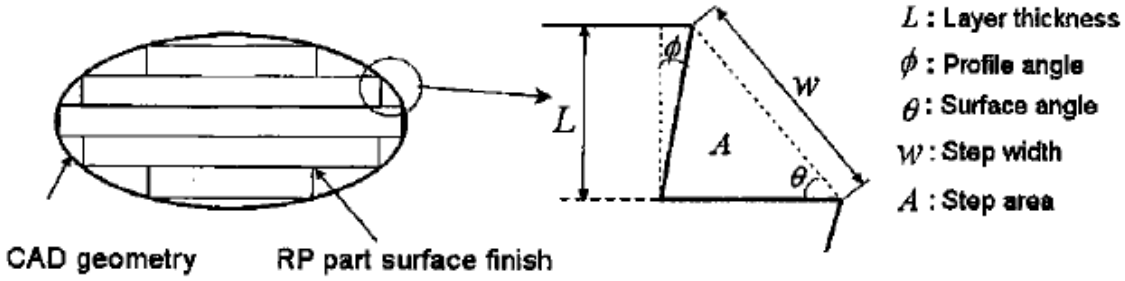

Figure 2-3 Surface profile of general layer-based manufactured part [8]

Byun and Lee [10] proposed a new profile rather than square corners to characterize the cusp profile and added two other parameters including fillet radius and corner radius as shown in Figure 2-4. The formula was used to determine the optimum build orientation considering three criteria: build time, surface roughness and cost. Their proposed formula to calculate the surface roughness was:

$$R_a = \frac{l_t}{4}cos\theta - \frac{(R_1^2 + R_2^2)\left(1 - {}^{\pi}/_{4}\right)sin\theta}{l_t} + \frac{\left\{(R_1^2 + R_2^2)\left(1 - {}^{\pi}/_{4}\right)\right\}^2}{l_t^3} tan\theta sin\theta \tag{2-4}$$

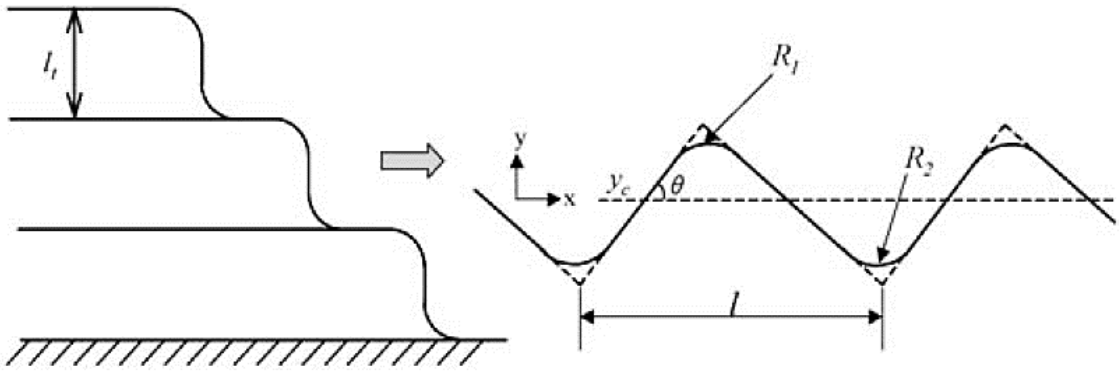

Figure 2-4 Proposed profile shape in [10]

Their results showed that part orientation is one the most significant factors in manufacturing a part with AM processes. They used a variable layer thickness in their research. The experimental results showed that the developed model can help users in choosing the optimal build orientation with three different objective functions.

Paul and Voorakarnam [11] used the average centerline method in calculating the surface roughness. Their results showed that orientation angle and layer thickness are the main parameters affecting the surface roughness. The experimental results revealed that the model is able to predict the roughness up to a certain layer thickness and after that shows poor performance. Perez et al. [12] studied the surface roughness of layer-base manufactured parts using the average centerline method. They considered the layer thickness and layer depression (horizontal space between the layers) in developing their model. Layer depression was defined based on the layer thickness and surface angle so the surface roughness was a function of layer thickness and surface angle. Their model had some difficulties in predicting the surface roughness for angles close to 0 and 90 degrees and needed some corrections. The developed theoretical model yields a maximum

roughness value so the results can be used as an upper bound in determining manufacturing strategies. For example, when the required surface roughness is known in advance, the maximum bound for roughness can be obtained. There can be two manufacturing strategies using the results of their study: manufacturing with a given R_a within a specified roughness tolerance, and second, manufacturing using a constant layer thickness. The results of these two strategies revealed that when a specified roughness is required, the layer thickness must be modified.

Pandey et al. [13] proposed a semi-empirical model to predict the surface roughness of a layer-based manufactured part by FDM. They approximated the layer edge profile by a parabola with base length of $t/cos\theta$ and height of 30-35% of base length, as shown in Figure 2-5. The areas A_1, A_2 and A_3 are used to calculate the surface roughness as shown in Equation 2-5. They observed a gap between the roads of filaments at surface angles from 70° to 90°. This gap was found to change the general model of the surface roughness. The results of this model are reported to be in good agreement with the experimental results.

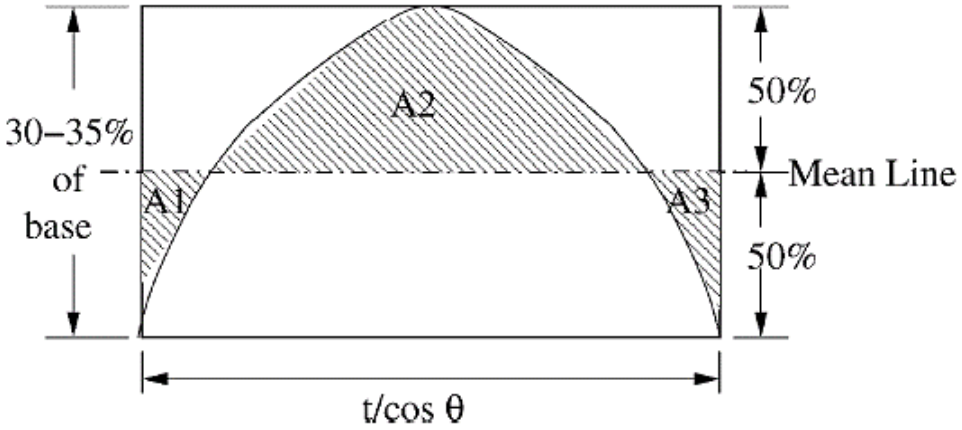

Figure 2-5 Surface profile approximation [13]

$$R_a = 1000 \frac{A_1 + A_2 + A_3}{t/cos\theta} \quad (2\text{-}5)$$

Ahn et al. [14] used experimental results of surface roughness to develop a theoretical model for surface angles of 0° to 180°, with 3° increments, on layer-base manufactured parts. The edge profile was considered as a sharp triangular edge similar to their previous works [8 and 9]. A distribution of surface roughness values versus surface angle was presented. For the unmeasured angles, interpolation method was used. The normal vector of the facet in CAD model alongside with the corresponding roughness from the distribution was used to predict the surface roughness at a specified surface angle.

Ahn et al. [15] considered the edge profile of a surface produced by FDM as an elliptical curve (Figure 2-6). Their model considers the cross section shape as well as the layer thickness and build orientation as the defining factors for surface roughness. In addition, the overlap interval between the adjacent layers is deducted from the actual layer thickness, thus the overlap is also considered. The effect of these factors were investigated and their results showed that the model could be used as a more detailed representation of surface roughness. They showed that for angles close to 90°, the effect of layer thickness is not significant on the surface roughness value.

Ahn et al. [16] used parabolic representation with different coefficients for surface profile of layer-based manufactured parts. They used average centerline method in calculating the surface roughness and the results of experiments was in good agreement with the predicted values.

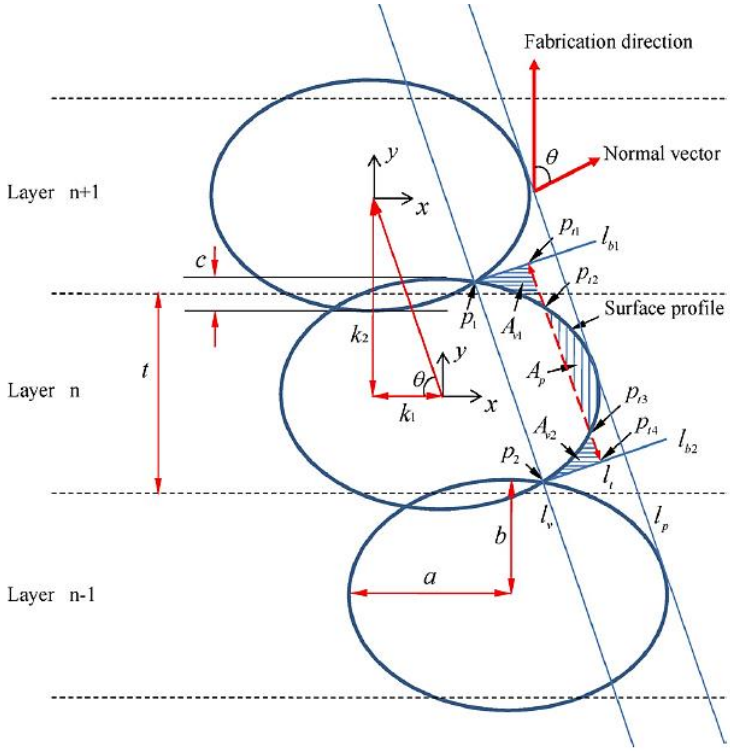

Figure 2-6 Elliptical representation of surface profile manufactured by layer-based methods [15].

Boschetto et al. [17–21] studied the 3D roughness profile of AM surfaces. They considered the edge profile as a sequence of circular arcs. They used average roughness values coming from a profilometric analysis in roughness analysis. They did a statistical analysis and concluded that the edge profile of the layer can be expressed by rounded curves. The proposed profile is useful for describing the micro-geometrical FDM surfaces. The third dimension makes the calculation of other roughness parameters such as amplitude, spatial and hybrid roughness parameters possible. The proposed model was validated by measuring the surface roughness of tubes with all surface angles from 0° to 180°, at 5° increments. A very good agreement was observed between the experimental and theoretical results; however, the mathematical difficulties have caused the theoretical

model fail to predict the roughness values for angles close to 0 and 180 degrees. They also have used neural network method in predicting the surface roughness value of FDM parts.

Barari et al. [22 and 23] developed a non-uniform rational B-spline (NURBS) model for representing the cusps geometry generated by layer-based manufacturing methods. They estimated the surface roughness based on the local surface gradient on the part and the selected layer thickness. Using their model, the local surface roughness was estimated effectively using Equation 2-6. The suggested surface profile is shown in Figure 2-7.

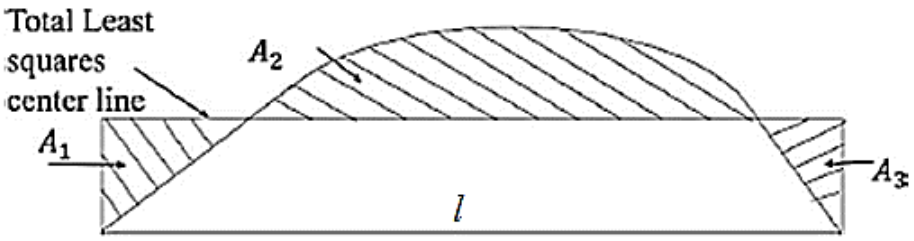

Figure 2-7 Schematic of surface profile of a layer-based method [22]

$$R_a = \frac{A_1 + A_2 + A_3}{l} \tag{2-6}$$

2.3. SURFACE TOPOGRAPHY

2.3.1. Surface texture parameters

In subtractive manufacturing methods, material is removed from a balk to create the desired shape. The removal of material by the manufacturing tool causes a scratch on the surface, which can also be referred to as a minute groove. As the manufacturing tool passes across the surface, the formation of minute grooves produces surface texture. The texture is determined within each of the created grooves on the surface, and it depends on the way that the material has been removed from the surface. If the tool is set up perfectly and

follows an accurate path, then the removed particles will be the same size and a flat plane will be resulted. However, if there are any irregularities on the tool surface itself or the path it follows, an undulating surface will be resulted. The case in the majority of the manufacturing processes is not perfect and roughness irregularities are left on the surface referred to as surface topography. In the case of additive manufacturing methods, the part is build by sequentially adding material layer by layer. For these type of manufacturing methods, the surface irregularities are again present because of the path that the solidifying head follows or any other type of layer creation method being used [24].

The ideal cycle of manufacturing and service life of a part is going directly from a manufactured part to working station with an acceptable performance, shown in Figure 2-8. The actual process conditions make this ideal cycle impossible and so there must be some measures to make sure the required performance is achievable. The process control needs to be done during or after the manufacturing process to identify the defects in the process and corrected them. In order to validate the performance of a part, standard definitions are required to define the goal and allowed deviations accurately. The surface texture and tolerance standards are developed to serve this goal [24–26].

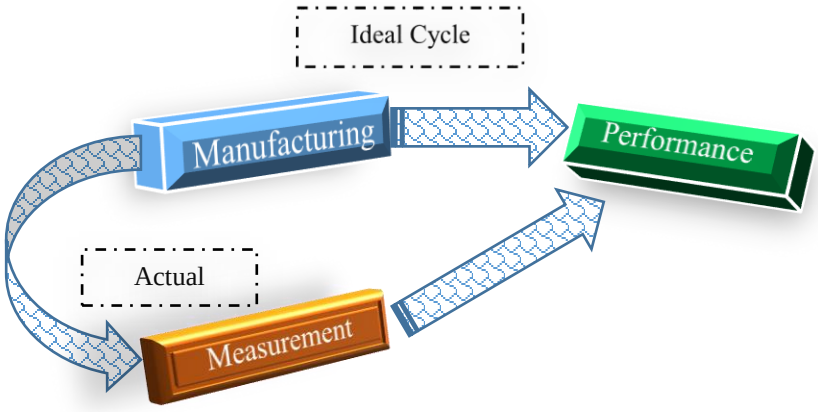

Figure 2-8 The ideal and actual cycle of manufacturing a part [24].

Surface irregularities define the surface topography and based on the spacing between them, a surface can be curved, wavy or rough. The waviness and roughness can coexist on a surface as shown in Figure 2-9. However, on an actual surface, the irregularities will not have a pattern and it can be randomly distributed. The roughness irregularities on a normal surface are so small to be visible by a naked eye so some magnifying devices are needed to explore the surface roughness. Figure 2-10 shows a schematic view of a magnifying device that is a basis for the majority of surface roughness equipment. The measuring technique is to draw a very sharp stylus across the surface at a constant speed for a set distance. An electrical signal is obtained and amplified to a much larger value. Then the signal is displayed on a screen output or as a graph to characterize the surface texture [24].

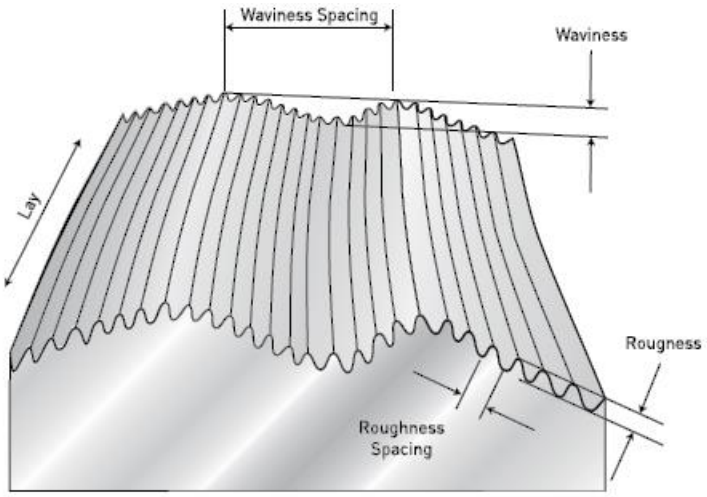

Figure 2-9 The waviness and roughness on a surface [24].

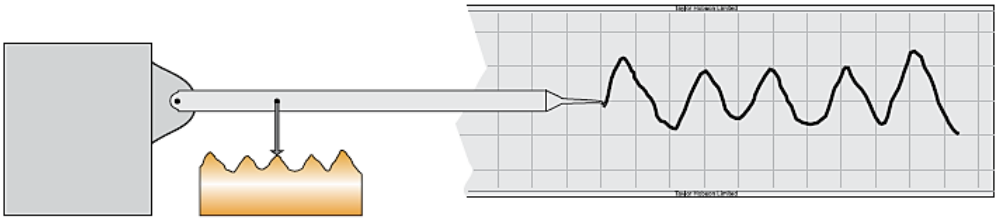

Figure 2-10 Schematic of a surface roughness device based on magnifying the surface topographies [24].

The distinction between the roughness and waviness often depends on the size of the workpiece. For instance, the irregular spacing might be regarded as roughness on a large shaft but considered as waviness on a watch staff. Another point of view is the number of waves on a functional length, which defines the classification criterion. One wave on a watch staff might be considered as curvature and part of the form of the part but on a longer component can be accepted as a waviness. A better way to classify these concepts is doing so according to their cause. Roughness is defined as the irregularities, which are inherent in the manufacturing process. For example, cutting tool or abrasive grids, etc. Waviness can be defined as the part of surface texture that the roughness is superimposed. The waviness can a result of vibrations, chatter or work deflections and strains in the material. It is hard to define a distinct point where waviness becomes a part of the form of the surface but form is usually defined as the general form of the surface. The qualitative definition of these concepts is not enough to use them in real manufacturing process. The surface texture needs to be quantified, which need a digital representation of the surface [24].

Characterizing the surface texture requires the extraction of texture related information from the surface topography information. The useful information must be extracted through the measurement, which capture relevant aspects of the texture such as heights, spacing and distribution of the features. International Standard Organization (ISO) has developed two standards to characterize the surface texture. The specific standards designed for this purpose are called Geometrical Product Specifications (GPS). The first one is surface texture: profile method-terms, definitions and surface texture parameters (ISO 4287:1997) [24] and the second one is surface texture: areal 2: terms, definitions and

surface texture parameters (ISO 25178-2) [26]. The ISO 4278 standard is concerned with terms, definitions, and parameters for profile measurement. However, ISO 25178-2 defines areal parameters for 3D texture analysis.

It is hard to put an individual number for characterizing the surface topography and be able to completely represent the surface complexity. Therefore, an accurate assessment of surface performance in service life needs exploring the surface parameters and quantify them. Surface profile parameters fall into three categories based on the surface they represent: amplitude parameters, which are defined by picks and valley heights or both, irrespective of the horizontal spacing between them, such as R_a. The second category are the spacing parameters, which are defined by the spacing of irregularities along the surface, such as RS_m. The third category are the hybrid ones, which are defined by amplitude and spacing combined, such as R_{dq}. Some of the surface texture parameters, which are more common, are explained in the following paragraphs according to ISO 4287:1998 [24 and 25]. The 3D texture parameters have distinct advantages over the profile parameters. As the surface topography is 3D in nature, thus any 2D profiles used in characterizing the surface result in an incomplete description of the real surface. Among the various surface texture parameters, some of them are recommended to be used in characterizing AM surfaces in the literature [29], so this parameters are explained in details in the following sections.

Roughness average, R_a, is the most frequently used parameter in surface topography analysis. Previously, this parameter was referred to as Center Line Average (CLA) or Arithmetic Average (AA). In calculation of R_a over a length, the mean line is found and

the areas below the mean line are inverted above the line and the mean height of them is called R_a, as shown in Figure 2-11 Schematic derivation of Ra [24]. Therefore, the unit for R_a is in length typically in microns. If the surface profile is digitized, as illustrated in Figure 2-12, which means the height of all points from the mean line is known, Ra can be found by Equation (2-7):

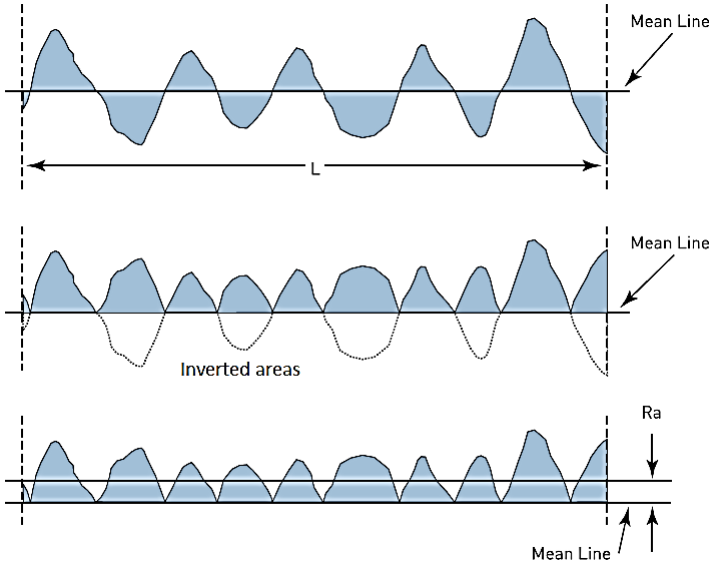

Figure 2-11 Schematic derivation of R_a [24]

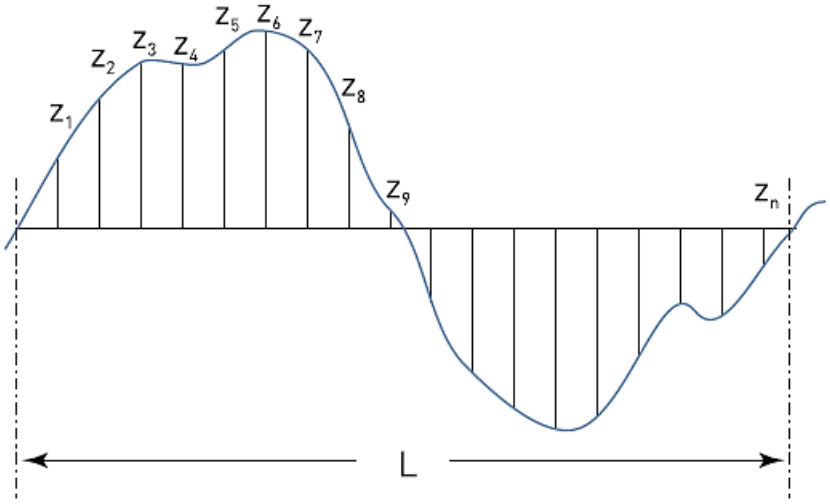

Figure 2-12 A digitized surface used in calculation of R_a [24].

$$R_a = \frac{|Z_1| + |Z_2| \dots |Z_n|}{n} = \frac{1}{n}\sum_{i=1}^{n}|Z_i| \quad (2\text{-}7)$$

Root Mean Square (*RMS* or R_q), is another way of calculating the average roughness obtained by squaring each height value and taking square root of the mean of them over an assessment length of *l*. The *RMS* value is referred to as R_q, too. The R_q values are more meaningful when being used in statistical works but graphical calculation of R_a is easier and that is why it was initially adopted.

$$RMS = \sqrt{\frac{1}{l}\int_0^l Z^2(x)\,dx} \quad (2\text{-}8)$$

Peak and Valley Height, R_t, is the maximum peak to valley height, which means the distance between the highest and lowest points on the profile over the assessment length. This parameter is sometimes referred to as R_{max}.

Mean Roughness Depth, R_z, is the arithmetic mean value of the single roughness depths of consecutive sampling lengths. There are many versions to R_z depending on the institution developing the standard. One of the frequent versions is the Japanese Institute of Standards (JIS) version, R_{zJIS}. The difference is in the number of the sampling over the length. It takes five peaks and five valleys, also referred to as ten point height. This factor is helpful in measuring small lengths (Figure 2-13).

Mean Width of Profile Elements, RS_m, this parameter is used to define the average spacing of the profile's peaks and valleys.

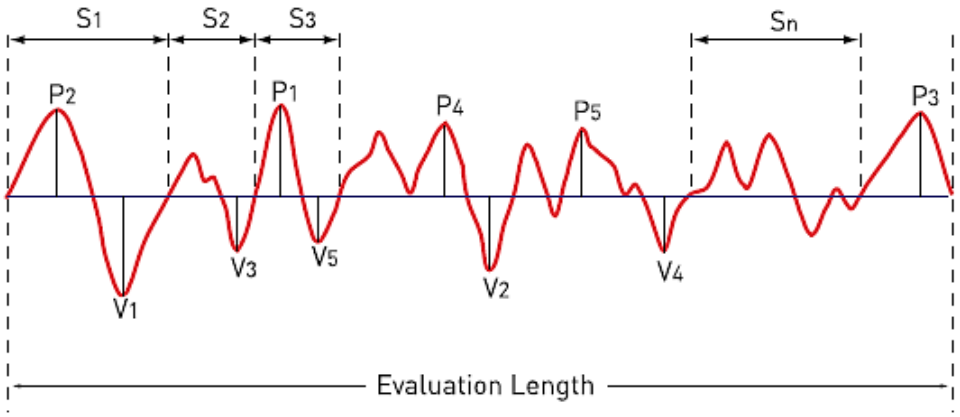

Figure 2-13 Schematic illustration of derivation of RS_m and R_zJIS [24].

$$R_zJIS = \frac{P_1 + P_2 + P_3 + P_4 + P_5 + V_1 + V_2 + V_3 + V_4 + V_5}{10} \tag{2-9}$$

$$RS_m = \frac{S_1 + S_2 + S_3 + \cdots + S_n}{n} \tag{2-10}$$

Slope, R_{da} and R_{dq}, of a profile is the angle that the surface makes with a line parallel to the centerline. The mean of the absolute value of slope calculated at each of the points in the profile within the sampling length is known as the average slope, R_{da} for arithmetical mean and R_{dq} for the rms value.

Amplitude distribution (Skew, R_{sk}, and Kurtosis, R_{ku}): the amplitude distribution curve illustrates the relative total lengths over which the profile graph attains any selected range of heights above or below the centerline. By plotting the density vs height (y), the way that the amplitude density is distributed over the entire profile can be represented. A profile with a regular shape yields an amplitude distribution symmetrical about the centerline. Any asymmetrical profile gives a skewed curved as shown in Figure 2-14. Depending on whether the bulk of the material is above or below the centerline, the direction of skew will be positive or negative, respectively. The skewness parameter R_{sk}

gives significant information about the shape of a surface profile. The two surfaces with the same R_a values but different profile can be distinguished by their R_{sk} value.

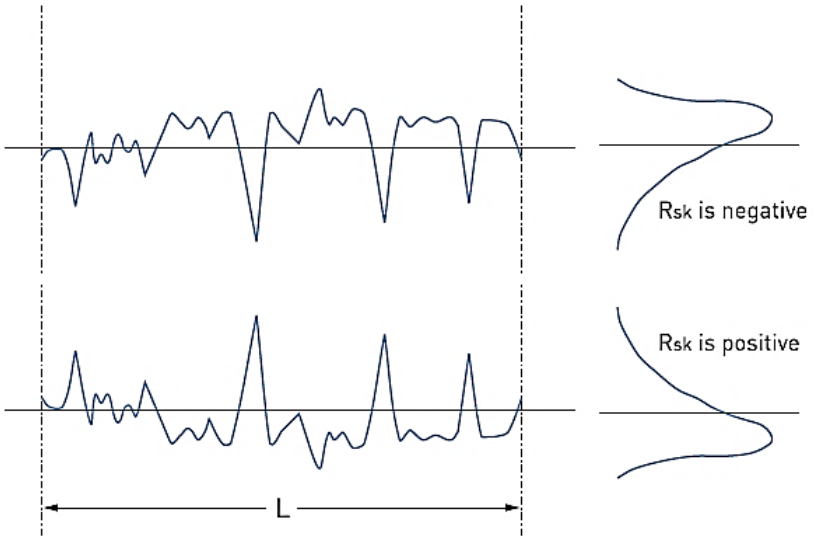

Figure 2-14 skew parameter distinguishes between two profiles with differing shapes [24].

Skew cannot detect whether the spikes are uniformly distributed about the mean line; however, Kurtosis is able to detect it. Kurtosis (R_{ku}) provides a measure of the sharpness of the surface, a "spiky" surface having a high Kurtosis value and a "bumpy" surface having a low Kurtosis value.

The 3D surface texture parameters are summarized in Table 2-1 Selected 3D surface texture parameters adopted from EUR 15178 EN and ISO 25178-2, The Development of Methods for the Characterization of Roughness in three dimensions.

Table 2-1 Selected 3D surface texture parameters

Amplitude Parameters		
Symbol	Description	Comment
S_a	Average absolute deviation of the surface.	The most commonly used and corresponds to R_a
S_q	Root mean square deviation of the surface.	Used to discriminate between different surfaces of the surface based on height information and to monitor manufacturing stability.
S_{sk}	Skewness of the surface.	Indicates aspects of load carrying capacity/lubrication.
S_p	Highest peak.	Largest peak height within the definition area.
S_v	Lowest valley.	Largest valley depth within the definition area.
S_z	Ten point height of the surface.	Used to evaluate extreme surface height deviations.
Spatial Parameters		
S_{ds}	Density of summits of the surface	Used to evaluate the density of peaks and pits in the surface.
S_{td}	Texture direction of the surface	Indicates the direction of the significant lay of the surface.
S_{tr}	Texture aspect ratio of the surface	Measures the isotropy of a surface.

2.3.2. Surface roughness measurement instruments

Contact based instruments:

One of the most common types of surface texture assessment, working based on contact of the measuring instrument with the surface is the stylus type instruments. In this type, a stylus follows the surface profile along a line and magnifies the profile for further study. These devices measure the profile along a line so for 3D cases, the measurements are done

several times and the average is considered as the result. Figure 2-15 shows the schematic roughness measurement by stylus instrument. According to Figure 2-15, the stylus travels across the surface and pickup converts its vertical movements into an electrical signal. This signal is then amplified and used to operate the recorder. The recorder gives the magnified surface profile. The magnified signal is filtered and then R_a value is displayed on a pointer or as a number on a screen. The illustration presented here is the basic principles of a stylus type roughness measurement, the more recent products have extra facilities but there is no difference in principles. A gauge is required to convert the vertical movements of the stylus into electrical signal. There are two main type of gauges: analog and digital transducers. The analog transducers can be divided into two types: position sensitive and motion sensitive [24].

i) Position sensitive: the signal is proportional to the displacement. The output depends on the displacement of the stylus and its position within its range of vertical movement irrespective of the movement of the stylus. Figure 2-16 shows an analog position sensitive transducer with variable inductance gauge.

ii) Motion sensitive: this type produces signal only when the stylus is moving. The output depends on the speed of the stylus movement. This type is more useful is measuring formed surfaces. This type has a piezoelectric crystal capable of creating electric signal when deformed.

In the case of digital gauges, as the stylus moves, pulses corresponding to multiples of the transducer resolution are fed into an up-down electric counter displaying the gauge displacement. The two gauges that are currently being used in commercial instruments are

based on interferometry. The principle used in interferometry-based devices is counting the light and dark "fringes" caused when two light beams interfere. The two types are laser and Phase Grating Interferometric (PGI). The PGI type offers a wider range of measurement and has a smaller size. Another advantage is that the measuring range is independent of laser wavelength. Figure 2-17 shows schematic diagram of a PGI gauge [24].

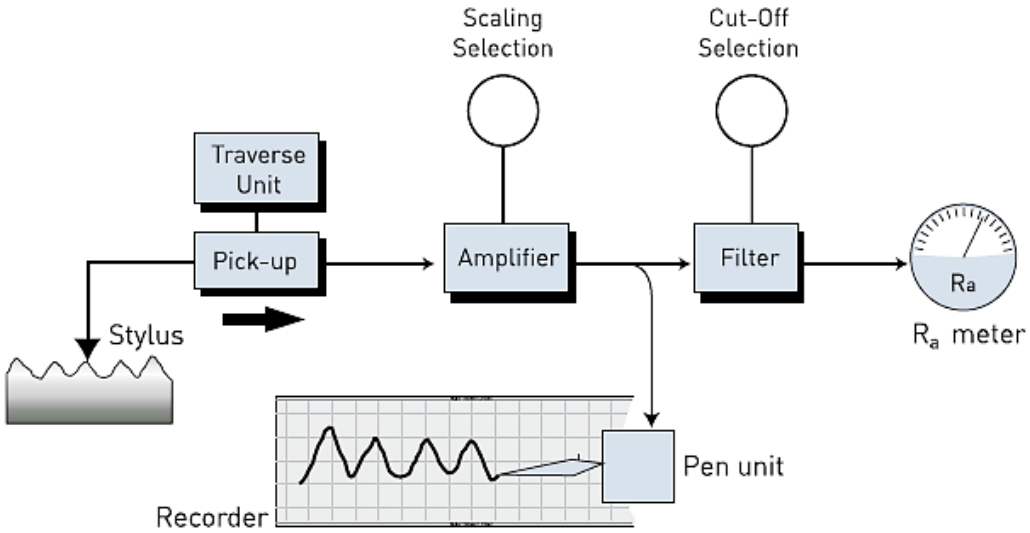

Figure 2-15 The components of a stylus type surface texture measuring instrument [24].

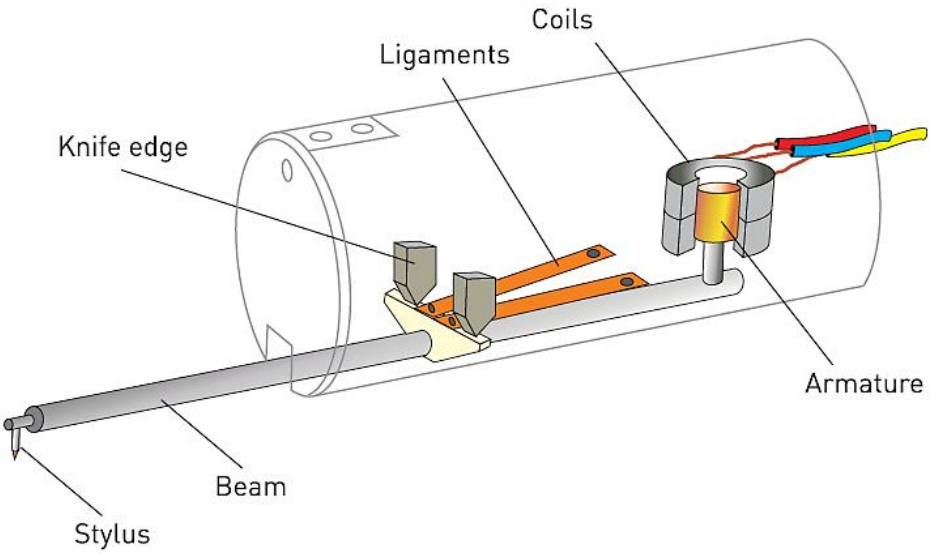

Figure 2-16 Schematic illustration of analog position sensitive gauges [24].

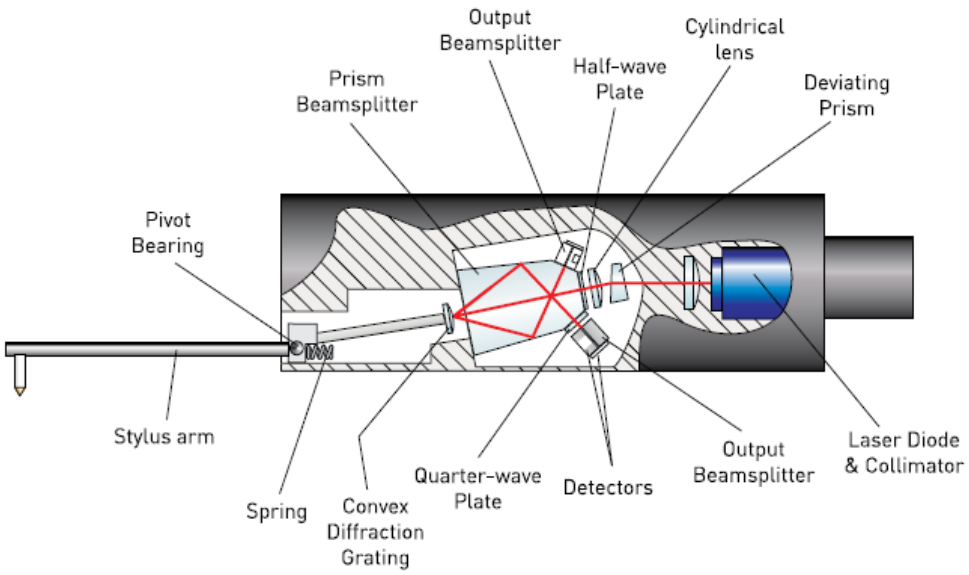

Figure 2-17 Schematic illustration of a PGI gauge [24].

Non-Contact roughness Instruments

There are also non-contact gauges for surface texture measurements including Capacitance systems, laser triangulation, Atomic Force Microscopy, Confocal Microscopy, Scanning Interferometer, etc. Each type is discussed briefly here.

Capacitance systems are the most basic form of surface measurement. This type used the surface as one of the plates of a capacitor. The air between the surface the probe, which is another plate, serves as the dielectric. The overall change in the surface profile causes a change in the distance between the probe and surface so the capacitor changes. The changes are converted to roughness values. This type does not provide the surface profile and in most cases gives the Ra for a specific material and surface geometry. Figure 2-18 (a) shows the schematic of a capacitance system [24].

Laser triangulation systems are one of the simplest types. The measurement is cheap and fast; however, gives poor vertical and lateral resolution. A focused laser beam is projected onto a surface. The illuminated point on the surface is imaged onto a position sensitive device that is calibrated in terms of *Z* height at the surface. Figure 2-18 (b) shows a graphical representation of a laser triangulation system [24].

In confocal microscopy, a rotating disc is used with a series of optical pinholes arranged in a spiral as shown in Figure 2-18 (c). This creates a series of images that progressively spiral outwards to give an overall picture of an area. As the disc spins, a voice coil motor is used to bring each new image into focus. Since the distance the voice coil has moved is known, the height of the surface at the focus point can be determined, hence building a 3D image of the surface. This method also has the limitation to small area and height of measurements [24].

In scanning interferometer, the conventional white light is used as the light source. A piezo drive system is used to "scan" the objective lens about a focal point. As the imaging system is "traversed" through its range by the piezo drive system, the focal point is noted for each pixel. The major benefit of such a measurement system is that large numbers of points (typically 1024x1024) can be measured with very high lateral resolution (0.3μm) and vertical resolution (typically less than 0.1nm) in just a few seconds. Figure 2-18 (d) shows the structure of this system graphically [24].

Atomic Force Microscopy (AFM) is a contact based system; however, as the applied force is too small it is considered as non-contact method. They work based on force not displacement. These systems provide very high resolution 3D representation of the surface.

They can resolve the individual atoms. The limitation of these systems are the very small area of measurement (100μm×100μm) and very small roughness values (5μm). The MEMS etching technology is used in making the AFM stylus out of silicon. The cantilever is about 50μm long and the stylus tip as small as 1nm diameter. The piezo electric activators built into the silicon are used to move the cantilever arm up and down, and deflection of the arm is measured by noting the deflection of a light beam reflected off the top of it, near the stylus. Horizontal actuators allow a scanning motion of the stylus. Figure 2-18 (e) represents the schematic view of this system [24].

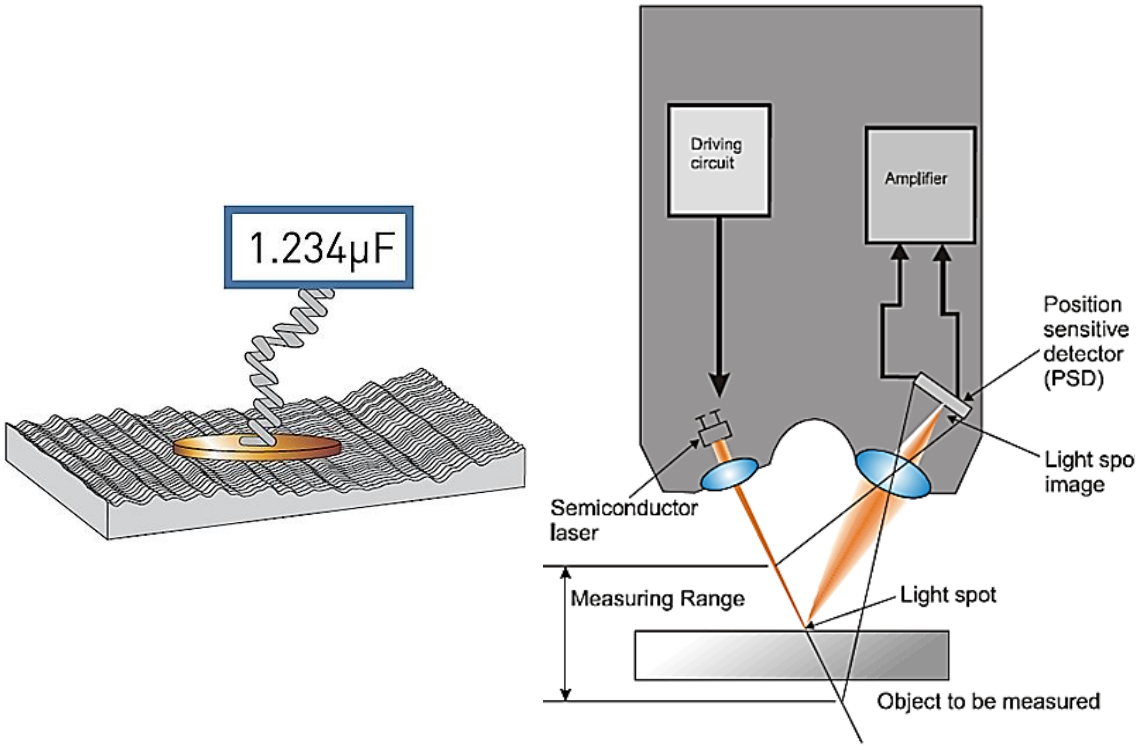

a) Capacitance system b) Laser Triangulation system

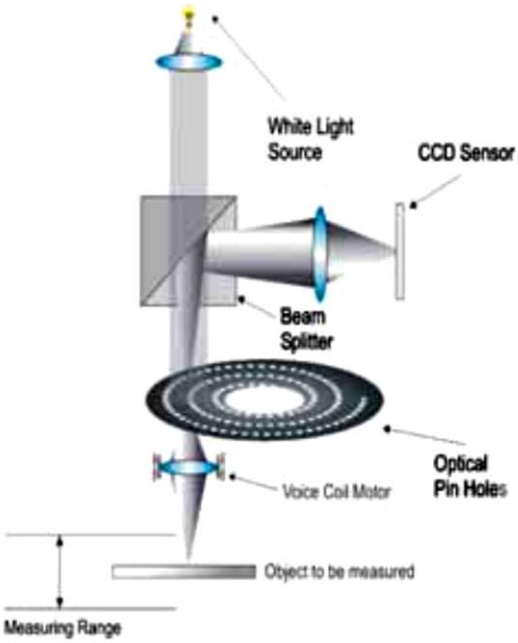

c) Confocal Microscopy

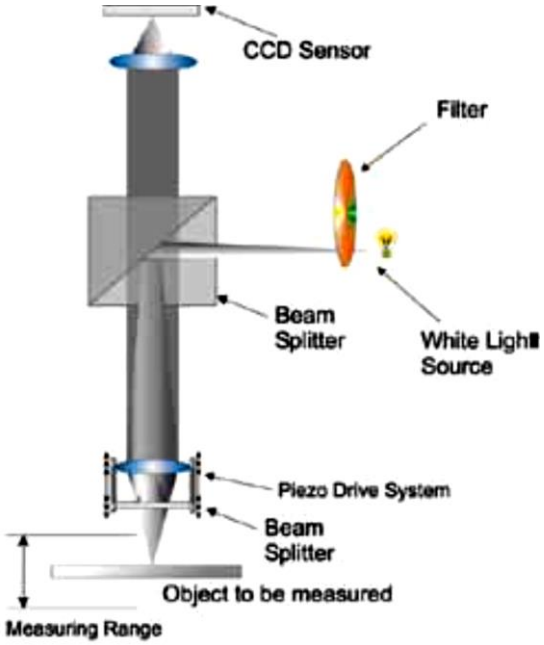

d) Scanning Interferometer

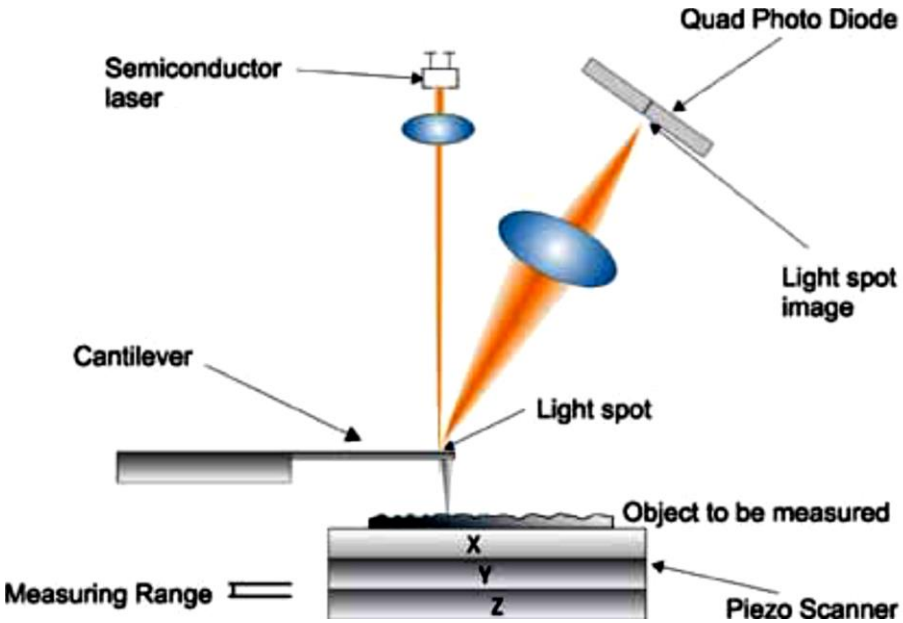

e) Atomic Force Microscopy (AFM)

Figure 2-18 Schematic representation of non-contact surface texture measuring systems [24].

2.3.3. Literature review on surface roughness measurement of AM parts

In many surface roughness measurements conducted on non-metallic additive manufacturing parts, the measurement device is a contact based surface roughness measurement system. As a well stablished method, the position sensitive contact based devices are the most commonly used roughness measurement systems for on non-metallic AM parts [6, 11–20]. Taylor Hobson Form profilometer and Mitutoyo are among the frequently used brands. The top surface of a layer-based manufacturing part will be affected by surface texture of the previously built layers, which contribute to the creation of the surface features at multiple spatial wavelengths (scales). Considering the process specific characterization for layer-based manufacturing methods, the following points must be considered when selecting a measurement technique. First, the scale of the features that the measuring technique needs to characterize. Second, the size and shape properties of the surface texture features to be measured from the part's final performance standpoint.

In the case of surface texture analysis for metallic AM parts, more research efforts are made. The spatial frequency of the irregularities on the manufactured surface, the nature of the material and topography of the surface define the choice of measurement system. The measuring systems are divided into two main categories: contact-based stylus devices need to consider the physical interaction of the probe and the surface to be measured. For instance, whether there is any risk of damage to the probe or the surface. In addition, the stylus radius and cone angle must be chosen carefully based on the surface characterizations to best catch the surface topography details [27].

On the other hand, non-contact devices, such as focus variation and confocal microscopy need to consider the reflective properties of the surface to be measured. The considerable differences between the AM metallic parts' surface and the traditional methods, are the challenging problems for any surface texture measuring system. A great majority of metal AM parts are made by powder-based methods, leading to a very irregular, and is characterised by sharp protrusions and recesses at multiple scales, with open pores transitioning into closed pores underneath the surface. Each AM manufacturing method creating metal parts, has its own surface characteristics, which might be hard to measure. For example, Powder Bed Fusion (PBF) methods cause specific patterns featuring balling, spatter formation, loose or partially melted particles, which are very hard to measure [27].

One of the main difficulties of the optical methods is their limited measuring range in vertical direction, also the small measuring area. The PBF methods sometimes cause large local surface slopes that may exceed the maximum limit of the optical method.

Contact-based topography or profile topography measurement of AM metallic parts has been reported in the literature by many researchers [28–32]. The non-contact based methods such as confocal microscopy [33 and 34], Focus variation microscopy [28 and 35], Chromatic confocal microscopy [36], Conoscopic holography [37], Coherence scanning interferometry [38], Atomic force microscopy (AFM) [39], Elastomeric sensor [40–42]. The literature survey showed that most of the choices were contact–based profile measurement via stylus instrument. In general, the profilometers are low cost and also have lower operator training costs. They also have high comfort level for machinists and inspectors. However, they fail to bring a good understanding of the surface 3D topography.

In this way, the non-contact based methods utilized, are mostly optical devices. The two more frequent optical devices are the variation and confocal microscopy methods. Both methods have difficulties in measuring the surface texture of AM parts because of the highly irregular nature of the surface topographies on AM surfaces. One of the main advantages of optical methods is less acquisition time compared to the contact-based methods. The scanning interferometry, also referred to as the scanning interferometry or white light interferometry, has more difficulties in terms of local slope and vertical scale of roughness in AM surfaces. The other non-contact method, AFM is rarely used since this method is so limited in terms of the vertical measurement range and the risk of damaging the stylus on the metallic AM surfaces.

The methods discussed so far intend to investigate the surface texture quantitatively and each has some sort of difficulty because of the specific surface characteristics of AM parts. The 2D imaging techniques such as Scanning Electron Microscopy (SEM) and optical microscopy are used to investigate the surfaces qualitatively. However, in some cases, if calibrated properly, these instruments have been used for quantitative measurement in the image plane [43–45]. As a special use of optical microscopy, Barari et al. [22] used this method for obtaining the edge profile of the FDM parts and quantified the roughness value. Based on these finding, the 2D imaging methods can be used in quantifying the surface roughness indirectly. However, its not a promising method and there are many obstacles in the way of their application in quantifying a surface texture.

One of the method having the potential capability of solving the current issues in surface topography measurement of AM parts is X-Ray Computed Tomography (XCT)

[46]. Using XCT, surface information can be extracted from the volumetric data with appropriate data processing method. This method obviates the limitations in vertical measurement range due to walls and undercuts. This method does not have the limitations of non-contact methods and also has an advantage over the contact-based methods since it is capable of extracting surface data from the inaccessible internal AM surfaces. The obstacles in the way of adapting XCT into surface topography measurement is in currently poor spatial resolutions of the measurement, and lack of complete understanding of metrological performance and error sources, necessary for a proper calibration of the surface extraction algorithms (mainly based on thresholding/edge detection) [47,48].

Another non-contact approach to quantify an AM surface has been reported in Ref. [49]. 3D laser scanner has been used to extract the point cloud data from the surface and finite difference methods are used to reconstruct the surface form the existing points from the surface. This approach highly depends on the accuracy of the points extracted from the surface and the estimation approach used to reconstruct the surface.

2.4. LITERATURE REVIEW ON POST-PROCESSING OF LAYER-BASED MANUFACTURING PARTS

When additive manufacturing process cannot satisfy the desired level of surface roughness of a product, the post processing via mechanical or chemical finishing methods need to be considered. AM surfaces include textures that are strongly related to the layer thickness, and filling pattern or the trajectories followed by the solidifying mechanisms such as the laser beam or polymer injection head, etc. The poor surface roughness is mainly a result of the layer by layer deposition of material, which creates the staircase effect. The

staircase effect is directly affected by layer thickness and thinner layers result in less staircase effect and so better surface roughness. The other main source of poor surface roughness is the chordal error coming from approximating part's surface by triangles (STL format) in the CAD software. This defect is mainly improved by reducing the maximum edge length of the triangles. The main sources of roughness can be divided into three main categories based on their importance: first, the inherent layer by layer characteristics of these methods. Second, the slicing and chordal errors and third, the fabrication parameters.

Beside all the advantages of AM process, lies its own design requirements that must be treated very seriously. The main factor is the requirement for support structures for some AM processes, in the cases that there is no material underneath to build on. The support requirement is one of the drawbacks of AM and its removal requires extra effort and cost. In addition, support removal leaves some defects on the surface, decreasing surface integrity. Another source of roughness is the remnants of the support removal process. Since not all additive manufacturing methods need support structure, this source is not included as one of the main categories. However, if there is a need for support structure, such as FDM, it becomes one of the main factors hurting the surface roughness.

The first category of the roughness sources of AM parts, staircase effect, can be improved by optimizing the third category (fabrication parameters). FDM has many process parameters such as, layer thickness, part orientation, raster angle, road width, air gap between roads and model temperature making this process more crucial from surface roughness aspect. Surface roughness is related to the mentioned parameters and studies have been conducted to improve them and examine their effect on the surface roughness

of the manufactured surfaces [50]. It is reported that the surface roughness and accuracy are the main drawbacks of AM process and even more challenging than the strength of AM parts [51 and 52]. The first logical procedure is to optimize all the pre-processing and processing factors. Optimizing the layer thickness based on the features complexity, and the triangulation step are the pre-processing steps to be considered. The layer thickness can be optimized based on the product's shape, which means adaptive slicing of the part. In adaptive slicing, the layer thickness is selected according to the features complexity and surface curvature [53–57]. However, according to all possible optimizations and improvements in pre-process and process factors, the surface roughness of AM parts are not still in an acceptable level, especially FDM parts that suffers from all main categories of roughness and support remnants as well. Post-processing is the only option to further enhance the surface roughness. The first approach is to minimize the required post-processing as much as possible. Therefore, after optimizing all the pre-processing and process parameters for objective functions such as mechanical properties, build time and etc., the next step is to do the optimization with an eye on minimizing the required post-processing as the objective function. Studies are conducted aiming at minimizing the required post-processing by optimally selecting the build orientation as main factor affecting the surface roughness of AM parts [58 and 59]. The post processing for metallic parts can be categorized into abrasive blasting, peening and laser polishing groups. The research works to improve the surface roughness of metallic AM parts is presented in the next section. Most of the research works in post-processing of non-metallic products are related to FDM parts as it suffers the most. The post-processing for non-metallic AM products is one of the main categories for improving the surface roughness. Post-processing

for non-metallic parts can be categorized into two groups as: mechanical and chemical processes, discussed in the following paragraphs.

2.4.1. Post-processing for metallic AM parts

The raw surface of the metallic parts made by Direct Metal Laser Sintering (DMLS) method have a surface roughness of approximately 8.75μm. Thus, a post processing stage is required to improve the surface roughness of DMLS parts, some of which are briefly introduced here adopted from Ref. [60].

Abrasive Blast (Grit & Ceramic), in which a stream of abrasive media is forcibly in propelled against the surface under high pressure. Abrasive blasting with grit and ceramic particles creates a stain and matte final finish on the surface. To a large extend, this method yields a uniform finish on the surface; however, it is not 100% uniform over the entire surface [60].

Shot Peening, is a cold working process to induce compressive residual stress on the manufactured surface to improve the mechanical properties such as fatigue life, etc. In this process, the manufactured surface is impacted by round metallic or ceramic or both, with a force enough to create small indentations or dimples. Shop peening is so similar to sandblasting, with the difference that in shot peening, the plasticity is the dominant deformation mechanism; however, in sandblasting, abrasion is the finishing mechanism. Figure 2-19 shows an impeller part made by DMLS method and after different shot peening processes [60].

a) as received DMLS part (R_a=10μm) b) shot Peened with metal particles (R_a=5μm) c) shot Peened with metal and ceramic particles (R_a=4μm)

Figure 2-19 Comparison of the roughness of surfaces as sintered and shot-peened with different particle materials [60].

Rossi et al. [61] studied the improvement of surface roughness and corrosion resistance of Direct Metal Laser Additive (DMLA) parts. The post processing methods used were blasting with corundum, shot peening with ceramic particles, micro grinding with grinder and emery polishing. The results revealed that the most promising methods for finishing the DMLA parts are the shot peening and emery polishing.

Polishing, is a metal finishing operation. The surface is finished by abrasive or mops in multiple stages. In the first stage, the coarse grid particles are used at high speed to remove the defects on the surface. The defects can be pits, nicks, lines and scratches. In the next steps, the fine-grained particles are used to finish the surface. In the final step, cotton mops are used to get a mirror like surface finish [60].

Electrochemical Polishing, also referred to as electro polishing, is a process in which the material is removed from the metal surface through polishing, passivation, and deburring. This process is reverse of electro plating in which by anodizing the surface, a thick layer is deposited on the surface. This process creates a bright finished surface and can be used instead of abrasive fine polishing in micro structural preparation [60].

Optical Polish, (Hand Finishing) is very cost effective and results a very bright finished surface. It's one of the best finishing options for low quantities of parts. This process removes 0.0075-0.025mm from a DMLS surface as there a porosities on the surface that need to be removed to get a bright surface at the end. Because of this material removal, it is better to considered an offset in design dimension for the post processing stage. One of the disadvantages of this method is that it creates inconsistent finish from part to part so it is not a proper choice for large quantities of parts [60].

CNC Finishing/Machining, is an appropriate method for achieving tight tolerances on the finial finished surfaces. Detail oriented precision can be achieved by 3-axis, 5-axis or 6-axis lathe machines. Because of the machining operation on the surface for finishing purposes, like optical polishing, the must be an offset considered for the dimensions in design stage. Figure 2-20 shows the difference between the raw material made by DMLS process and CNC finished ones [60].

Figure 2-20 the difference between the raw surface and CNC finished part [60].

Abrasive Flow Machining (AFM), (Extrude Hone Polishing), is used for getting accurate radius in internal surfaces. In this way, an abrasive media is extruded through the

internal surface of the part and the surface finish is improved. The process is particularly useful for difficult to reach internal passages, bends, cavities, and edges. A more uniform surface finish is resulted from this process but it's an expensive choice for DMLS parts with no tolerance requirements [60].

Electroplating, in a method in which electrical current is used to reduce the ions of a desired material from a solution and coat a conductive object on the surface. Electroplating can be used to build up thickness on undersized parts, so it can be used to improve the surface roughness of the parts. This process is an inexpensive method of improving the surface roughness [60 and 62].

Micro Machining Process (MMP) is a mechanical-physical-chemical surface treatment applied to items placed inside a treatment tank, providing highly accurate selective surface finishes. The advantage if this process is its capability in improving the surface roughness locally and wherever desired. MMP begins with a detailed analysis of the surface state of the item to be treated, establishing the processing parameters required to meet the customer's objectives. This process is ideal for parts requiring precision tolerance finishing and for large quantities of parts, as well as parts with internal passages that cannot be reached by an alternate method [60].

Atmospheric Plasma Spraying (APS) is a coating process that deposits a ceramic layer on the AM metal part. According to the results of Ref. [63], a relatively low surface roughness can be achieved by APS ceramic coating on the SLM parts.

Abrasive Fluidized Bed (AFB) [64], the finishing is done by rotating the part inside a fluidized bed of abrasives at high speeds. The final roughness can be as low as 1.5μm. The finishing mechanisms are essentially the micro-ploughing/micro-cutting of the semi-molten metal due to high speed impacts with the fluidized abrasives and, secondly, the local micro-fatigue/micro-cracking created by the penetration of the harder abrasive edges into the softer metal workpiece. The geometric shape of the abrasive particles have a very significant effect in establishing the final morphology of the workpiece. The spherical abrasive particles are more prone to act by micro-ploughing finishing mechanism alone, while angular abrasive combines both micro-ploughing and micro-cutting with some material removal. The rotating speeds of the workpiece are important on the effectiveness of AFB finishing. Higher speeds lead to better surface fishing because of the almost complete removal of the larger semi-molten powder agglomerates of the starting morphology of the parts. In general, AFB could be used as an easy-to-automate, low cost, low time consuming and industrially sustainable finishing technology for metal parts made by metal additive manufacturing.

Laser Polishing, is based on laser irradiation. In this method, a smoother surface is achieved by melting a microscopic layer on the surface by a laser beam. The melted layer then re-solidifies under shielding gas protective conditions, resulting in a smoother surface as shown in Figure 2-21 from a Selective Laser Additive (SLA) process. The laser energy acting on the surface must be controlled carefully; it should be strong enough to melt a layer deep enough to include the roughness peaks, but it must not melt the surface deeper than the valleys. The three primary factors of the process are: the surface material, its initial

topography and the energy density of the laser beam. The high energy density of the laser beam (energy per surface unit) with respect to other plasma-arc heat sources makes it possible to melt a microscopic layer locally without affecting the surrounding areas. This is a key factor in laser-polishing process [65–70].

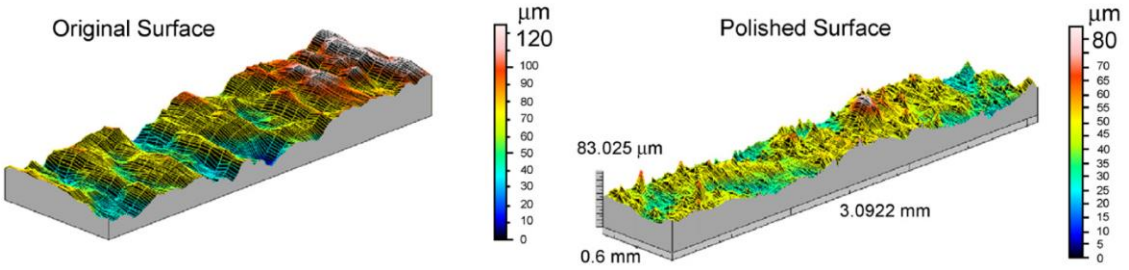

Figure 2-21 Left: the as received SLA surface, right: the laser polished surface [67].

Laser polishing is applied on Additive Laser Manufacturing (ALM) parts [71]. In ALM process, the powder is projected into the melting zone under the laser beam, and enables the direct manufacturing of complex metallic parts, larger than the parts manufacturable SLA. The result showed very smooth surfaces on thin ALM parts because of laser polishing.

2.4.2. Post processing for non-metallic AM products

Kulkarni and Dutta [72] proposed CNC machining using ball end mill, with a focus on tool path generation algorithm. The main disadvantages of this approach are inaccessibility of some sections, the need for clamping the workpiece, delicate features on AM parts, and details of the ball end mill. Another research utilizing CNC machining for finishing FDM parts, done recently, focuses on a variable cutting depth to prevent inner defects from being created and removing the initial surface morphology [73]. In their research, the authors have tried to link the FDM process parameters to CNC machining parameters and couple

them in a more efficient way. The cutting depth is derived as a function of deposition angle (surface slope with the horizontal axis). Pandey et al. [13] attempted to improve the surface roughness of FDM parts by Hot Cutter Machining (HCM) of the surface and reported 0.3μm surface finish with 87% confidence level. This approach suffers from inaccessibility of all sections of the AM parts, also the need for clamping the part. This is limited by tool size and available movements on the machine to access different parts of the sample to machine. However, the author stated that development of a hybrid machine that does the cutting, while layer by layer depositing the material, would solve this problem. Another mechanical approach used to enhance the surface roughness of AM parts is Abrasive Flow Machining (AFM). This method is used on Stereo Lithography (SL) parts [74], which also suffer from poor surface roughness because of layer-based nature of this process. It is reported that the media pressure, grit size and the type of abrasive particles and built orientation are the most significant factors. The minimum surface roughness obtained with this process is 1.27μm. However, the inaccessibility of some sections that the flow of material is not feasible, such as: slots, blind holes and intricate features, etc. are the main drawbacks of this method. In addition, there is no way to control the pressure based on the surface profile and as a result, some parts may be machined unwantedly reducing the accuracy of the model. Leong et al. [75] have used Abrasive Jet Deburring (AJD) method to improve the surface roughness of SLA parts. The process parameters including flow pressure and time are considered and dimensional errors and roughness reduction are studied. The main downfalls of mechanical processes for finishing AM parts are inaccessibility of some parts, higher process costs and their need for clamping the part. The clamping can hurt the mechanical and geometrical properties, and it is time consuming. It

mainly depends on the part's shape to be finished, thus they are limited in this aspect as well. Therefore, methods not requiring clamping are more favourable. A non-clamping mechanical process used to improve the surface roughness of FDM parts is Barrel Finishing (BF) [18 and 76]. The results of these research works showed FDM and BF methods being successfully coupled with each other. The BF method is mainly affected by the build orientation. An important parameter found to be essential was BF working time, by increasing which, the surface roughness was improved at each specific surface slope. However, BF technology might not be applicable for products with extremely delicate and fragile parts and there might be some regions that the process cannot finish them, such as small holes and corners. Considering all the cons and pros of the mechanical finishing processes, yet they cannot fulfill the requirements of a functional and efficient finishing process. An efficient method should be able to improve the surface roughness while keeping the mechanical and geometrical properties constant, improving the surface roughness all over the surface without limitation, and without requiring clamping and extra costly operations.

The chemical post processing uses acetone and can be applied to Acrylonitrile Butadiene Styrene (ABS) parts. The Dimethyl Ketone (acetone) smoothing process is used to improve the surface finish of the ABS parts fabricated by the typical additive manufacturing processes. Acetone is a colorless, mobile, flammable liquid, and is the simplest ketone with the Boil temperature 56 °C. ABS is a common thermoplastic. Its glass transition temperature is approximately 105 °C (221 °F). ABS is amorphous and therefore has no true melting point. It is a polymer with a low reticulation degree, including nitrile

functionality. ABS have weak interaction with polar solvents such as acetone, ester and chloride solvents. Acetone is chosen for the smoothing process due to its low cost, very low toxicity and to its very high diffusion. The interaction of acetone and ABS doesn't result a chemical change in the ABS. ABS is sufficiently polar for acetone vapour to make an "ABS + acetone" slurry. However, acetone can cause a profound geometrical change in ABS. The process involves boiling acetone in a chamber and suspending a part in the resulting vapour. By repeatedly soaking the part in the vapour for some set period, interaction of acetone and ABS results in a slurry of ABS and acetone on the surfaces of the work piece. As acetone evaporates, the ABS polymer strands will be left behind, with only their macroscopic shape being altered by the surface tension of the acetone/ABS solution [77]. This process results in smoother surfaces for the FDM part made of ABS. However, the amount of smoothing and its effect on the surface roughness and part's dimensional accuracy needs some focused investigation.

Contrary to the mechanical approaches, chemical finishing improves the surface roughness significantly without the limitations pointed out for mechanical approaches. However, it has material restrictions that makes it not applicable for all parts and it can be used for parts made of ABS. Galantucci et al. [78 and 79] showed that chemical post-treatment of the ABS parts improves the surface roughness significantly at a negligible expense of prototypes dimension change. They used acetone vapour bath and immersed the samples for 300 seconds. A minor reduction was found in tensile strength but a greater ductility was also observed after post-processing. Bending tests showed better flexural strength. The build orientation, which is the main factor affecting the mechanical properties

shows less influence after the finishing process. In Ref. [80], the authors reduced the vapour smoothing process time and concluded that the smoothing time is a function of surface area and the relation is linear. Garg et al. [81] studied the effect of part orientation on the surface roughness and dimensional accuracy treated by acetone vapour. The results showed that the staircase effect is dramatically reduced. In addition, there was a minimal change in dimensional accuracy; however, the dimensional deviation was reduced.

The literature survey proves that the chemical methods outweigh the mechanical ones in many aspects. This thesis attempts to study the post processing procedures for FDM parts; therefore, the aim of this research is to investigate the parameters affecting this process and provide a thorough approach for designing a part as it relates to the final surface roughness requirements and steps to take for achieving that. From product design perspective, there is a necessity for a model to develop, so the designer can predict the surface roughness after post-processing. For instance, it is reported that build orientation has a major effect on the result of post-processing. Thus, in design stage, if there is a need for a specific surface roughness value, a model for predicting the post finishing roughness can help the designer to design based on that, and change the design if need at the very beginning of the design process. The necessity of such model has served as motivation to thoroughly investigate the process parameters and consider the number of cycles for immersion in the bath and duration of each cycle at different surface angles (build orientation) as the main process parameters to develop a useful model for predicting the final surface roughness of FDM parts.

3. METHODOLOGY

3.1. INTRODUCTION

The methodology section is divided into three parts. First, the analytical surface roughness modeling procedure is discussed in order to develop the arithmetical surface roughness formula. Second, the inspection procedure taken to measure the surface roughness of FDM parts is explained. Third, the design of specimens and the post processing stage setups are introduced.

3.2. DEVELOPING THE ARITHMETICAL SURFACE ROUGHNESS FORMULA

Although the recent research works reported good results in estimation and modeling of the details in cusps geometry but an accurate relationship between the overall shape of cusps and the arithmetical surface roughness is not derived yet. We believe that the current deficiency in predicting the surface roughness of additive manufactured parts is due to a wrong assumption of the mean centerline (or the best substituted fitted surface) in calculation of the arithmetic average roughness. Although understanding the details of the profile cusp geometry is very important but this study shows the employed criteria in stablishing a proper mean centerline having a more significant effect on the calculated arithmetical surface roughness. The models developed for estimation of the surface profile with different curves are essentially dealing with the ridge shape. The two main factors of

an AM part surface is staircase effect and ridge pattern. The staircase effect and ridge shape are in macro and micro scales, respectively. Therefore, the staircase effect is the most important one and we have developed out methodology based on staircase effect.

As the first step in deriving the arithmetical surface roughness formula, the common trigonometry with the assumption of square cornered profile is utilized. Figure 3-1 schematically shows the simplified profile view of the surface manufactured by layer based additive manufacturing processes such as FDM. The average surface roughness is defined as the arithmetic average deviation of each point on the profile from the centerline [46]. The traditional assumption used in the previous works in stablishing the centerline was that the centerline passes through the midpoint of each cusp edge. The arithmetical roughness of a surface can be calculated by Equation (3-1) where *f(x)* is surface profile and *l* denotes assessment length.

$$R_a = \frac{1}{l}\int_0^l |f(x)|dx \tag{3-1}$$

Using the basic trigonometry, the cusp geometry is described by three parameters *b*, *t*, and *l*, where *t* is the layer thickness and *b* is called the layer depression (horizontal distance on each layer).

$$b = t \times \cot(\alpha) \tag{3-2}$$

$$l = \frac{t}{2 \times \sin(\alpha)} \tag{3-3}$$

Based on Equation (3-1), and the assumption that the surface is created by the same cusp geometry repeating over the entire surface, the roughness value can be obtained by only considering one cusp unit representing the profile, as the shaded area in Figure 3-1.

The integration of f(x) over the assessment length (l), which due to uniformity of the profile is also considered as the measurement cut-off, is the shaded area in Figure 3-1. Therefore, the arithmetic roughness value, R_a is calculated as follows:

$$A_{shaded} = \frac{1}{2} \times \frac{t}{2} \times \frac{b}{2} = \frac{t^2}{8}\cot(\alpha) \tag{3-4}$$

$$R_a = \frac{A_{shaded}}{l} = \frac{\frac{t^2}{8}\cot(\alpha)}{\frac{t}{2 \times \sin(\alpha)}} = \frac{t}{4}\cot(\alpha) \times \sin(\alpha) = \frac{t}{4}\cos(\alpha) \tag{3-5}$$

According to the above calculation, when φ is zero, the formula proposed in Ahn *et al*. [9] must result into what is presented in Equation (3-5). This discrepancy happens because of another assumption made as it considers the entire step with no centerline and calculates the roughness as half of cusp height that is also not correct. The above formulation is in accordance with the formulas proposed in Reeves *et al*. [4] and Campbell R.I, *et al*. [5].

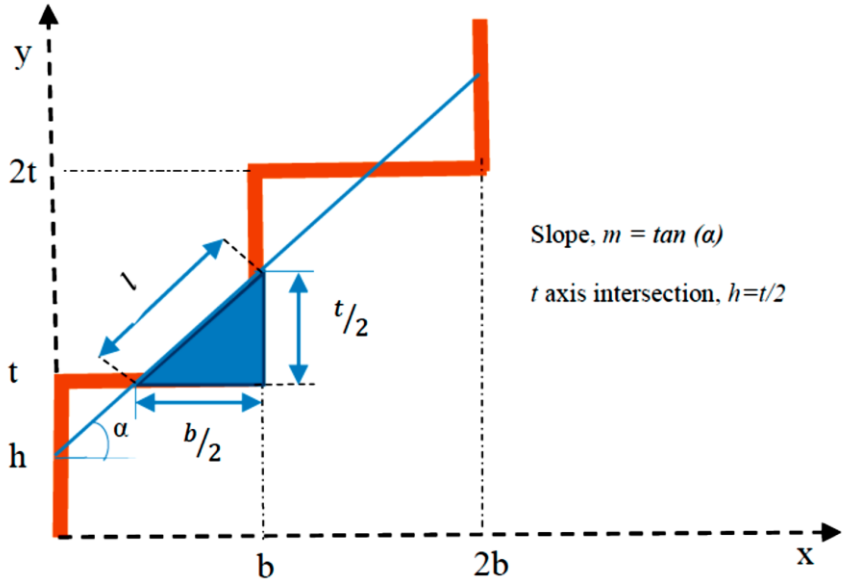

Figure 3-1 The simplified approach using wrong centerline in calculation of arithmetical roughness for layered based manufactured surfaces.

3.2.1. Total Least Square (TLS) Method

The methodology presented in this thesis is developed using a more general definition for centerline. The centerline is defined as a line that the total distance of all point on the cusp profile from it is minimum, called TLS method. In the standard, the centerline is considered as known to the metrologist. The method to find the centerline is not discussed in the standards of surface roughness. In order to find the surface roughness of a measured surface, especially while dealing with point clouds, the normal practice to define the substitute plane is to fit a total least square plane, which minimizes the summation of square distances of all point from the fitted plane. Therefore, proper establishment of centerline requires fitting the best substitute plane on the cut-off length of the surface being neglected in deriving the Equation (3-5) for layered based manufactured surfaces. Considering this issue, a new formulation is derived here without assuming that the centerline passes through the midpoint of each edge. Based on Equation (3-1), instead of calculating the shaded area in Figure 3-1, the integral is taken for each cusp edge to find the actual arithmetic roughness. Figure 3-2 shows the new configuration proposed in this work. The distance of a point in x-y plane (x_i , y_i) from a specified line defined by Equation (3-6) can be represented as follows:

$$ax + by + c = 0 \tag{3-6}$$

$$E = \frac{ax_i + by_i + c}{\sqrt{a^2 + b^2}} \tag{3-7}$$

where a, b and c are the line parameters in x-y plane and E stands for distance from the line.

The integral should be taken over each vertical and horizontal line and the sum of them will give us the total distance of every point on the vertical and horizontal lines from the centerline, specified by equation (3-8).

$$y = mx + h \tag{3-8}$$

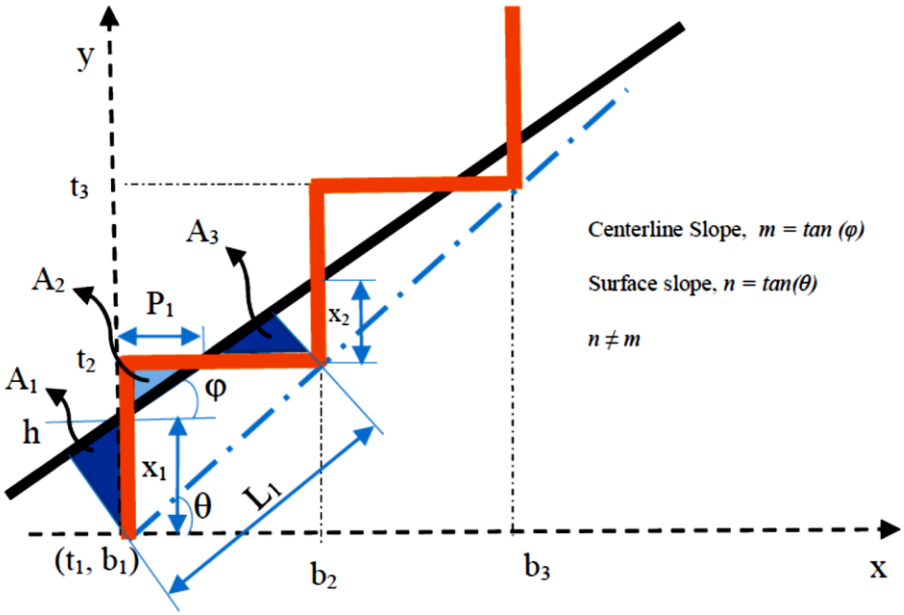

Figure 3-2 The mean centerline established based on total least square fitting

For the first vertical and horizontal line, the integration will result E_{v1} and E_{h1}, respectively, as follows:

$$E_{v1}^2 = \int_{t0}^{t1} \frac{(mb_0 - y + h)^2}{m^2 + 1} dy = \frac{-1}{3(m^2+1)} \{(mb_0 - t_1 + h)^3 - (mb_0 - t_0 + h)^3\} \tag{3-9}$$

$$E_{h1}^2 = \int_{b0}^{b1} \frac{(mx - t_1 + h)^2}{m^2 + 1} dx$$
$$= \frac{1}{3m(m^2+1)} \{(mb_1 - t_1 + h)^3 - (mb_0 - t_0 + h)^3\} \quad (3\text{-}10)$$

where E_{v1}^2 and E_{h1}^2 are the sum of squares of the distances of all the points from the centerline for the vertical and horizontal lines, respectively. *m* denotes the slope of the line with horizontal axis *x*, *h* is the intersection of the line with the vertical axis *y*, and (b_0, t_0) and (b_1, t_1) are the *x* and *y* coordinates of the start and end point of the edge profile, respectively.

The upper and lower bounds of the integrals change for the other layers. The total value is the sum of the results of the vertical and horizontal integrals and for two layers it can be written as follows:

$$E^2 = \frac{-1}{3(m^2+1)} \{(mb_0 - t_1 + h)^3 - (mb_0 - t_0 + h)^3\} +$$
$$\frac{1}{3m(m^2+1)} \{(mb_1 - t_1 + h)^3 - (mb_0 - t_1 + h)^3\} -$$
$$\frac{1}{3(m^2+1)} \{(mb_1 - t_2 + h)^3 - (mb_1 - t_1 + h)^3\} +$$
$$\frac{1}{3m(m^2+1)} \{(mb_2 - t_2 + h)^3 - (mb_1 - t_2 + h)^3\} \quad (3\text{-}11)$$

The general formula for *n* number of layers will be as follows:

$$E^2 = \frac{1}{3(m^2+1)}\sum_{i=1}^{n}\{(mb_{i-1} - t_i + h)^3 - (mb_{i-1} - t_{i-1} + h)^3\} + \frac{1}{3m(m^2+1)}\sum_{i=1}^{n}\{(mb_i - t_i + h)^3 - (mb_{i-1} - t_i + h)^3\} \quad (3\text{-}12)$$

The aim of these calculations is to find an analytical model representing the centerline for a given set of cusps. The final centerline can be represented using the two parameters, *m* and *h* in Equation (3-8). According to the definition of centerline in the standard, it is necessary to find the parameters *m* and *h* such that they minimize the total calculated *E* in Equation (3-12). This can be achieved by setting the derivatives of *E* equal to zero with respect to *m* and *h*. Solving the two resulting equations simultaneously will result in the optimum centerline with *m* and *h* values minimizing *E*. The derivatives of Equation (3-12) with respect to *m* and *h* are as follows:

$$\frac{\partial E^2}{\partial h} = \frac{-1}{(m^2+1)}\sum_{i=1}^{n}\{(mb_{i-1} - t_i + h)^2 - (mb_{i-1} - t_{i-1} + h)^2\} + \frac{1}{m(m^2+1)}\sum_{i=1}^{n}\{(mb_i - t_i + h)^2 - (mb_{i-1} - t_i + h)^2\} = 0 \quad (3\text{-}13)$$

$$\frac{\partial E^2}{\partial m} = \frac{-1}{3(m^2+1)}\left\{\sum_{i=1}^{n} b_i\{(mb_{i-1} - t_i + h)^2 - b_{i-1}(mb_{i-1} - t_{i-1} + h)^2\}\right.$$
$$\left. - \frac{6m}{3(m^2+1)}\{(mb_{i-1} - t_i + h)^3 - (mb_{i-1} - t_{i-1} + h)^3\}\right\}$$
$$+ \frac{1}{3m(m^2+1)}\left\{\sum_{i=1}^{n} 3b_i\{(mb_{i-1} - t_i + h)^2\right.$$
$$- 3b_{i-1}(mb_{i-1} - t_{i-1} + h)^2\}$$
$$\left. - \frac{3m^2+1}{3m^2(m^2+1)^2}\{(mb_i - t_i + h)^3 - (mb_{i-1} - t_i + h)^3\}\right\} = 0 \quad (3\text{-}14)$$

It is difficult to solve the Equations (3-13) and (3-14) using an analytical approach. Thus, they are solved numerically in this work. In order to solve these equations, the layer thickness and depression of all layers are considered equal and increased at the amount of thickness and depression increments, respectively. The assumption made here is that all layers belonging to a triangular patch of the Stereolithography file (STL) have the same thickness (*t*) and depression (*b*), which makes the final calculations a lot simpler.

In order to find the roughness values, *N* number of layers are considered. For each layer, the areas between the obtained centerline and edge profile are calculated, and the sum of all these areas is divided by *L* (length of each layer). According to Figure 3-2, the following calculations are done to find the roughness value:

$$x_i = mb_i + h - t_i \quad (3\text{-}15)$$

$$A_I = \frac{(x_i)^2 \sin(2\varphi)}{4} \tag{3-16}$$

$$P_i = \frac{t_{i+1} - h}{m} - b_i \tag{3-17}$$

$$A_{II} = \frac{(t_{i+1} - t_i - x_i) \times P_i}{2} \tag{3-18}$$

$$A_{III} = \frac{\big((b_{i+1} - b_i) - P_i\big)\sin(2\varphi)}{4} \tag{3-19}$$

$$A_1 = A_I + A_{II} + A_{III} \tag{3-20}$$

$$L_i = x_i \sin(\varphi) + \frac{P_i}{\cos(\varphi)} + (b_{i+1} - b_i - P_i)\cos(\varphi) \tag{3-21}$$

$$R_a = \sum_{i=1}^{N} \frac{A_i}{L_i} \tag{3-22}$$

So far, the analysis results have revealed that the centerline angle (φ) is different from the surface angle (θ). This finding brings in another significant issue, which is the relationship between the layer thickness (t) and depression (b). Considering Figure 3-2, they are related by $tan(\theta) = \frac{t}{b}$.

3.3. INSPECTION PROCEDURES

Inspection of layer-based manufacturing parts for surface roughness purposes required an adequate measuring span to cover the patterns on the surface. At least three ridges need to be present on the measuring span and around 5 mm in length. In this research, an area of 4mm×4mm is measured to have enough details from the surface. Most of the non-contact methods presented in literature review do not have the required measuring area for layer-based manufacturing surfaces, also the vertical range of them is not enough for texture

assessment of layer-based manufacturing parts. There is not a specific procedure or a standard to measure the layer-based surfaces and more research needs to be done.

In this thesis, a new methodology using Total Least Square (TLS) method is developed to calculate the surface roughness. The point cloud data extracted from each surface is examined. The point cloud is the 3D coordinates of the points from the surface, which is scanned by a laser scanner, Faro Arm (Figure 3-3). In order to obtain the surface roughness value of each surface, a plane from which the total sum of arithmetic distance of all points is minimum, is fitted to the data points. This plane is called the Total Least Square (TLS) plane. In this regard, a computer program is developed that by getting the point cloud data of the surface, calculates the TLS plane and the deviations from this plane is used in finding the surface roughness.

This procedure is an effective method for Layer Manufacturing (LM) parts. However, the ridge pattern must be large enough so the laser scanner resolution can catch the details for roughness purposes. In the case of FDM parts, the build orientation and layer thickness were the defining factors for using point cloud data. The laser scanners range of measurement was enough for examining the surface texture of the FDM parts with 0.010 and 0.013 inch layer thickness before doing the post-processing stage. However, after conducting the finishing process for 0.010 inch layer thickness of FDM parts, the experimental results revealed that this method can be used for surface angles below 30 degrees. For larger layer thickness values, bigger angles would be possible. The 3D discrete point cloud data captured from one patch of specimens is shown in Figure 3-4 (a) from two different views and part (b) shows the corresponding best plane fitted to the entire data set.

Figure 3-3 Inspection of an FDM part with Faro Laser Arm.

In the next step, the distance from the TLS plane is calculated and the surface roughness is found using Equation 3-23.

$$S_a = \frac{\sum_{i=1}^{n} |dis|}{n} \tag{3-23}$$

where *n* is the number of points extracted from the surface and *dis* is the arithmetic distance of each point from the TLS plane. The approach starts with importing the coordinates of points into a computer program developed here to calculate the surface roughness values.

The surface reconstruction is done by PolyWorks software coming with Faro Laser Arm.

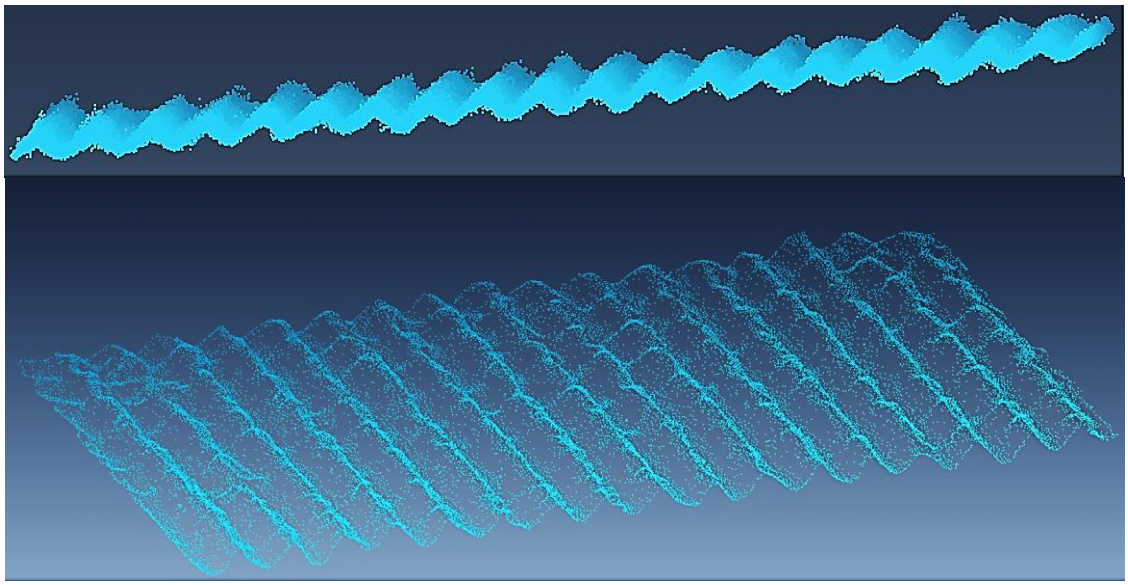

a) The discrete points obtained from a FDM surface (60 deg.) depicted from two views.

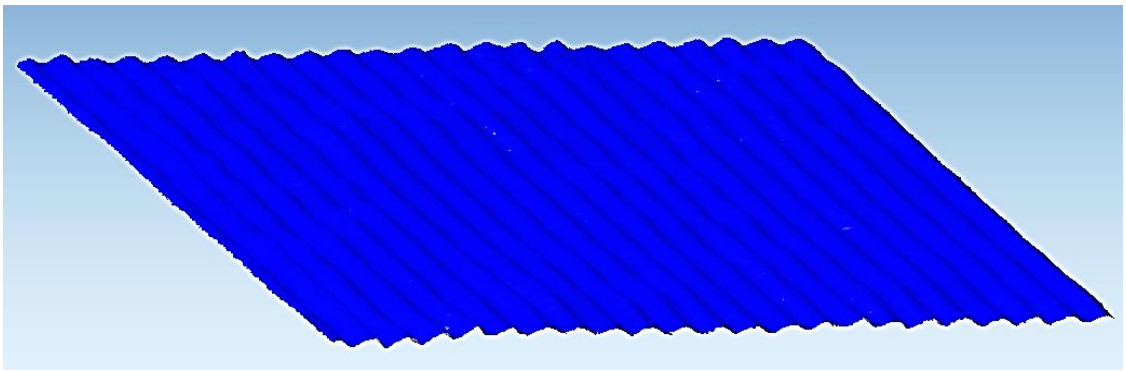

b) The surface fitted to the points (60 deg.).

Figure 3-4 The results of the surface 3D digitizer device and the surface fitted to the points from a sample with 60 deg. build orientation.

As mentioned, the point cloud data are efficient in surface roughness calculation of angles below 30° in our cases of experiments. Therefore, it depends on layer thickness and build orientation. One of the most frequently used devices for surface texture assessments is the mechanical position sensitive device from contact-based category. For the surfaces, which their details are hard to be caught by laser scanner or are out of its range of accuracy, a contact based mechanical roughness device, position sensitive, is used. The angles below 30 were out the range of the mechanical device and the Faro Laser Arm could be used for

angles up to 60° with 0.010 inch layer thickness. This overlap was used to verify the compliance of the two devices. At 30°, the mechanical profilometer gave 34.22 μm surface roughness and the Laser Arm data yielded 35.68 μm. This results show that the two devices are giving close results so the measuring device was switched to mechanical profilometer after 30° with 0.010 inch layer thickness. In the case of 0.013 inch layer thickness, after 60° surface slope, the mechanical profilometer was used and the results at 60° and 65° were 0.7 and 0.4% different. Based these observations, it was decided to merge the results and use the devises according to their measuring ranges. The Laser arm measurement used in these cases was too time consuming and it took approximately 30 min to measure a surface with 60° surface slope and 0.010 inch layer thickness. On the contrary, the mechanical roughness device does the task in less than 10 minutes. It would be possible to measure all angles by the mechanical roughness; however, the one available for us does not cover the large details on the surfaces below 30 degrees. Figure 3-5 shows the mechanical roughness device while functioning on an 85 deg. surface with 0.010 inch layer thickness. The mechanical roughness device used in this research is Mitutoyo SJ 210, 178-951A model, with stylus radius of 5μm.

All samples were examined by a 3D optical surface topography microscope as well. This microscope has a camera capturing pictures from the surface at different heights and creates a stack of figures. A software then processes the pictures and reconstructs a 3D topography of the surface. The software used is called MicroPhase from GetPhase Inc. Figure 3-6 Shows the microscope while measuring a 60 degrees surface by it. The surface topography and surface profile of this sample is shown in Figure 3-7. The main concern in

measuring the surface roughness using the optical methods is the transparency of the surfaces and also calibration of these devices. The device works based on the light intensity at different height that the picture is taken; however, if the surface is translucent by any degree, the results will not be promising for surface roughness values. They are designed mostly for measuring metal surfaces, and for using them on polymer surfaces, other calibration procedures must be taken. In addition, the optical microscopes work based on the light reflected from the surface. The AM parts, FDM parts in particular, have surface patterns that is out of the vertical range of optical devices. It also has a short range and best works at higher build orientations above 75° for 0.010 inch layer thickness. Increasing the layer thickness makes the measurements more difficult.

Figure 3-5 The mechanical roughness device functioning on a sample at 85°.

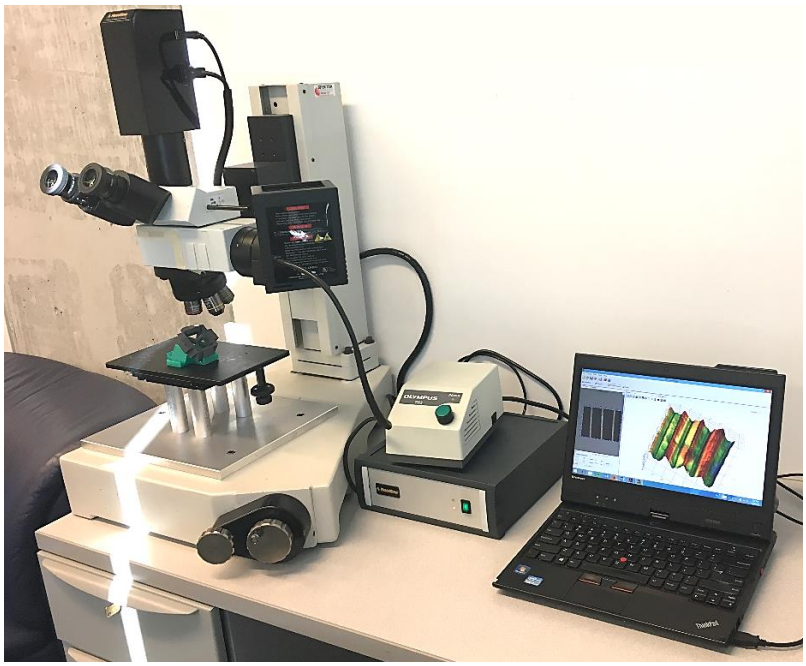

Figure 3-6 The 3D optical surface topography microscope measuring a 60° with 0.010 inch layer thickness surface.

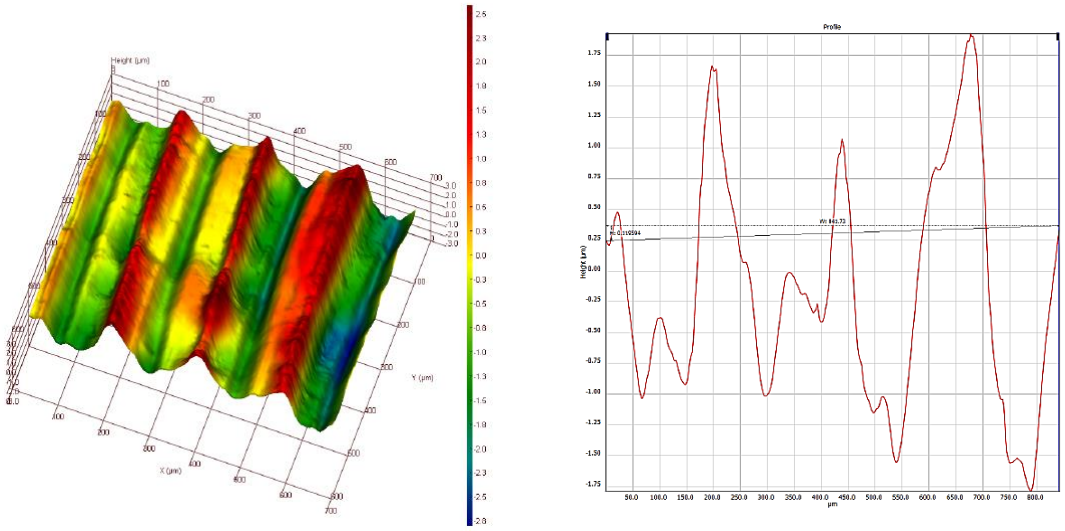

a) Surface topography b) 2D surface profile

Figure 3-7 Surface topography and 2D surface profile of an FDM surface with 0.010 inch layer thickness and 50° build orientation.

In this research, the 3D optical microscope was only used for investigating the surface topography shapes qualitatively not for roughness measurements. The important use of 3D

microscope results was in studying the effect of post processing stage on the surface roughness. The grooves and ridges on the surface were investigated to see the differences before and after finishing step.

One of the main concerns in all measuring operations is holding the specimen in an appropriate position. Most of the measuring devices require the sample to be hold horizontally, perpendicular to measuring direction. In this research, some jigs with inclined surfaces with the same angles as the samples are designed and printed with an FDM machine as shown in Figure 3-8 (a). The jig have four sides, each with an angle from 5 to 90 degrees at 5 degree increments. Figure 3-8 (b) shows a sample on a jig at 50 degrees.

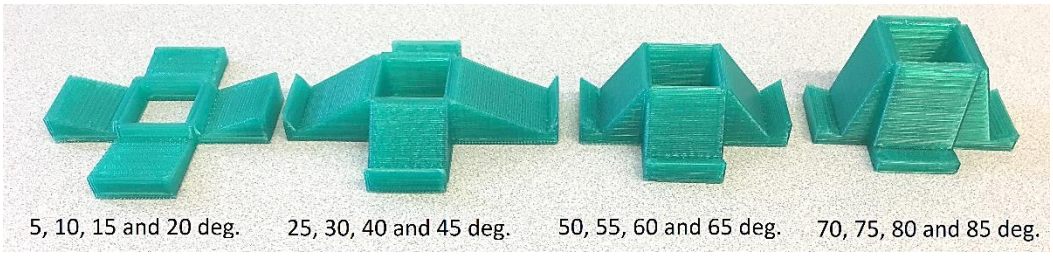

a) The designed jige to keep the samples horintally

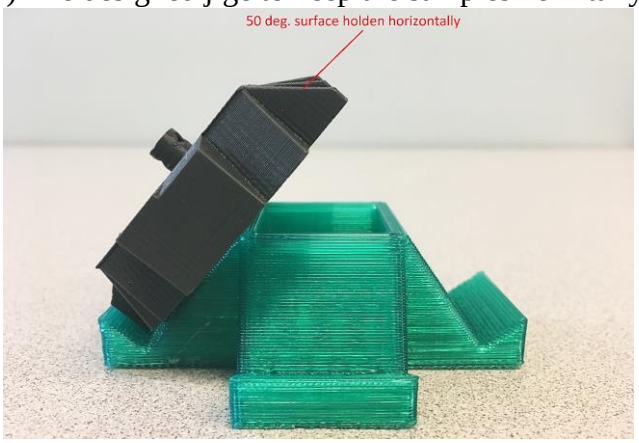

b) A sample with 50 deg. build orientation on a jig

Figure 3-8 The jigs and their application in keeping a surface in horizontal position.

3.4. DESIGN OF EXPERIMENTS

In order to validate the developed analytical model and the post processing stage, an experimental setup for fabrication of specimens, Inspection, and roughness analysis is stablished. FDM process is used as a platform to implement the conceptual methodology. However, the concept can be implemented for any other layer-based AM process. The final specimen was designed to maximize the number of angles that can be measured, while minimizing the overall size and complexity in order to make it cheap and easy to print. To this end, a cubical shape was used as the basis for the part. By placing four angles on each side, sixteen different angles are available for analysis. These angles range from 5-85 degrees in increments of 5°, skipping 35°. On the interior, five smaller surfaces are included on each side, these increase in increments of 1 degree from 30 to 49, so 35° is also present on the surface. Figure 3-9 (a) shows the designed specimen. The specimens are manufactured with two different layer thicknesses as 0.010 and 0.013 inch as shown in Figure 3-9 (b).

The smoothing parameters are divided into two parts as the number of cycles and cycle duration. Three levels are considered for each one resulting in $3^2=9$ smoothing setups, considering full factorial method in design of experiments (Table 3-1). The full factorial method is chosen since there is not enough data about the behaviour of the surface roughness at each surface slope. The full factorial method gives a more comprehensive output from the experiments using the input parameters. In general, $9\times36=324$ experiments need to be conducted. Acetone vapour bath is used as the smoothing method and the parts are hung in the bath according to the smoothing setup and the results are studied.

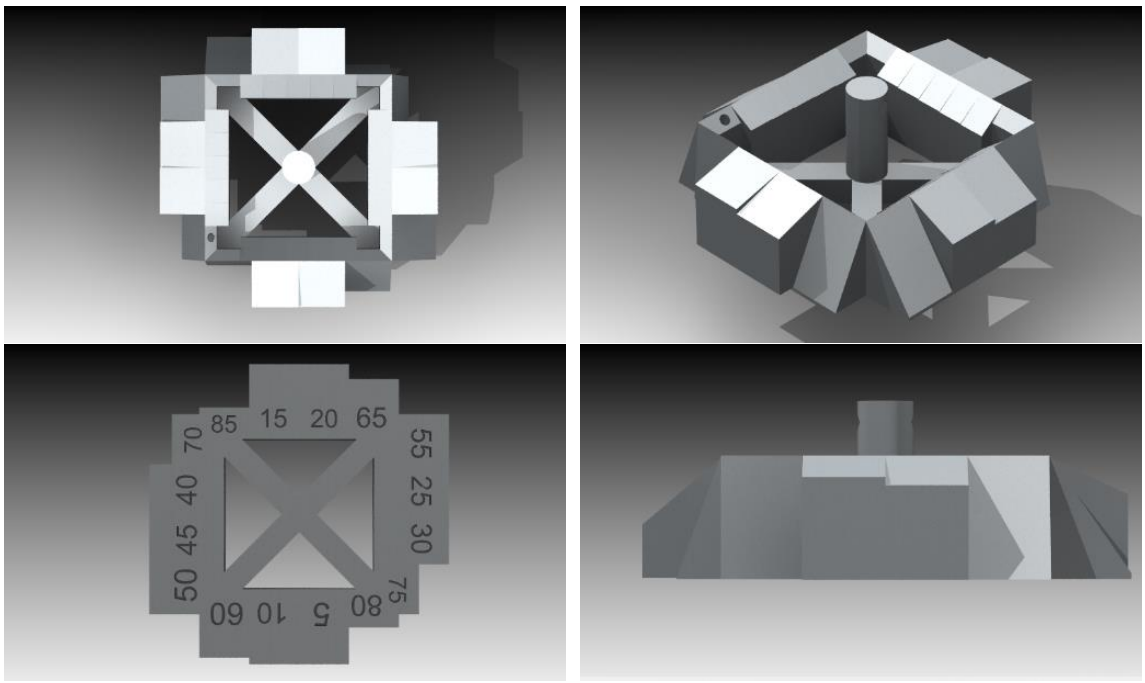

a) The designed specimen for surface roughness evaluation.

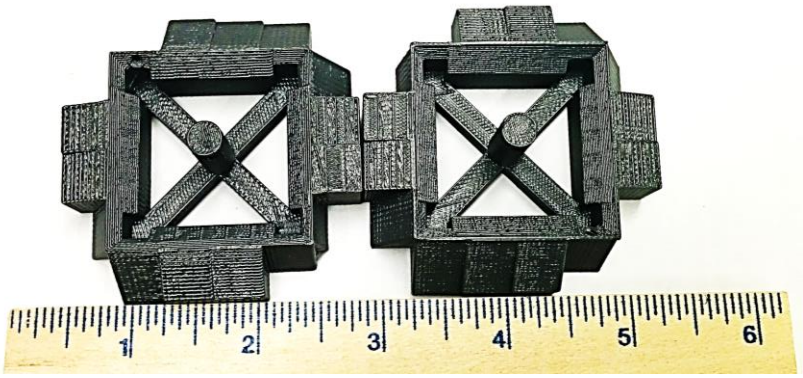

b) The typical final manufactured specimens (inch).

Figure 3-9 The designed (a) and the manufactured specimens (b).

The total time during which the part is exposed to acetone vapour can be calculated for each set of smoothing parameters, referred to as Total Exposure Time (TET). This parameter is used as the main smoothing parameter. Another parameter called Roughness Reduction Percentage (RRP) is defined (Equation 3-24) to see the amount of reduction in surface roughness for each smoothing setup.

$$RRP = \frac{S_a^i - S_a^f}{S_a^i} \times 100 \tag{3-24}$$

where S_a^i and S_a^f are the initial and final roughness, respectively.

Table 3-1 Smoothing factors.

Factor 1, Number of cycles	Factor 2, Cycle Duration (Seconds)
2	8
3	10
4	15

4. RESULTS AND DISCUSSIONS

4.1. INTRODUCTION

This chapter presents the results of the analytical solution compared to the experimental results for different angles. Then the experimental results of the post processing stage are presented and experimental models are fitted to the data for predicting the surface roughness values. Based on the results of this research, the best post processing setup, main factors affecting the roughness values, and the best model for predicting the surface roughness are stablished.

4.2. ANALYTICAL SOLUTION RESULTS

The developed analytical model for predicting the surface roughness is used here and the values are compared to the experimental ones. The two layer thicknesses are 0.010 and 0.013 inch and the depression is found by $b = t/\tan(\theta)$. A computer algorithm is developed to find the achievable angle considering the new centerline established in this study. This output is a measure of the required number of layers and layer depression to create a particular angle. Before 45° surfaces, with respect to horizontal plane, the achievable angle increases and converges to a certain angle, which might be smaller or bigger than the aimed angle. The point is that the desired angle might be anywhere in this trend with a certain number of layers. Figure 4-1 (a) represents the trend of the achievable

surface angle for ideal surface angle of 40 degrees. As it can be seen in Figure 4-1 (a), by increasing the number of layers, the achievable angle converges to 39.8° after 27 layers. However, for other cases it may converge to a larger angle so the best choice can be found with fewer number of layers before convergence. At 45° surface, the trend changes and that's the angle at which the achieved angle is always the same as the aimed one and it converges to 45° with only three layers. For the surfaces with more than 45° with respect to horizontal plane, the achievable angle starts from a larger angle for few numbers of layers and decreases toward a close angle to the desired one. However, the angle that the curve converges to, can be either smaller or larger than the aimed angle. For instance, at 50° (Figure 4-1 (b)), the best result with 100 number of layers is 51.3407° and actually it converges to this value after 91 layers. A noteworthy point here is that both trends start from a too smaller or too larger angle than the desired one for few numbers of layers, conveying the fact that for fewer numbers of layers, the issue addressed above is more significant. In order to solve this problem, it is suggested that the layer thickness be reduced to increase the number of layers and achieve a better result.

The layer thicknesses available on the machine is of great importance in selecting the number of layers for the achievable angle closest to the desired one. The product design specifications and dimensions define the available space to manufacture a certain surface angle on the machine. Therefore, considering the available space and the desired angle, the designer can check the required number of layers based on the curves obtained in this work. This will lead to the layer thickness necessary to have that number of layers in the space available. Then the approach is to check the available layer thicknesses on the machine,

the required layer thickness should be equal or bigger than the options on the machine. If its equal to one of the options so the surface can be easily manufactured but if it is larger, number of layers should be increased, which can lead to some error in surface angle. Taking this discussion in to account in deciding about the process parameters ends in some back and forth between number of layers and the final possible approach considering machine limitations and design requirements.

Figure 4-2 (a-f) shows the results of different angles from 5 to 90 degrees with 5 degrees increments versus the number of layers. In design application and during service life of a product, the surface properties are the other significant parameters, which can be of assembly, authentic etc. requirements. Surface roughness is one of the surface properties and is one of the substantial process design parameters. Considering the fact that the desired angle is not always the angle that the corresponding curve convergence to and also there are other choices available for a specific angle with some error, surface roughness resulting from each of the choices can be another criterion to select between two available options.

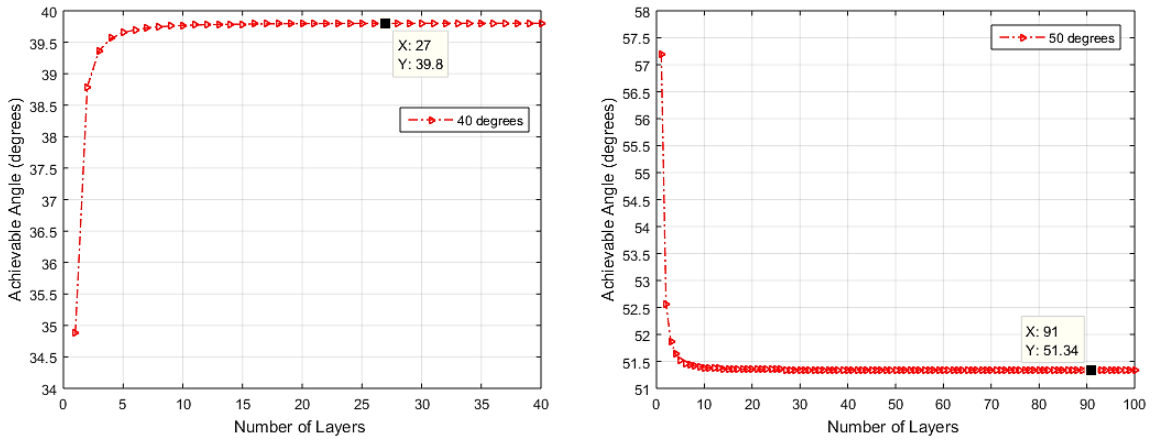

(a) $\theta = 40°$ (b) $\theta = 50°$

Figure 4-1 Resulting angle versus number of layers for aimed angles of $\theta = 40°$ *and* $50°$ when depression is constant and equal to $(\frac{t}{\tan(\theta)})$.

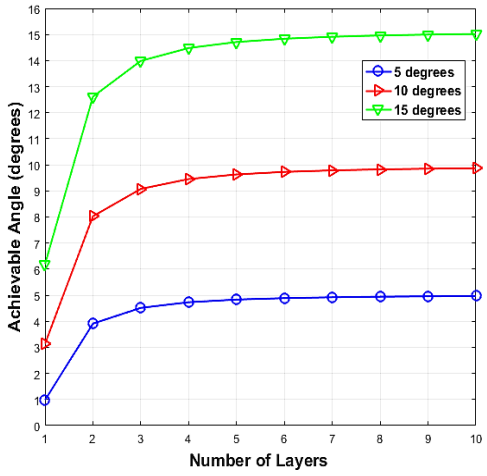

a) At 5, 10, and 15° surface angles

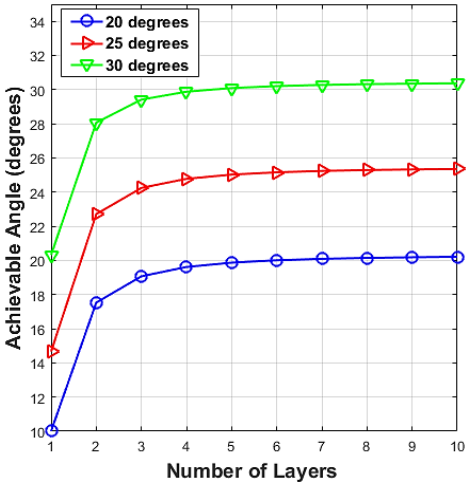

b) At 20, 25, and 30° surface angles

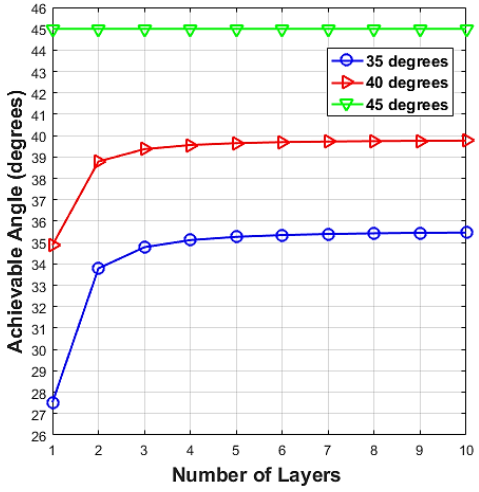

c) At 35, 40, and 45° surface angles

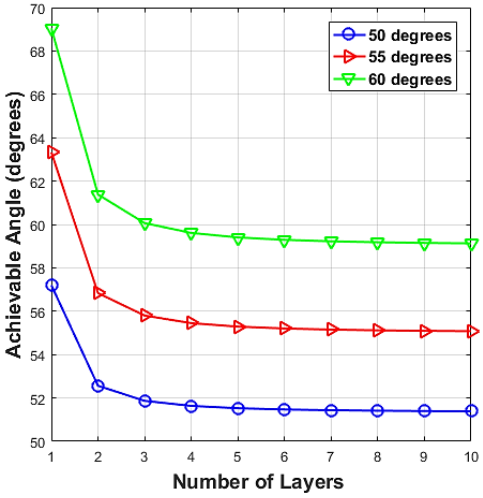

d) At 50, 55, and 60° surface angles

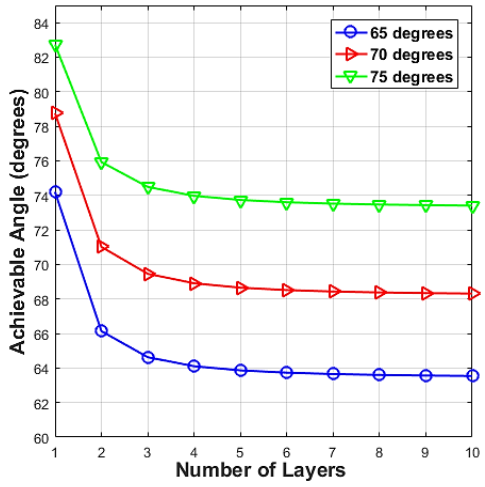

e) At 65, 70, and 75° surface angles

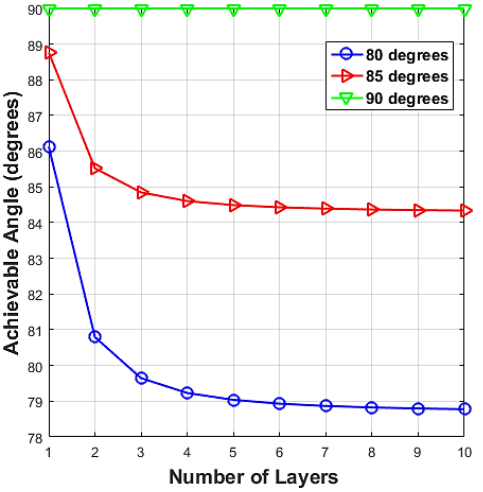

f) for 80, 85 and 90 degrees surface angle

Figure 4-2 Achievable angle vs number of layers at each surface angle.

The process designer can choose the number of layers based on two factors. The two factors are minimizing the surface roughness and the accuracy of the resulting angle. Table 4-1 shows the corresponding possible angles and a parameter defined as the surface roughness divided by layer thickness for each number of layers at 15°. In order to achieve an angle of 15°, about 10 layers are required to get an angle of 15.0205° and after that the resulting angle increases slightly and with 100 layers the resulting angle is 15.1230 degrees, that is more than 15°. Regarding the preferred surface roughness, the designer can decide about the angle. An increase in the number of layers causes an increase in surface roughness and based on the application that a higher or lower surface roughness is desirable, the number of layers can be selected. In fact, if the angle is not the main factor and an angle of 14.480° is acceptable leading to a lower surface roughness, the number of layers can be changed to 4 layers instead of 10.

Table 4-1 Resulting angle and corresponding depression (b) needed from 1 to 20 layers at 15° surface angle.

No. Of Layers	Resulting Angle (Deg.)	R_a/t	No. of Layers	Resulting Angle (Deg.)	R_a/t
1	6.190	0.11061	11	15.038	0.18909
2	12.614	0.17174	12	15.052	0.18918
3	13.987	0.18178	13	15.063	0.18925
4	14.480	0.18525	14	15.071	0.18931
5	14.711	0.18684	15	15.078	0.18936
6	14.837	0.18771	16	15.083	0.18940
7	14.913	0.18823	17	15.088	0.18943
8	14.962	0.18857	18	15.092	0.18945
9	14.996	0.18880	19	15.095	0.18948
10	15.0205	0.18897	20	15.098	0.18949

The results can also be used to decide on the most accurate angle that can be obtained, where an accurate angle is the most significant goal. As it can be inferred from the results, for 10° as the goal, the possible angle with 20 layers is 9.931° and 9.9498° with 100 layers. This means that in order to have a more accurate angle for 10°, the designer should aim at a larger angle to get an accurate 10 degrees surface. In other words, the analytical solution presented here provides the designer with a tool to get a more accurate angle on the final part by aiming at another angle achievable from the analytical solution. Table 4-2 shows the suggested angles to achieve each angle at 5° increments with 0.02° error. For each particular desired angle, there is a suggested angle, which should be selected so that on the final part the angle will be close enough to the desired one. At each angle with 20 layers, there might be a good accuracy with 20 layers; however, the possibility of that accuracy with 20 layers depends on the space available for it and the minimum layer thickness available on the machine. For instance, at a five-degree surface slope, if the aim is chosen 5°, a good accuracy will be achievable but with 20 layers which might not be feasible at the moment, either because of limited space or minimum feasible layer thickness on the machine. Therefore, the other purpose should be focusing on minimizing the number of layers. For instance, aiming at 5.2° will yield 5.0076° only with 5 layers that is more reasonable. In the case of small features, where there is only a limited space (i.e. 1 mm) for building the feature with an FDM machine or any other layer based 3D printing machine, the layer thickness and number of layers will be the crucial factors. Within 1 mm space, it is possible to get a 5° angle with 10 layers which means 0.1 mm layer thickness but with 100 layers, it might not be feasible to have 0.01 mm layer thickness. As a result, the number

of layers should be minimized by aiming at a more appropriate angle leading to a more feasible layer thickness.

According to the results in Table 4-2, after a certain angle (20 degree) the designer can aim at the actual desired angle because it yields the final angle without any need to change it. It can be concluded that for small features with small angles (lower than 20°), the designer can use the proposed method to change the angle to get the final desired angle. In order to summarize these results, based on the design requirements and machine specifications, the designer has different options to select. If the goal is to have an accurate angle, these results suggest that for small features, aiming at another angle slightly different from the desired one leads to a better result. In addition, if the surface roughness is important, number of layers can be changed to get the preferred surface roughness but it should be noted that this might cause some error in the desired angle. However, while selecting an angle to be manufactured, the possible layer thicknesses on the machine also affects the number of layers and if there are not options to have the desired layer thickness, the aim must be reducing the number of layer with losing some accuracy in angle.

Table 4-2 The suggested angle, corresponding final angle and the required layers for the suggested angle.

Desired angle (deg.)	Suggested angle (deg.)	Achievable angle (deg.)	Required layers	Error (%)
5	5.2	5.0076	5	0.076
10	10.2	10.0248	9	0.248
15	15.1	15.0204	10	0.204
20	20	20.0079	10	0.079
25	25	25.0246	5	0.246

4.3. VALIDATION OF ANALYTICAL SOLUTION WITH EXPERIMENTAL RESULTS

In order to validate the analytical study presented here, an experimental setup for fabrication of specimens, measurement, and roughness analysis is utilized. Layer thickness and the horizontal depression between the subsequent layers define the overall shape of the cusp for any profile of the product. Traditionally, the horizontal depression is calculated based on trigonometry and the local slope of the desired profile curvature. Therefore, modelling the resulting surface roughness as a function of layer thickness and the local slope of the desired profile will be a practical approach to use for predicting and process controlling applications. The commercially available AM machines are still very limited in terms of layer thickness variation. In addition, dynamic change of layer thickness is not an option in many commercial systems. As a result, the surface local slope will be the most adjustable parameter to control and conduct the required experimental study. FDM process is used as a platform to develop and implement the conceptual methodology. However, the concept can be implemented for any other layer-based AM processes.

The point cloud data is captured for each patch of specimens and a surface is fitted to the data. Figure 4-3 shows the reconstructed surface topographies of two sets of the specimens with 0.010 and 0.013 inch layer thickness at 10, 35 and 90° surface angles obtained by Faro Laser Arm. Appendix A shows all reconstructed surface topographies for all angles from 5 to 90° with 5° increments.

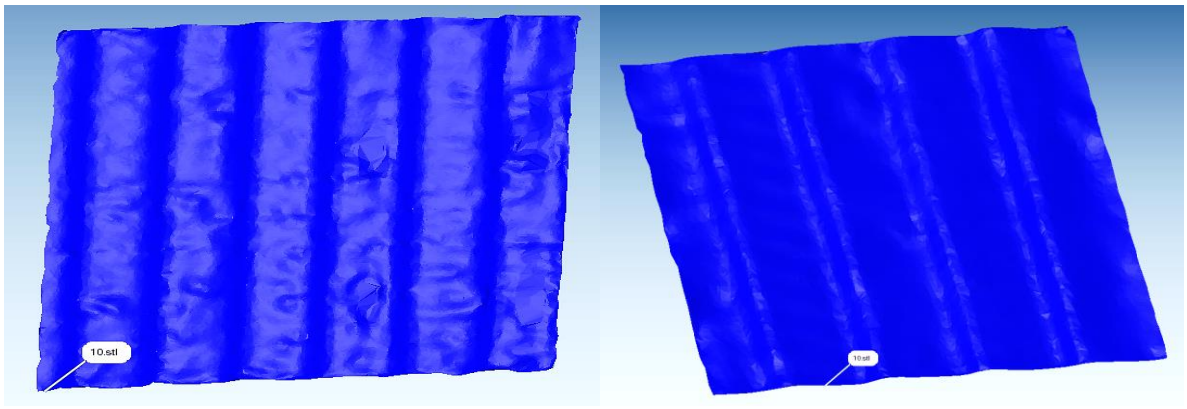

a) 10° surface angle (left is 0.010 inch and right is 0.013 inch layer thickness)

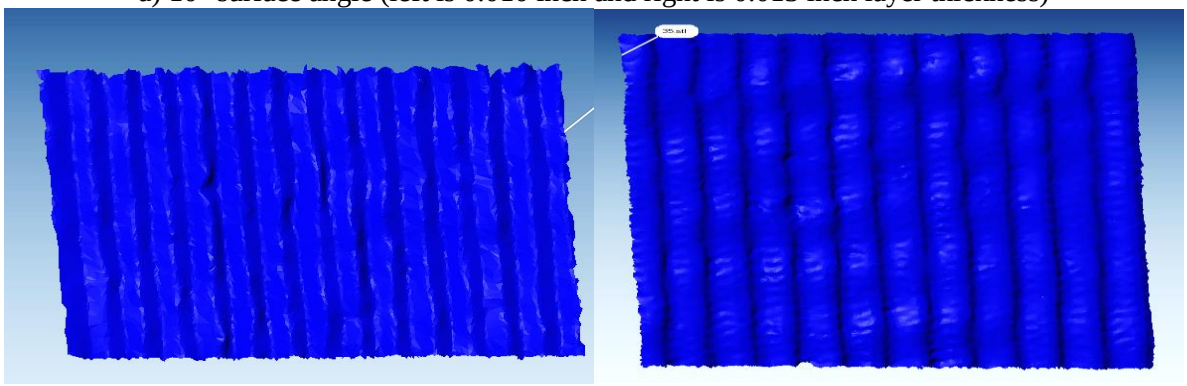

b) 35° surface angle (left is 0.010 inch and right is 0.013 inch layer thickness)

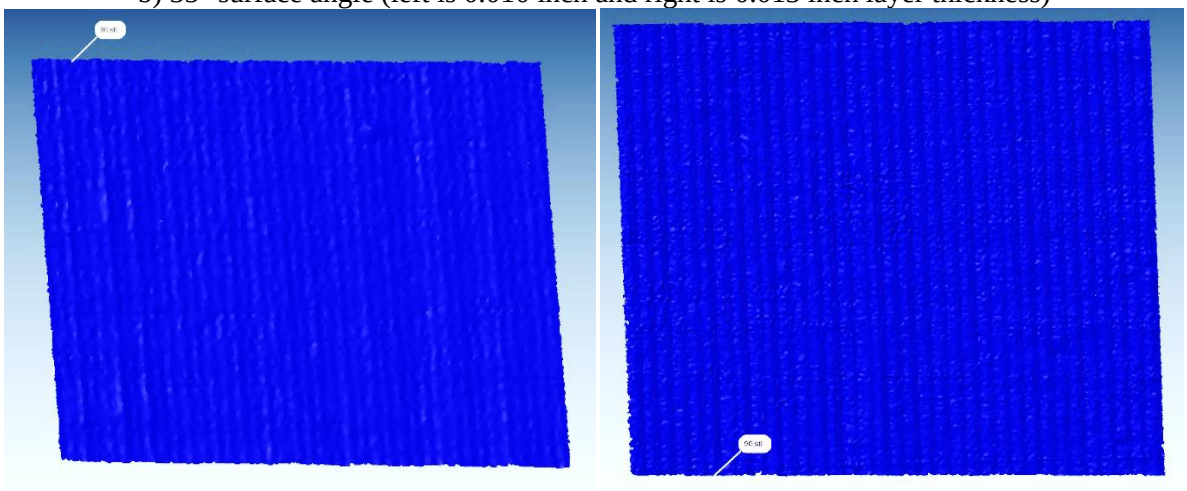

c) 90° surface angle (left is 0.010 inch and right is 0.013 inch layer thickness)

Figure 4-3 3D representation of the surfaces with 0.010 and 0.013 inch layer thickness at different surface angles after surface reconstruction from point cloud data.

In the next step, the results of the analytical formulation and the actual surface roughness values calculated using the point cloud data of the manufactured surfaces are

compared as shown in Figure 4-4. In the theoretical solution the surface is considered perfectly smooth and there is no waviness. The only thing considered is the square stair-step shape of layers on the top of each other. However, the surface created by FDM process has waviness on it as a result of machine vibration, acceleration, deceleration of head during printing, etc., which is not taken into account in analytical solution. The other effect that is not considered is the filling underneath surfaces which is visible on 5 and 10° surfaces. The infill material can be seen on the surface making it too different from the ideal surface. At higher surface slopes such as 80° and 85°, the waviness is dominating and after a certain degree (70°) the trend is locally changed to increasing by increasing the angle. This behaviour can be attributed to the waviness effect. In addition, in the theoretical model, the surface is considered as steps with square edges, which is another reason for getting different results.

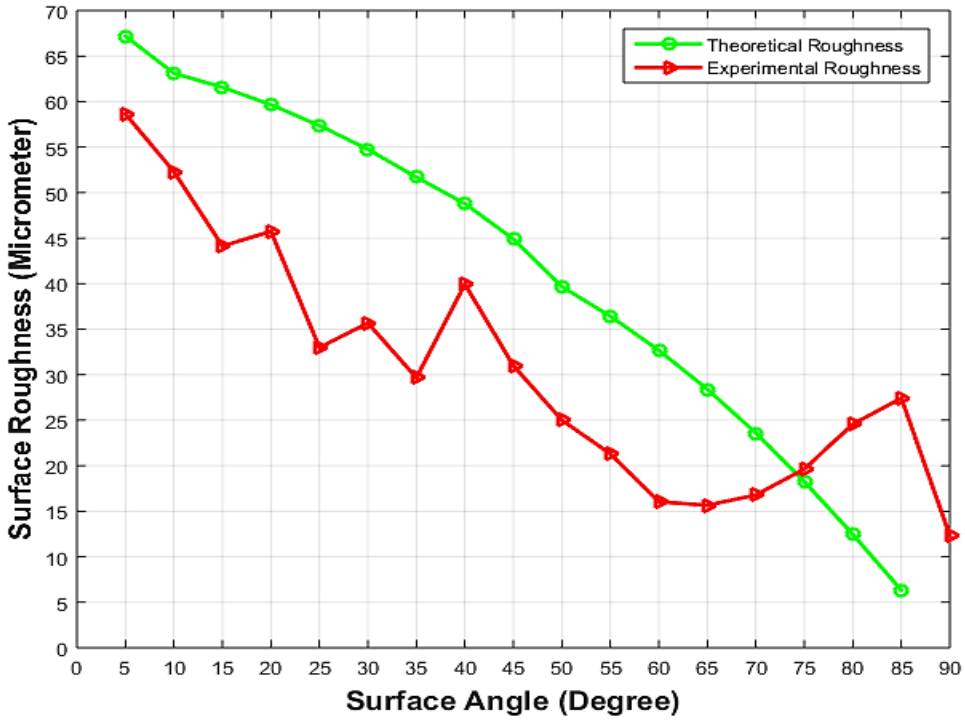

a) The surface roughness results of the specimen with 0.010 inch layer thickness.

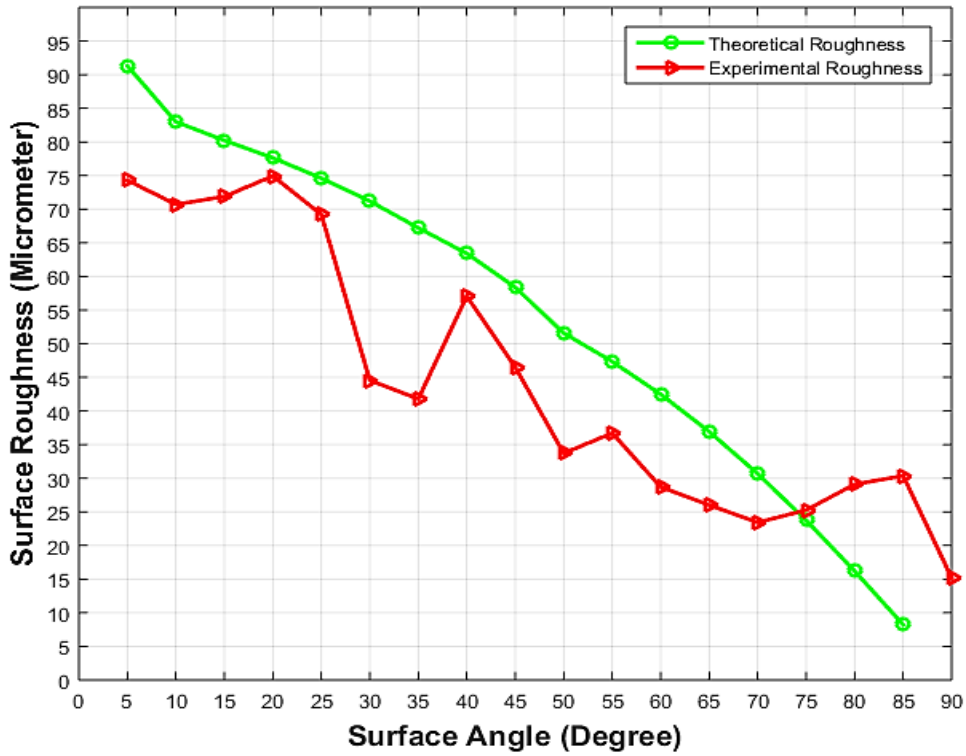

b) The surface roughness result of the specimen with 0.013 inch layer thickness.

Figure 4-4 The theoretical and experimental surface roughness of the specimens.

4.4. RESULTS OF POST-PROCESSING STAGE

The smoothing process in acetone vapour bath on FDM parts made of ABS removes the staircase effect on the part's surface dramatically and yields a smoother surface. Figure 4-5 (a) and (b) show the pre and post-smoothing surfaces for the 90 degrees surface slopes for 0.010 and 0.013 inch layer thickness, respectively. Figure 4-5 (a) shows the pre-smoothing surface for 0.010 inch layer thickness and (b) shows the smoothed surface with 4 cycles and 15 seconds cycle duration. As it can be seen in these figures, the smoothing process has a profound effect on the surface to the end that the staircase effect is almost removed and only some grooves have remained on the surface. For the layer thickness of 0.013 inch the staircase effect is more and the same smoothing process has less effect on removing that and as it can be seen in Figure 4-5 (c) and (d), few amount of peaks and valleys still remain on the surface compared to the pre-smoothing surface. This result confirms that layer thickness has a significant effect of smoothing process by acetone. The surface topographies obtained by optical microscope showed the same behaviour about the pre and post-processing result. Figure 4-6 shows some typical results of 3D optical microscopy.

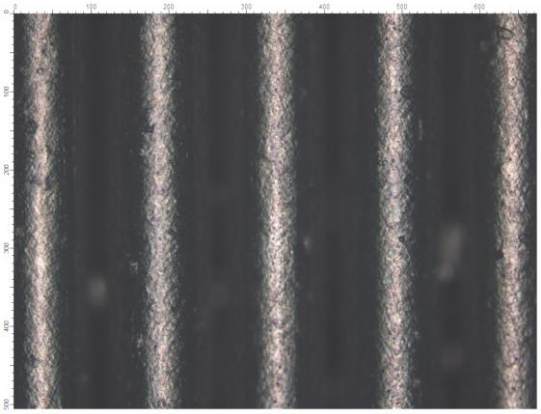

a) Pre-smoothing surface for t=0.010 inch.

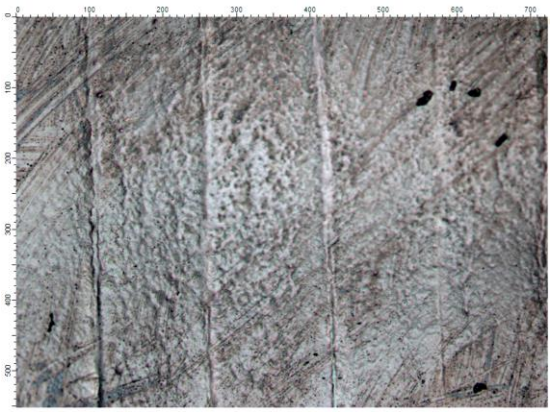

b) 4 cycles for 15 seconds for t=0.010 inch.

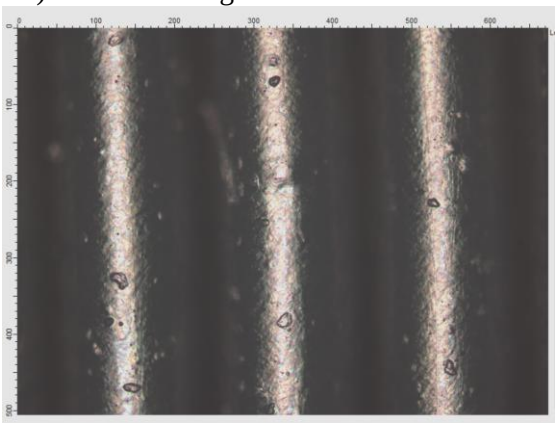

c) Pre-smoothing surface for t=0.010 inch.

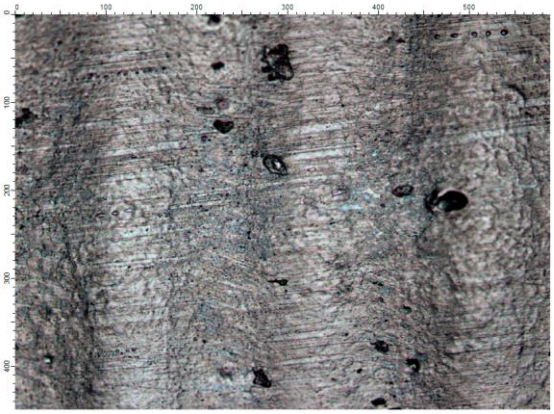

d) 4 cycles for 15 seconds for t=0.013 inch.

Figure 4-5 Pre and post-smoothing surfaces for t=0.010 and 0.013 inch and 4 cycles for 15 seconds.

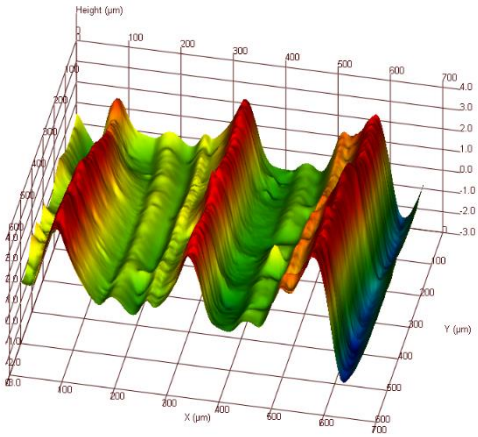

a. 50° before

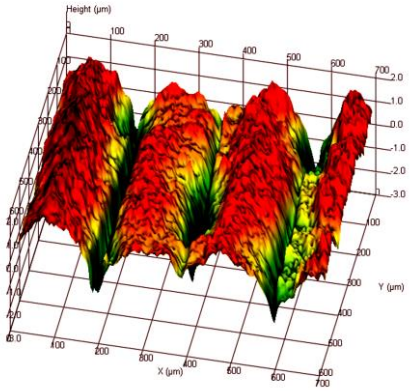

b. 50° after

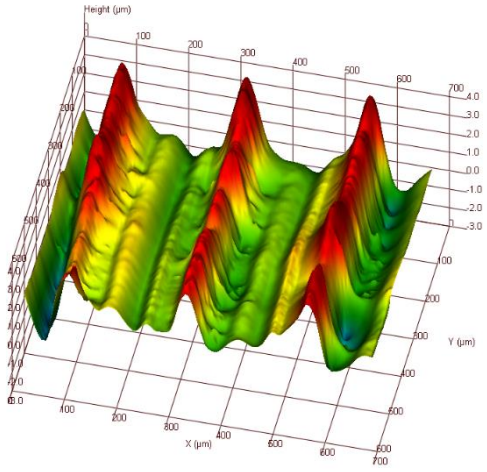

c. 55° before

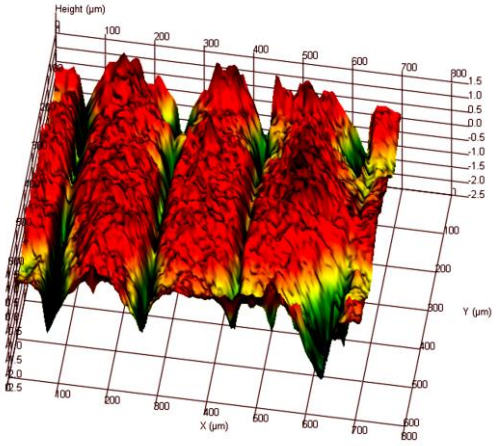

d. 55° after

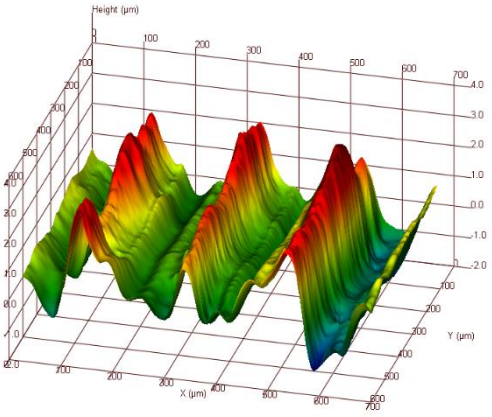

e. 65° before

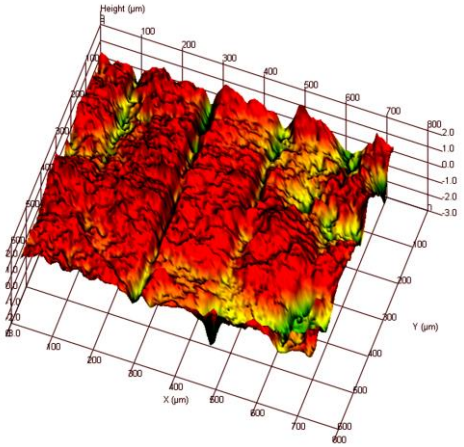

f. 65° after

Figure 4-6 3D roughness evaluation of the post processed surfaces before and after post-processing with 4 cycles each for 15 seconds and 0.013 inch layer thickness.

In order to find the optimum smoothing parameters to get a specific surface roughness on the FDM surfaces, 9 experiments with different smoothing setups have been conducted for each layer thickness. Figure 4-7 illustrates the final surface roughness values resulted from each smoothing set of parameters for 0.010 inch layer thickness. The notation used in the figures are as "Ra a-b", the first number (a) indicates the number of cycles and the second (b) stands for the duration time. For example, "Ra 2-8" means the part has been smoothed for two cycles, each for 8 seconds. Compared to the original roughness values, smoothing process has affected the surface roughness significantly, especially for angles above 40 degrees. In addition, after smoothing process, the fluctuations in the curves attributed to process parameters, machine vibrations etc. are removed from the surface and the curves behave smoother. This behaviour indicates the fact that smoothing process also removed surface irregularities resulted from process parameters and machine instabilities. The surface roughness decreases by increasing the surface angle showing more important effect of surface slope. As it can be inferred from Figure 4-7, as the cycle number increases, smoother surfaces are resulted, also increasing the cycle time leads to smoother surfaces. It can be concluded that 4 cycles with 15 seconds results the smoothest surface; however, there should be a relation between the number of cycles and cycle time and which one has the more significant effect on the surface roughness. Figure 4-8 shows the results for the layer thickness of 0.013 inch, and it confirms the same results as of 0.010 inch layer thickness. Considering these two results, surface slope is the main design factor affecting surface roughness.

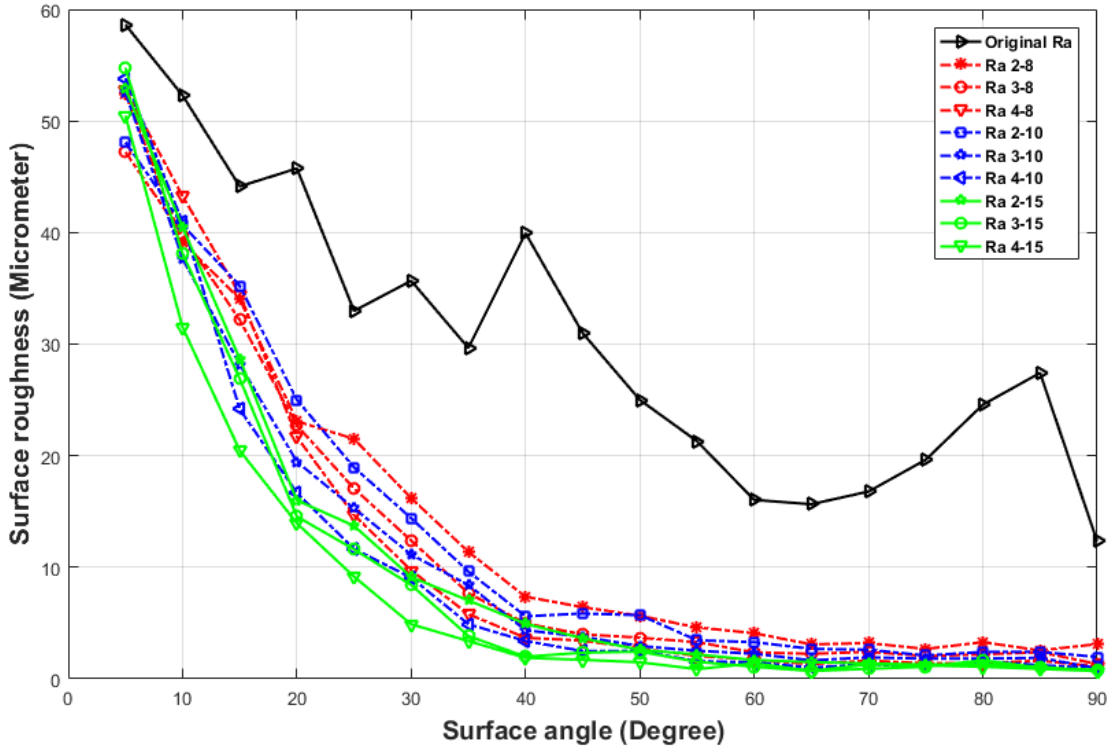

Figure 4-7 Post-Smoothing surface roughness values for different smoothing cycles and time for 0.010 inches layer thickness.

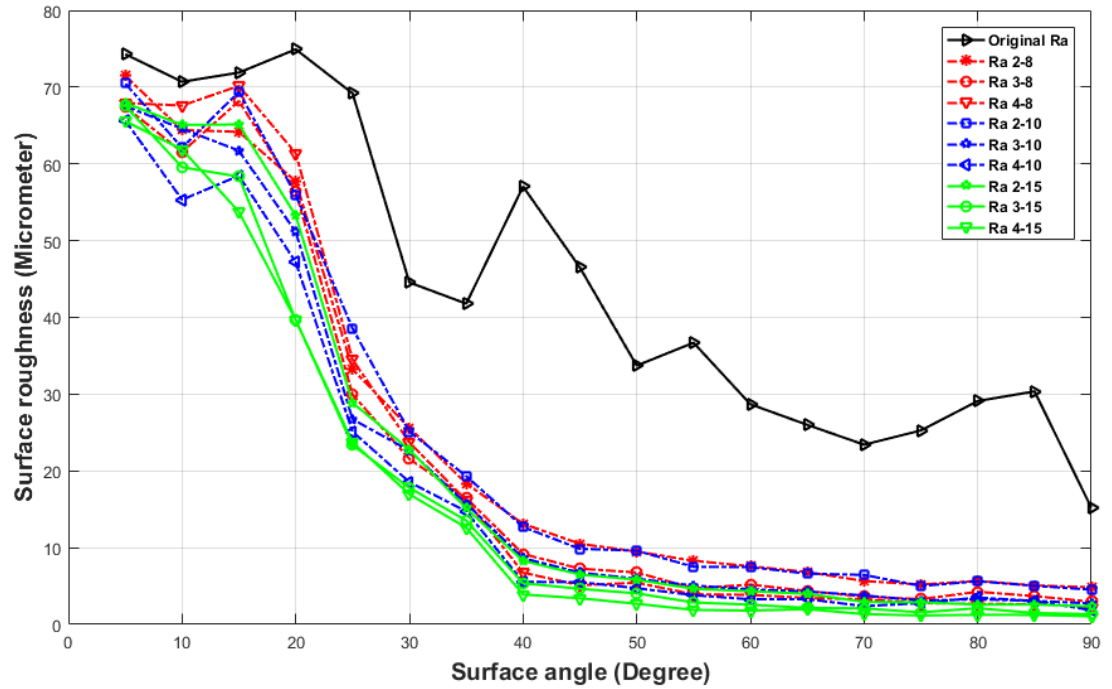

Figure 4-8 Post-Smoothing surface roughness values for different smoothing cycles and time for 0.013 inch layer thickness.

It seems that the most important parameter affecting the surface roughness is TET and the two parameters individually do not have such a significant effect. Figure 4-9 shows the effect of TET for both layer thicknesses based on the RRP parameter. In the legend of Figure 4-9, the first column is the number of cycles, second is the cycle time and the third column is the TET. As it can be understood from the results, after 40° the curves become stable and converge to a certain RRP and before 40° the results are so sensitive to the surface slope. It means that at angles less than 40°, a change in surface slope results in a very different roughness value and if they are present on a part together, the final surface will not be homogenously smoothed. On a surface having angles larger than 40°, more homogeneous results will be achieved. These results suggest that in design stage, the surfaces required to be smooth and have various angles with respect to horizontal axis (like a free surface), be designed in such a way that at a specific build orientation, all angles fall above 40° when printing. In general, the sensitivity to surface slope decreases after 40°. Surface Roughness Sensitivity (SRS) to surface slope can serve as an indicator to choose the build orientation at in order to have a smoother surface SRS should be as low as possible. These results can be used as a design tool that helps the designer to decide on the product's build orientation. At design stage, each surface slope will yield a different surface roughness, which is predictable using the available results from pre-processing step. For a part that a particular surface roughness is required at some areas, the designer can calculate the corresponding RRP and use the results of Figure 4-9 to decide on the appropriate post-processing parameters. In this way, at design stage, the build orientation can be selected so as to give the proper surface slope and the corresponding post-processing parameters.

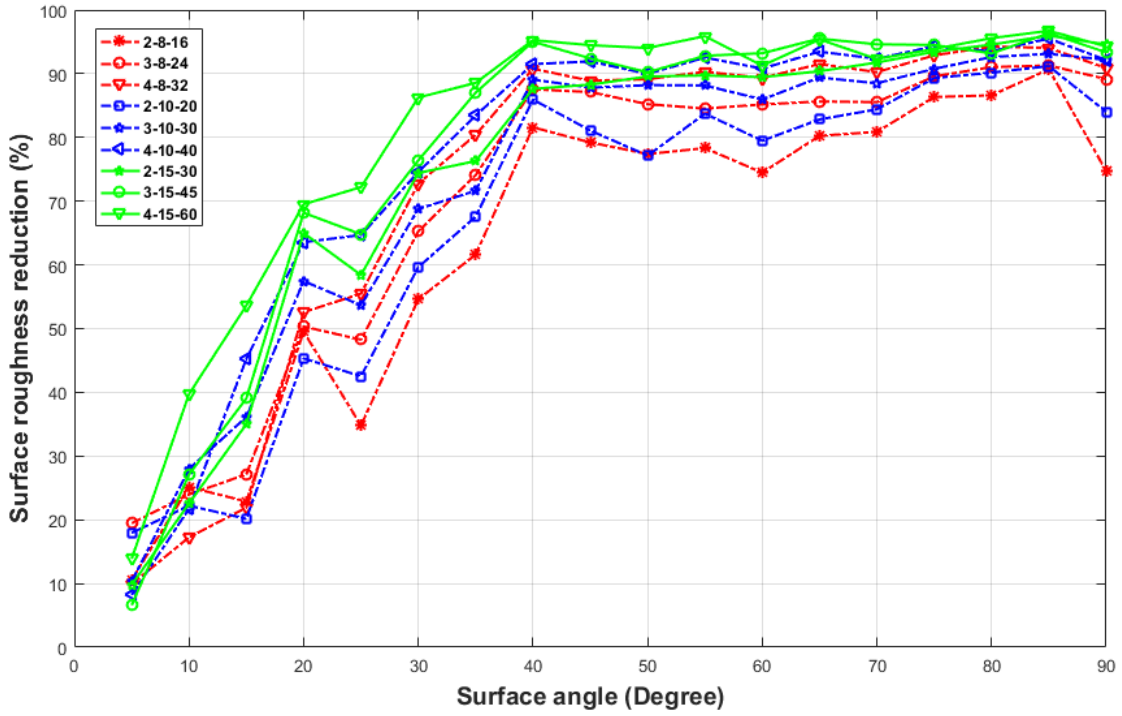

a) RRP for 0.010 inch layer thickness for various smoothing settings

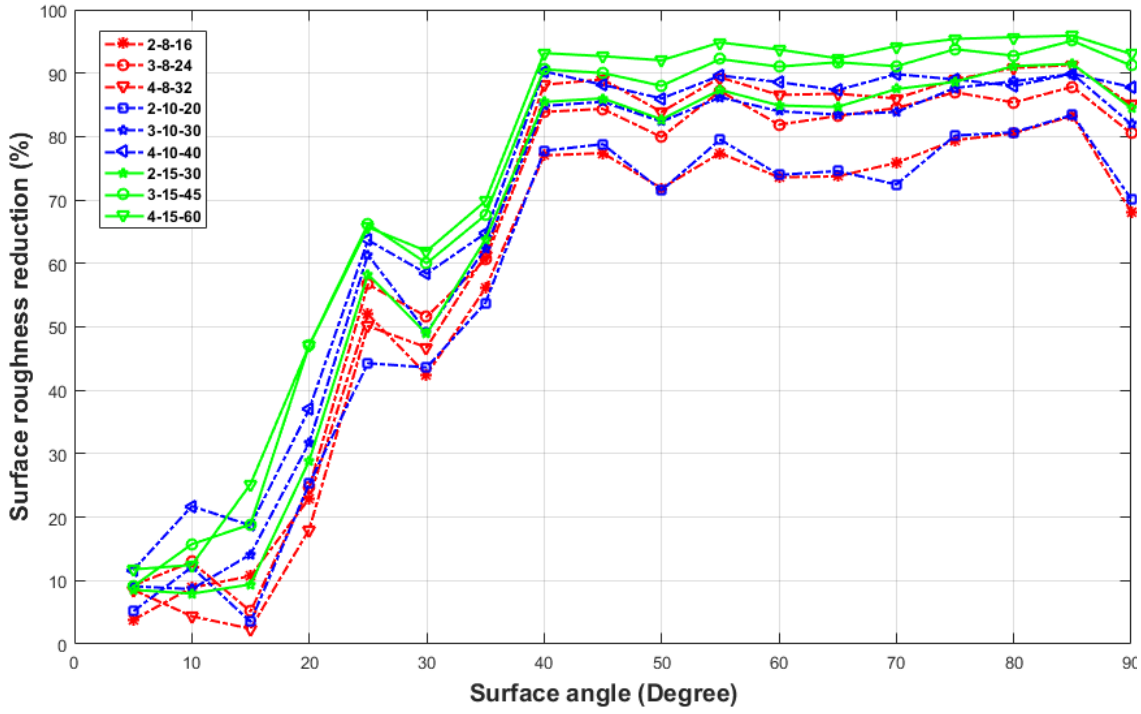

b) RRP for 0.013 inch layer thickness for various smoothing settings

Figure 4-9 Effect of different smoothing parameters on RRP.

In order to study this idea that TET is the main factor, the two cases having the same TET: 2 cycles of 15 seconds and 3 cycles of 10 seconds are compared. The RRP for these two sets are presented in the following column diagram (Figure 4-10). As it is obvious, almost in all cases, 2 cycles of 15 seconds results in a smoother surface than 3 cycles with 10 seconds, which shows that duration time has more effect on the surface roughness. It is worth noting that 2 cycles with 15 seconds is easier and more cost effective than 3 cycles with 10 seconds for it needs less cycle changes resulting in less effort necessary to conduct the smoothing process but in order to decide whether it's a significant variation, a statistical analysis should be conducted. Another set of smoothing parameters which are close in TET are 4 cycles of 8 seconds (32 seconds) and 3 cycles of 10 seconds (30 seconds). The column diagram for this case is shown in Figure 4-11. Although TET is less in the case of 3 cycles by 2 seconds but the results are almost the same or even better with fewer cycle with longer time.

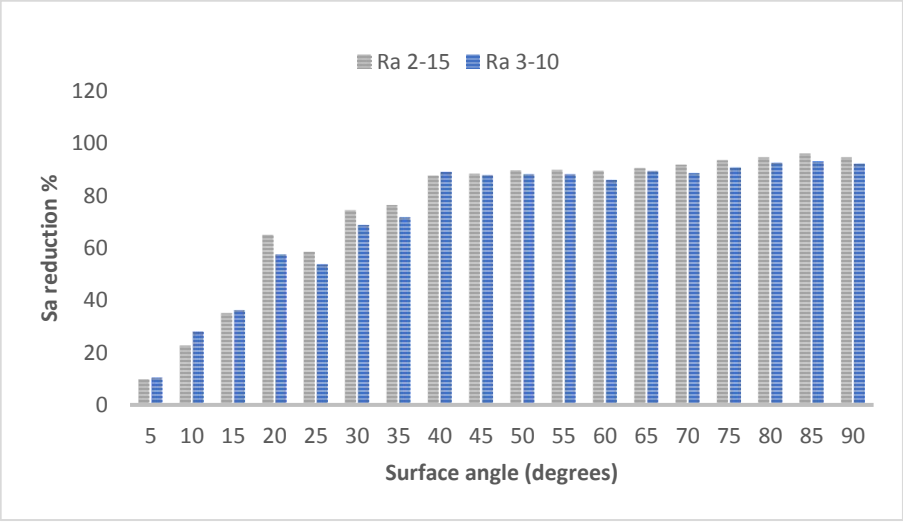

Figure 4-10 The RRP versus surface angle for TET of 30 seconds by 2 cycles of 15 seconds and 3 cycles of 10 seconds for t=0.010 inch.

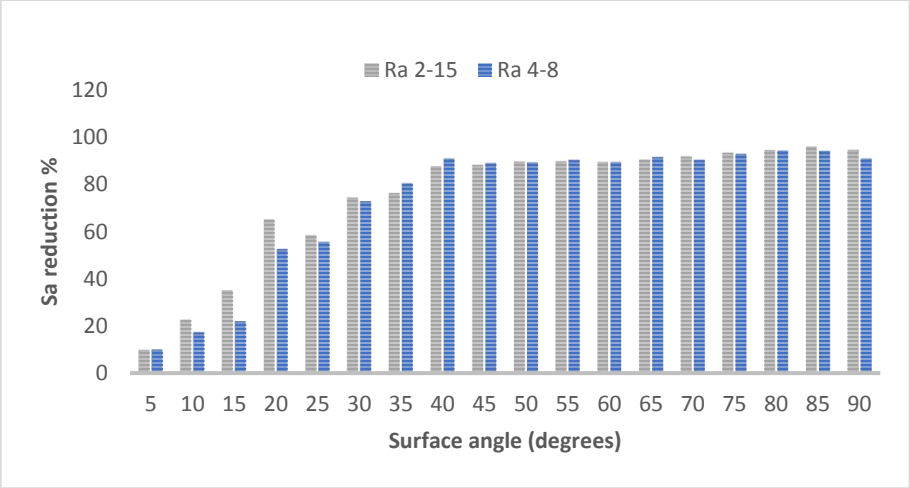

Figure 4-11 RRP versus surface angle for 2 cycles of 15 seconds and 4 cycles of 8 seconds.

In order to decide which factor has more effect on the surface roughness, at each cycle number, time is increased and reduction in surface roughness with respect to original roughness is represented and in the other case, the time duration is kept constant and number of cycles are increased for 0.010 inch layer thickness (Figure 4-12 (a-f)). The important fact about these results is that by increasing the surface angle, the reduction percentage increases until 40 degrees and after that the behaviour becomes more stable and surface roughness reduction does not change significantly by increasing the surface angle. In the case of constant number of cycles, increasing the duration time from 8 to 10 seconds results in reduction of surface roughness as reduction percentage increases. However, increasing duration time from 10 to 15 seconds gives more reduction in surface roughness. This result shows that increase in duration time leads to smoother surface and has more effect on the surface roughness. On the other hand, when duration time is constant and number of smoothing cycles are being increased, from 2 to 3 cycles, the surface roughness is decreased but as opposed to constant cycle case, from 3 to 4 cycles, the reduction in

surface roughness is less than from 2-3 cycles. This result proves that duration time has more effect on surface roughness. After 3 cycles, the effect of number of cycles is decreased as it can be seen in Figure 4-12 but the effect of duration time becomes more by increasing it. This behaviour is more obvious in the case of 0.013 inch layer thickness (Figure 4-13). Increasing the time from 8 to 10 seconds has the least effect and surface roughness does not change significantly but from 10 to 15 seconds there is a significant increase in RRP. The reverse is observed for constant duration time as from 3 to 4 cycles, the increase in RRP is less than 2 to 3 cycles, supporting the fact that effect of number of cycles is becoming less. This trend for 0.013 inch layer thickness also confirms the more significant effect of duration time than number of cycles. In general, these differences suggest that when a TET is achievable with two different configurations, the one with less number of cycles is preferred from either cost or smoother surface aspects.

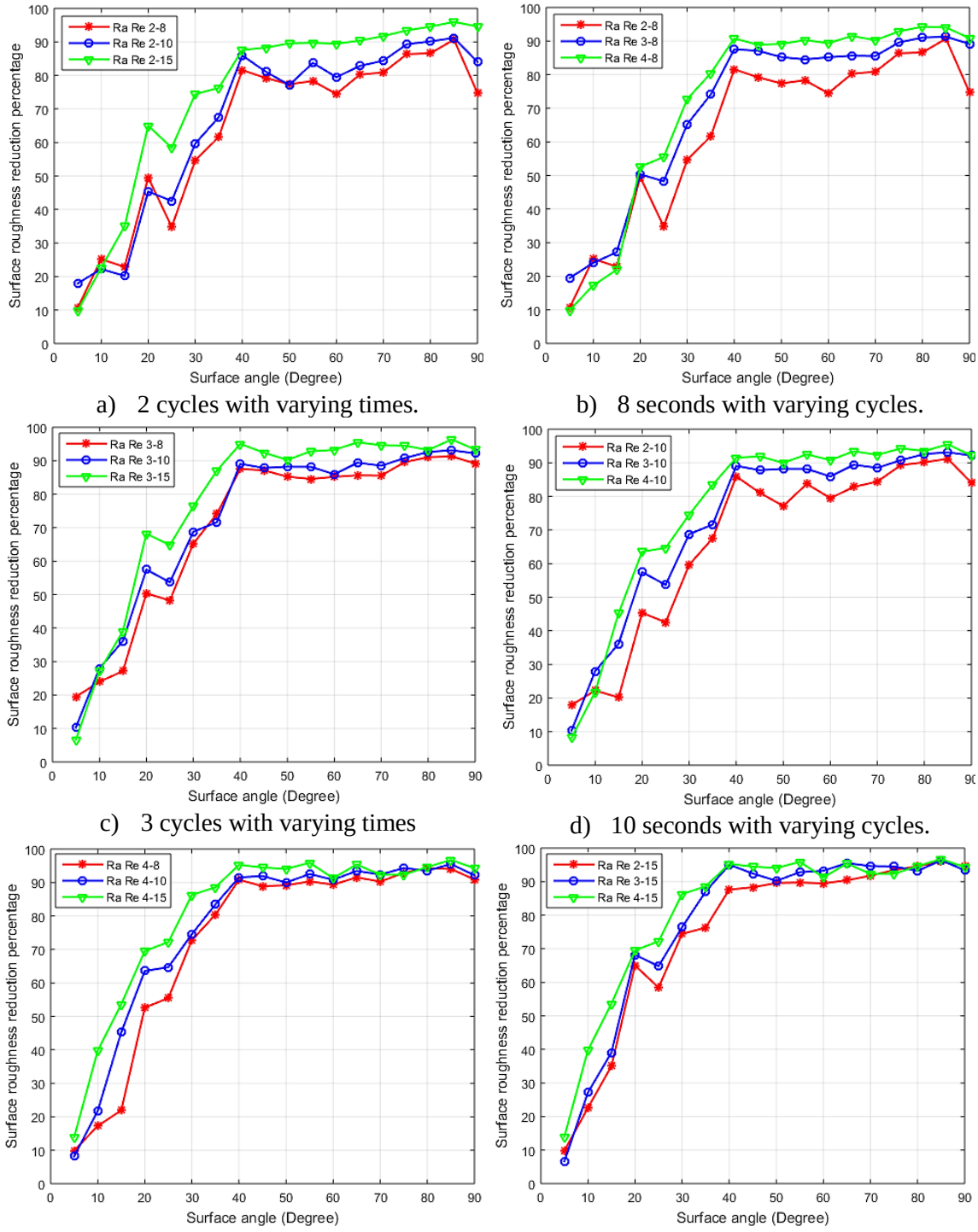

Figure 4-12 Surface roughness versus surface angle for different duration time and number of cycles for 0.010 inch layer thickness.

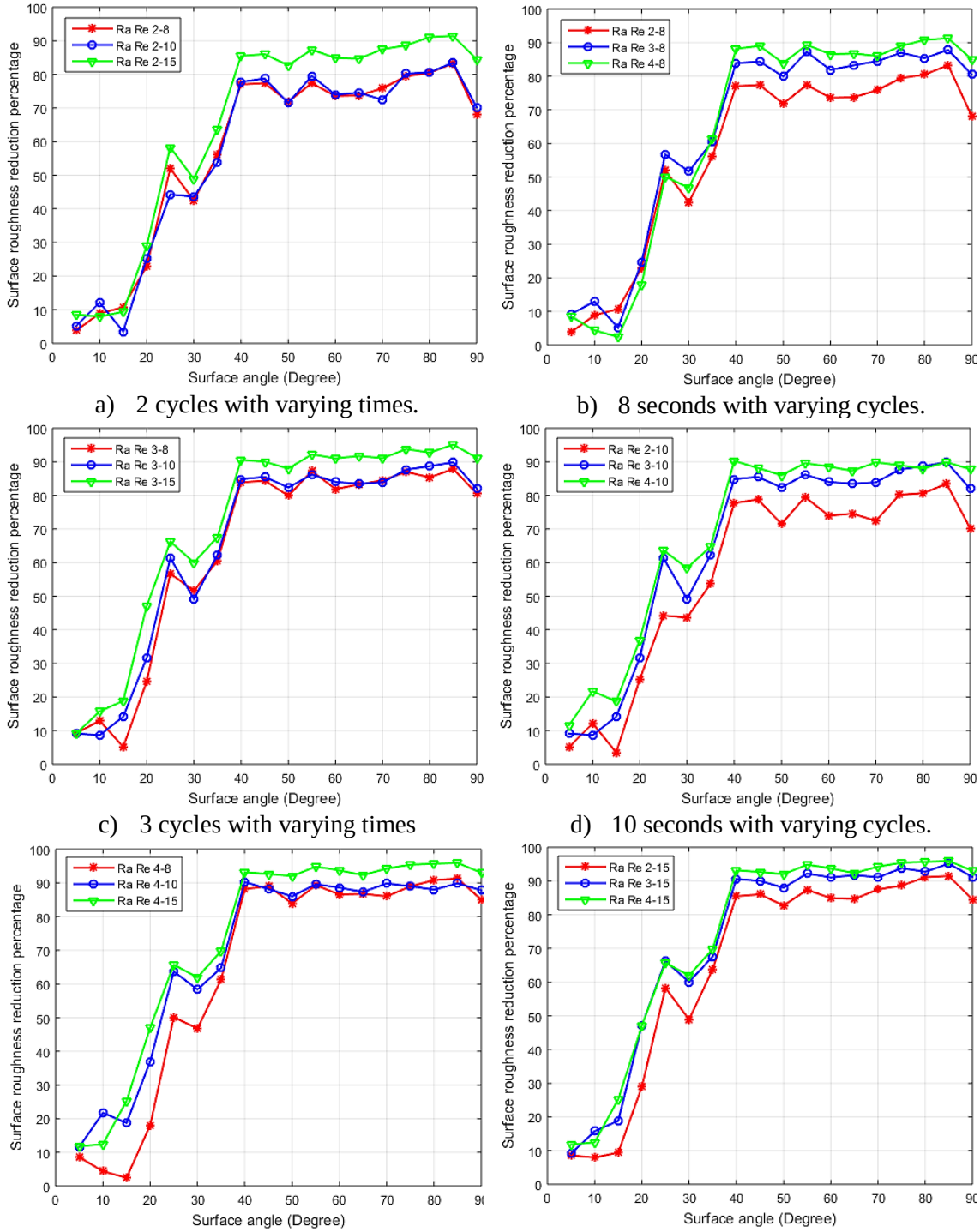

Figure 4-13 Surface roughness versus surface angle for different duration time and number of cycles for 0.013 inch layer thickness.

4.5. STATISTICAL ANALYSIS AND MODEL DEVELOPMENT

The statistical analysis used here is the 6-Sigma method, which suggests that if the difference between the minimum and maximum value of results (maximum deviation) is less than 6 times of standard deviation of the results, the data distribution can be considered as normal distribution. Then a regression analysis will lead to a model fitted to the data set. The result of 6-Sigma analysis showed that for all cases and both layer thicknesses the variation between minimum and maximum roughness values is less than 6 times of standard deviation of that case, suggesting that the distribution can be considered normal based on 6-Sigma method.

At each surface angle, a linear and a quadratic model with 95% confidence level are fitted to the results and the outputs show that the quadratic model better fits to the experimental data for both layer thicknesses. Figure 4-14 shows the models for 65° surface angle for both layer thicknesses.

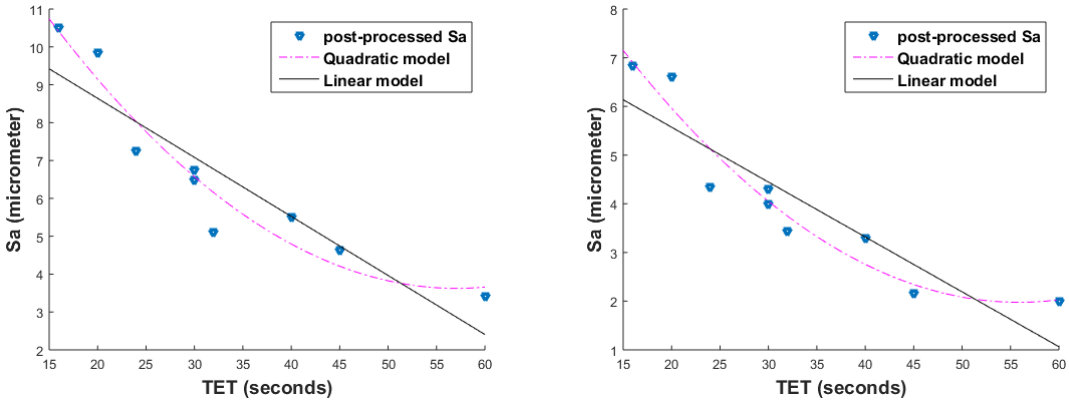

a) 65 degrees with t=0.013 inch b) 65 degrees with t=0.013 inch

Figure 4-14 Linear and quadratic models fitted to experimental data for t=0.010 and 0.013 inch.

Table 4-3 and Table 4-4 show the linear and quadratic models fitted to the data for 0.010 and 0.013 inch layer thickness, respectively.

Table 4-3 Linear models fitted to the experimental results for 0.010 inch layer thickness.

Angle (*Deg.*)	**Surface roughness linear model for t=0.010 *inch***	**Surface roughness linear model for t=0.013 *inch***
5	S_a=0.0580×t+49.7667	S_a=-0.1165×t+71.7994
10	S_a=-0.1588×t+44.3042	S_a=-0.0944×t+65.5741
15	S_a=-0.3288×t+40.2188	S_a=-0.3356×t+74.3322
20	S_a=-0.2584×t+27.7633	S_a=-0.4830×t+67.3221
25	S_a=-0.2695×t+23.7395	S_a=-0.2975×t+39.1561
30	S_a=-0.2349×t+18.3481	S_a=-0.2128×t+28.6594
35	S_a=-0.1805×t+12.8705	S_a=-0.1449×t+20.5677
40	S_a=-0.1188×t+8.1616	S_a=-0.2159×t+15.2914
45	S_a=-0.1049×t+7.2035	S_a=-0.1559×t+11.7592
50	S_a=-0.0918×t+6.3366	S_a=-0.1579×t+11.2722
55	S_a=-0.0785×t+5.0519	S_a=-0.1364×t+9.2474
60	S_a=-0.0582×t+4.0727	S_a=-0.1358×t+8.9994
65	S_a=-0.0563×t+3.5207	S_a=-0.1127×t+7.8270
70	S_a=-0.0455×t+3.3550	S_a=-0.1068×t+7.0268
75	S_a=-0.0329×t+2.7212	S_a=-0.0906×t+6.0773
80	S_a=-0.0388×t+3.1485	S_a=-0.0976×t+6.6614
85	S_a=-0.0420×t+3.0610	S_a=-0.0890×t+6.0394
90	S_a=-0.0412×t+2.6573	S_a=-0.0863×t+5.5088

Table 4-4 Quadratic models fitted to the experimental results for 0.013 inch layer thickness.

Angle (*Deg.*)	Surface roughness quadratic model for t=0.010 *inch*	Surface roughness linear model for t=0.013 *inch*
5	S_a=-0.00621×t^2 + 0.52621×t + 42.10279	S_a= 0.00364×t^2 - 0.39114×t + 76.29453
10	S_a=-0.00995×t^2 + 0.59090×t + 32.03211	S_a= 0.00204×t^2 - 0.24795×t + 68.08728
15	S_a= 0.00005×t^2 - 0.33284×t + 40.28458	S_a= -0.00501×t^2 + 0.04250×t + 68.14335
20	S_a= 0.00423×t^2 - 0.57697×t + 32.97755	S_a= -0.00233×t^2 - 0.30711×t + 64.44273
25	S_a= 0.00587×t^2 - 0.71215×t + 30.98490	Sa= 0.00557×t^2 - 0.71760×t + 46.03292
30	S_a= 0.00370×t^2 - 0.51390×t + 22.91406	Sa= 0.00195×t^2 - 0.36001×t + 31.06966
35	S_a= 0.00416×t^2 - 0.49427×t + 17.99590	Sa= 0.00236×t^2 - 0.32301×t + 23.48368
40	S_a= 0.00253×t^2 - 0.30930×t + 11.28027	Sa= 0.00544×t^2 - 0.62614×t + 22.00622
45	S_a= 0.00288×t^2 - 0.32228×t + 10.76196	Sa= 0.00402×t^2 - 0.45902×t + 16.72069
50	S_a= 0.00296×t^2 - 0.31522×t + 9.99323	Sa= 0.00341×t^2 - 0.41465×t + 15.47403
55	S_a= 0.00204×t^2 - 0.23272×t + 7.57532	Sa= 0.00329×t^2 - 0.38415×t + 13.30206
60	S_a= 0.00279×t^2 - 0.26889×t + 7.52135	Sa= 0.00332×t^2 - 0.38578×t + 13.09134
65	S_a= 0.00186×t^2 - 0.19640×t + 5.81363	Sa= 0.00310×t^2 - 0.34623×t + 11.64925
70	S_a= 0.00206×t^2 - 0.20092×t + 5.89896	Sa= 0.00258×t^2 - 0.30135×t + 10.21198
75	S_a= 0.00149×t^2 - 0.14500×t + 4.55536	Sa= 0.00190×t^2 - 0.23358×t + 8.41749
80	S_a= 0.00150×t^2 - 0.15188×t + 4.99923	Sa= 0.00214×t^2 - 0.25907×t + 9.30434
85	S_a= 0.00107×t^2 - 0.12288×t + 4.37554	Sa= 0.00194×t^2 - 0.23562×t + 8.43790
90	S_a= 0.00229×t^2 - 0.21421×t + 5.48851	Sa= 0.00255×t^2 - 0.27873×t + 8.65848

In order to draw a quantitative comparison between the linear and quadratic models, the Sum of Square of Errors (SSE) and Root Mean Square Error (RMSE) for both models are compared (Table 4-5 and Table 4-6). For both indicators, the quadratic model has a smaller average than the linear model in both indicators. Therefore, the quadratic model is found to be the best model to explain the trend of surface roughness based on TET. Using

these models, the proper TET to get a specific S_a value at a certain surface angle on a surface can be selected. Figure 4-15 illustrates the results of SSE and RMSE for both models. As it can be understood from Figure 4-15, for angles below 30 degrees, the two models are not capable of representing the results efficiently. This can be explained by considering the larger staircase effect on these angles the initial value of the surface roughness.

Table 4-5 SSE and RMSE of linear and quadratic models for 0.010 inch layer thickness.

t=0.010 in	**Linear Model**		**Quadratic Model**	
Angle	SSE	RMSE	SSE	RMSE
5	47.29409518	2.599288232	35.70678138	2.439493847
10	48.76684644	2.639449251	19.05592715	1.782130146
15	44.1930235	2.512625931	44.19217028	2.71391999
20	34.51134362	2.220403555	29.14777355	2.204078551
25	13.08862686	1.367407707	2.732554547	0.674852397
30	10.05956861	1.198783229	5.946718647	0.995549986
35	8.76250979	1.118832924	3.574121434	0.771807557
40	3.390495225	0.695957226	1.471797317	0.495277249
45	3.228593086	0.679137382	0.730646056	0.348961807
50	4.621605365	0.812544976	1.983776918	0.575003901
55	1.594604441	0.477284647	0.338414958	0.23749209
60	2.684938731	0.61932437	0.338659628	0.237577927
65	1.082575188	0.393260217	0.045383976	0.086971236
70	1.505519932	0.463761012	0.228847874	0.195298009
75	0.844059258	0.347246158	0.18039798	0.173396453
80	1.426644084	0.451449109	0.750953231	0.353777998
85	0.852647707	0.349008331	0.50655805	0.290562113

90	2.476100087	0.594750859	0.894801719	0.386178223
Average	12.79909984	1.085584173	8.212571372	0.831240527

Table 4-6 SSE and RMSE of linear and quadratic models for 0.013 inch layer thickness

t=0.013 in	**Linear Model**		**Quadratic Model**	
Angle	Sum of Square of Errors (SSE)	Root Mean Square Error (RMSE)	Sum of Square of Errors (SSE)	Root Mean Square Error (RMSE)
5	10.3011898	1.213094614	6.314920468	1.025907766
10	88.8668319	3.563041075	87.6208633	3.821449622
15	86.89294451	3.523248187	79.33694452	3.63632013
20	138.4800067	4.447792498	136.8444214	4.775709744
25	88.24291609	3.550511353	78.91349217	3.626602914
30	13.83872336	1.406044267	12.69269582	1.454458422
35	5.428228531	0.880602759	3.750833999	0.790657321
40	12.13807846	1.316818594	3.243040116	0.735191598
45	7.812803896	1.056463365	2.956620449	0.701975836
50	5.631933453	0.896973758	2.148949549	0.598463247
55	6.057395555	0.930237723	2.814179329	0.684857568
60	4.464382169	0.798604333	1.161144052	0.439913638
65	4.385742539	0.791539417	1.503653977	0.500608626
70	4.846885522	0.832113104	2.845459263	0.688653186
75	2.264205905	0.568733669	1.1838437	0.444192845
80	4.215320357	0.776008133	2.837345214	0.687670611
85	2.786344043	0.630911364	1.651424587	0.524630757
90	2.527556015	0.600898852	0.570438847	0.308339328
Average	27.17674938	1.543535392	23.79945948	1.41364462

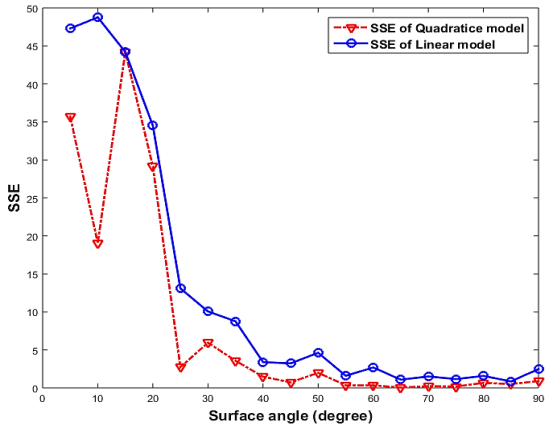

a) SSE of linear and quadratic models for 0.010 inch layer thickness

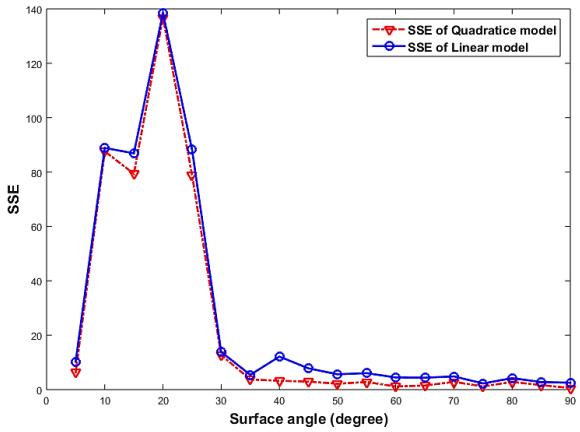

b) SSE of linear and quadratic models for 0.013 inch layer thickness

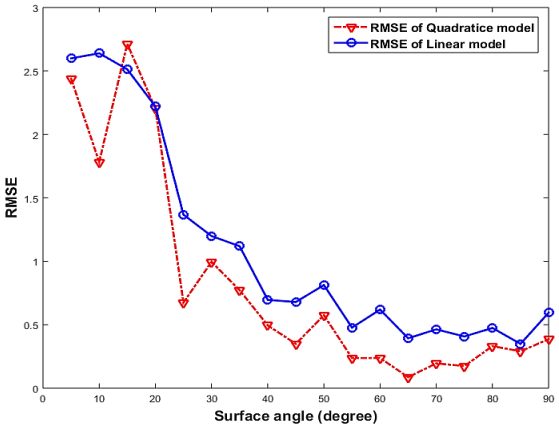

c) RMSE of linear and quadratic models for 0.010 inch layer thickness

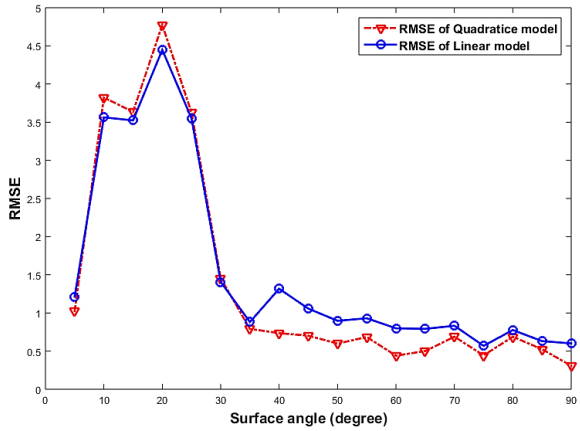

d) RMSE of linear and quadratic models for 0.013 inch layer thickness

Figure 4-15 Graphic representation of SSE and RMSE of linear and quadratic models for both layer thicknesses.

4.6. DESIGN MODELS

The application of the experimental models is in deciding about the proper TET to achieve a specific surface roughness on the surface of a product. Figure 4-16 shows a typical example of the models developed in this study at 45° and the TET of 30 seconds. The models fitted for all surface angles from 5 to 90°, with 5° increments, are represented in Appendix B. Supposedly, if a layer thickness between the ones used in this study is chosen, the final surface roughness can be interpolated between them. If the layer thickness of the product is something other than the two values considered in this study, for example 0.012 inch, the surface roughness of the product after 30 seconds of exposure can be

interpolated using the two available curves. The following linear interpolation can be done to calculate the surface roughness of a 0.012 inch layer thickness ($S_{a\,(0.012)}$) product:

$$\frac{S_{a\,(0.012)} - 3.8}{0.012 - 0.010} = \frac{6.6 - 3.8}{0.013 - 0.010}$$

$$S_{a\,(0.012)} = 5.667\ \mu m$$

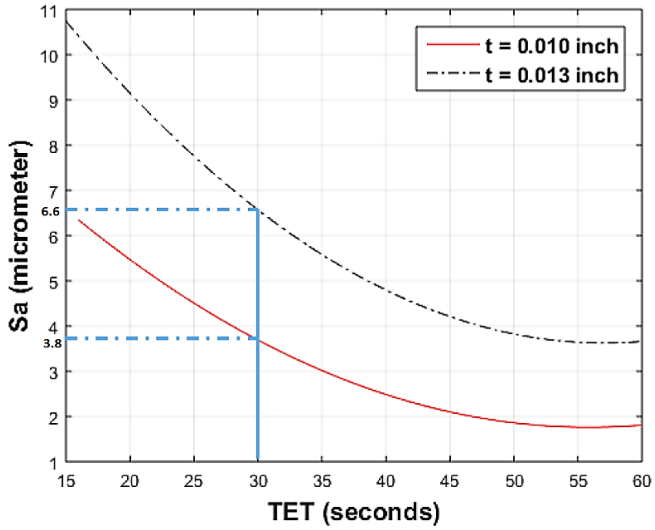

Figure 4-16 Surface roughness calculation of products with other layer thicknesses for a particular TET

4.7. DIMENSIONAL ACCURACY

The overall size of specimens with the different surface angles is a 60×60×20 mm cube. In order to check the dimensional change of the specimens after the post processing, they are measured and the results are shown in Figure 4-17-a. The maximum observed dimensional change is 0.082 millimetre, which is a negligible change. It can be concluded that the post-processing stage does not have a significant effect on the dimensional accuracy of the products. As it can be seen in the results of 2 and 3 cycles, increasing duration time decreases the dimensions. However, the results of smoothing with 4 cycles, shown by downward triangles in Figure 4-17-a, are not consistent comparing to the results of the other cycles. It is observed that increasing number of cycles is not as efficient as increasing the duration time in each cycle. Therefore, it is found that smoothing with 3 cycles gives the most efficient result in terms of a better surface roughness, less time and

cost, and also less inconsistency in dimensional accuracy. The roughness improvement gained by using 4 cycles is not significant and as a result, smoothing with 4 cycles is not recommended.

Figure 4-17-b shows the results of dimensional measurement without fourth cycle. Considering all the observations and as a general rule of thumb for quick planning, the dimensional accuracy of the parts after smoothing in acetone vapour bath is maintained the most using 3 cycles of 15 seconds duration, which gives a desirable surface roughness when dimensional accuracy is still within an acceptable range.

$$Error\ Percentage\ \% = 0.0045(TET) - 0.0568$$

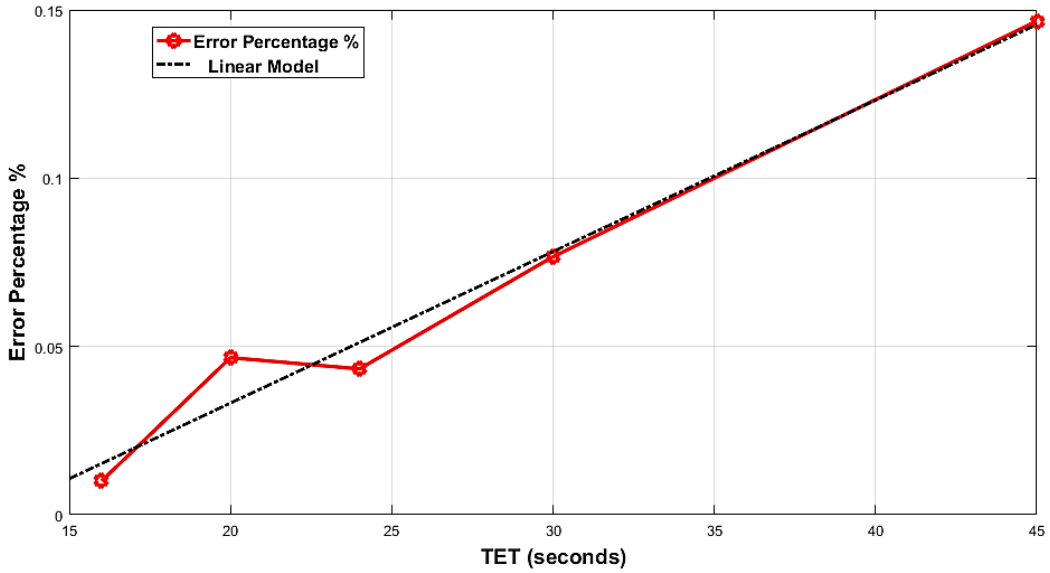

Figure 4-17 Dimension of the cube versus TET with and without the forth cycle

5. CONCLUSION AND RECOMMENDATIONS FOR FUTURE RESEARCH

The three primary stages to thoroughly investigate and improve the surface quality were followed. These stages are modeling the surface profile, inspection and post processing. A new analytical modeling of the surface profile was developed. The developed model considers the centerline not passing through the center of each edge profile line. Instead, the centerline was found by minimizing the total distance of points on the surface profile from a line. The defining parameters of that line were found using a minimization process. The line found was considered as the centerline and roughness was found more accurately in this way. The results showed that the new algorithm is most useful for small features at small surface angles with respect to horizontal plane and for low number of layers. Before any post-processing, the inspection was done using a 3D digitizer (FARO Laser Arm) and processed by a computer program developed in this study to find the roughness values. The theoretical and experimental results were slightly different. The differences can be attributed to the process parameters of the machine including vibration of the printing head, the acceleration and deceleration of the axes while printing. The theoretical procedure does not work on 90 degrees because of cosine of 90° becomes zero. As the surface becomes smoother by increasing the angle toward 90°, the effect of process parameters becomes

more influential and after a certain angle (70°) they dominate the amount of roughness. From 70-85° surface angles, surface waviness, which because of process errors, dominate the staircase effect. This leads to an increase in roughness until 85° but at 90° the roughness becomes minimum compared to all other angles.

The results of analytical solution show that based on the aim of the designer, different approaches may be considered. When the goal is to get a more accurate surface angle while reducing number of layers, aiming at an angle slightly different than the desired one can maintain both purposes especially for angles smaller than 20 degrees. In addition, the results can be used for finding the number of layers required for the aimed angle. The results also showed that between the available options, the one yielding a better surface property could be chosen.

The rough surface of AM parts before post-processing, and specifically for FDM parts, mandated a 3D representation of the manufactured surface. There are many pattern details and AM specific textures that need to be considered in measurement process. Therefore, in this thesis, a 3D surface reconstruction from point cloud data was generated and the point cloud data from FDM part surface was used to calculate the surface roughness. In conclusion, it can be said that for rough unfinished FDM surfaces or any other AM processes that create a rough surface at the end, a 3D surface texture inspection is more crucial to detect all pattern and surface details.

In this research, acetone vapour bath smoothing was employed to enhance the surface roughness of FDM parts made of ABS. The roughness values are profoundly improved and

a reduction percentage of maximum 95% was observed. The results showed that the main input factor in smoothing process is total exposure time. When breaking down the total exposure time into number of cycles and cycle duration, cycle duration proved to be the more important factor. The surfaces angles more than 40° slope with respect to the horizontal axis, the surface roughness values become less sensitive to surface slope. An experimental model is develop to predict the resulting surface roughness within a good accuracy. The main finding of this study can be summarized as follow:

- The theoretical model predicts the roughness more accurately than the previous models and its significance is revealed for fine features on the surface.
- The theoretical model can be also be used in selecting the minimum number of layers to achieve an accurate angle ion the surface. This was also observed more on lower surface slope with respect to the horizontal plane.
- For rough additive manufacturing surfaces, a 3D representation of the surface texture is more vital because of the details on the surface. 3D point cloud data was used to study the surface texture of unfinished FDM parts. After post-processing, the angles below 30 degrees for 0.010 inch layer thickness was also investigated by point cloud data. For 0.013 inch layer thickness until 50 degree surface slope was done by point cloud data as this surface was rougher.
- 3D optical microscopy was used for qualitative study of the effect of post-processing and the results were used to compare the surfaces before and after post-processing.

- Layer thickness is the main design factor affecting the surface roughness and reducing it results in reduced surface roughness.
- The surface roughness values become less sensitive to surface slope after 40 degrees.
- Total exposure time is found to be the main smoothing factor and between the number of cycle and cycle duration, cycle duration is the more important one.
- The maximum roughness reduction percentage of 95% is observed and is achievable by angles above 40 degrees.
- Smoother surfaces can be achieved at low surface roughness sensitivity values.
- The experimental models are developed to predict the results of the smoothing process and design based on them. The quadratic model better fits the results. At high surface roughness sensitivity values the two models are very close.
- The dimensional changes are negligible after the post-processing step. The best smoothing setup is 3 cycles with 15 seconds.

The main contributions of this study in each stage of surface integrity improvement can be summarized as follows:

- The analytical model is developed based on the true definition of centerline using total least square method. Because the staircase effect is the main roughness factor for inclined surfaces, the sharp square corner edge profile is assumed in developing the model. The edge profile shape is the second factor and its effect is in micro level compared to staircase effect.

- In order to inspect the additive manufactured surfaces in 3D, an approach is proposed and has resulted in acceptable accuracy. There is not a specific device capable of inspecting additive manufactured surfaces in 3D. A 3D surface topography is achieved by 3D point cloud data of the surface. A computer program is developed to process the point cloud data and find the surface roughness.
- The post processing stage is investigated and best number of cycles and cycle duration are found for each surface angle. Experimental models are developed for post processing of FDM parts made of ABS. For each surface angle one can find the required post processing time and setup.

For further investigation, it can be recommended to study other profile geometries and find the centerline using total least square method. More research can be done for 3D inspection of additive manufacturing surfaces. The methodology presented in this thesis was about the FDM surfaces. Other additive manufacturing processes need more investigation to study their surface texture.

REFERENCES

1. Turner, B. N. and Gold, S. A. “A review of melt extrusion additive manufacturing processes: II. Materials, dimensional accuracy, and surface roughness”. *Rapid Prototyp. J.* **21,** 250–261 (2015).

2. Agarwala, K. M., Jamalabad, R. V., Langrana, A. N., Safari, A., Whalen, J. P. and Danforth, C. S. “Structural quality of parts processed by fused deposition”. *Rapid Prototyp. J.* **2**, 4-19 (1996).

3. Reeves, P. E. “Reducing the surface deviation of stereolithography components”. PhD Thesis, University of Nottingham, UK, 1998.

4. Reeves, P. E., Cobb, R. C. and Cobb, R. C. “Reducing the surface deviation of stereolithography using in-process techniques”. *Rapid Prototyp. J.* **3,** 20-31 (2002).

5. Campbell, R. I., Martorelli, M. and Lee, H. S. “Surface roughness visualisation for rapid prototyping models”. *CAD Comput. Aided Des.* **34,** 717–725 (2002).

6. Rahmati, S. and Vahabli, E. “Evaluation of analytical modeling for improvement of surface roughness of FDM test part using measurement results”. *Int. J. Adv. Manuf. Technol.* **79,** 823–829 (2015).

7. Nourghassemi, B. “Surface Roughness Estimation for FDM Systems”. Masters Thesis, Ryerson University, Canada (2011).

8. Ahn, D. K., Kim, H. C. and Lee, S. H. “Determination of fabrication direction to minimize post-machining in FDM by prediction of non-linear roughness characteristics”. *J. Mech. Sci. Technol.* **19,** 144–155 (2005).

9. Ahn D. K., Kwon, S.M., Lee, S.H. “Expression for Surface Roughness Distribution of FDM Processed Parts. International Conference on Smart Manufacturing Application”. April. 9-11, 2008 in KINTEX, Gyeonggi-do, Korea (2008).

10. Byun, H. S. and Lee, K. H. “Determination of optimal build direction in rapid prototyping with variable slicing”. *Int. J. Adv. Manuf. Technol.* **28,** 307–313 (2006).

11. Paul, B. K. and Voorakarnam, V. “Effect of layer thickness and orientation angle on surface roughness in laminated object manufacturing”. *J. Manuf. Process.* **3,** 94–

101 (2001).

12. Luis Pérez, C. J., Vivancos Calvet, J. and Sebastián Pérez, M. A. "Geometric roughness analysis in solid free-form manufacturing processes". *J. Mater. Process. Technol.* **119,** 52–57 (2001).

13. Pandey, P. M., Reddy, N. V., and Dhande, S. G. "Improvement of surface finish by staircase machining in fused deposition modeling". *J. Mater. Process. Technol.* **132,** 323–331 (2003).

14. Ahn, D., Kim, H., and Lee, S. "Surface roughness prediction using measured data and interpolation in layered manufacturing". *J. Mater. Process. Technol.* **209,** 664–671 (2009).

15. Ahn, D., Kweon, J. H., Kwon, S., Song, J., and Lee, S. "Representation of surface roughness in fused deposition modeling". *J. Mater. Process. Technol.* **209,** 5593–5600 (2009).

16. Ahn, D., Kweon, J. H., Choi, J., and Lee, S. "Quantification of surface roughness of parts processed by laminated object manufacturing". *J. Mater. Process. Technol.* **212,** 339–346 (2012).

17. Boschetto, A., Giordano, V., and Veniali, F. "3D roughness profile model in fused deposition modelling". *Rapid Prototyp. J.* **19,** 240–252 (2013).

18. Boschetto, A. and Bottini, L. "Roughness prediction in coupled operations of fused deposition modeling and barrel finishing". *J. Mater. Process. Technol.* **219,** 181–192 (2015).

19. Boschetto, A., and Bottini, L. "Accuracy prediction in fused deposition modeling". *Int. J. Adv. Manuf. Technol.* **73,** 913–928 (2014).

20. Boschetto, A., Giordano, V., and Veniali, F. "Modelling micro geometrical profiles in fused deposition process". *Int. J. Adv. Manuf. Technol.* **61,** 945–956 (2012).

21. Boschetto, A., Giordano, V.,and Veniali, F. "Surface roughness prediction in fused deposition modelling by neural networks". *Int. J. Adv. Manuf. Technol.* **67,** 2727–2742 (2013).

22. Barari, A., Kishawy, H. A., Kaji, F., and Elbestawi, M. A. "On the surface quality of additive manufactured parts". *Int. J. Adv. Manuf. Technol.* (2016).

doi:10.1007/s00170-016-9215-y

23. Kaji, F. “Inspection & modelling of cusp geometry in additive manufacturing to predict product’s surface roughness”. Masters Thesis, University of Ontario Institute of Technology, Canada (2015).

24. Taylor Hobson. “Exploring Surface Texture: A fundamental guide to the measurement of surface finish”. Taylor Hobson Ltd, UK (2011).

25. ISO 4287 BE. BS EN ISO 4287. “Geometrical product specification (GPS): surface texture: profile method: terms, definitions and surface texture parameters”. British Standards Institute; 1997.

26. ISO 25178-2 DIN EN ISO 25178-2. “Geometrical product specifications (GPS)—surface texture: areal—part two: metrological characteristics for areal-topography measuring methods”. ISO; 2012.

27. Townsend, A., Senin, N., Blunt, L., Leach, R. K. and Taylor, J. S. “Surface texture metrology for metal additive manufacturing: a review”. *Precis. Eng.* **46,** 34–47 (2016).

28. Triantaphyllou, A., Giusca, C. L., MacAualy, G. D., Leach, R. K. and Milne, K. a. “Surface texture measurement for additive manufacture”. *Proc. ASPE Spring Top. Meet. Dimens. Accuracy Surf. Finish Additive Manuf.* **3,** 127–130 (2014).

29. Mumtaz, K. and Hopkinson, N. “Top surface and side roughness of Inconel 625 parts processed using selective laser melting”. *Rapid Prototyp. J.* **15,** 96–103 (2009).

30. Król, M., Dobrzański, L. and Reimann, I. “Surface quality in selective laser melting of metal powders”. *Arch. Mater. Sci.* **60,** 87–92 (2013).

31. Yasa, E., and Kruth, J. “Application of Laser Re-Melting on Selective Laser Melting Parts”. *Adv. Prod. Eng. Manag.* **6,** 259–270 (2011).

32. Strano, G., Hao, L., Everson, R. M. and Evans, K. E. “Surface roughness analysis, modelling and prediction in selective laser melting”. *J. Mater. Process. Technol.* **213,** 589–597 (2013).

33. Safdar, a., He, H. Z., Wei, L.-Y., Snis, A. and Chavez de Paz, L. E. “Effect of process parameters settings and thickness on surface roughness of EBM produced Ti-6Al-4V”. *Rapid Prototyp. J.* **18,** 401–408 (2012).

34. Grimm, T., Wiora, G. and Witt, G. “Characterization of typical surface effects in additive manufacturing with confocal microscopy”. *Surf. Topog. Metrol. Prop.* **3,** 14001 (2015).

35. Krolczyk, G., Raos, P. and Legutko, S. “Experimental analysis of surface roughness and surface texture of machined and fused deposition modelled parts”. *Tehnički vjesnik.* **21,** 217-221 (2014).

36. Jamshidinia, M. and Kovacevic, R. “The influence of heat accumulation on the surface roughness in powder-bed additive manufacturing”. *Surf. Topog. Metrol. Prop.* **3,** 14003 (2015).

37. Galantucci, L. M., Lavecchia, F. and Percoco, G. “Experimental study aiming to enhance the surface finish of fused deposition modeled parts”. *CIRP Ann. - Manuf. Technol.* **58,** 189–192 (2009).

38. Temmler, A., Willenborg, E. and Wissenbach, K. “Laser Polishing”. *Proc. SPIE* **8243,** Laser Applications in Microelectronic and Optoelectronic Manufacturing (LAMOM) XVII, 82430W (February 9, 2012); doi:10.1117/12.906001 (2012).

39. Köpplmayr, T., Häusler, L., Bergmair, I. and Mühlberger, M. “Nanoimprint Lithography on curved surfaces prepared by fused deposition modelling”. *Surf. Topog. Metrol. Prop.* **3,** 24003 (2015).

40. Vetterli, M., Schmid, M. and Wegener, K. “Comprehensive Investigation of Surface Characterization Methods for Laser Sintered Parts”. *Proc. Fraunhofer Direct Digit. Manuf. Conf.* ETH-Zürich, 1–6 (2014). http://dx.doi.org/10.3929/ethz-a-010357719

41. Johnson, M. K. and Adelson, E. H. “Retrographic sensing for the measurement of surface texture and shape”. *2009 IEEE Comput. Soc. Conf. Comput. Vis. Pattern Recognit. Work. CVPR Work. 2009* 1070–1077 (2009). doi:10.1109/CVPRW.2009.5206534

42. Johnson, M. K., Cole, F., Raj, A. and Adelson, E. H. “Microgeometry capture using an elastomeric sensor”. *ACM Trans. Graph.* **30,** 1 (2011).

43. Gharbi, M., Peyre, P., Gorny, C., Carin, M., Morville, S., Masson, P. L., Carron, D., and Fabbro, R. “Influence of various process conditions on surface finishes induced by the direct metal deposition laser technique on a Ti-6Al-4V alloy. *J. Mater. Process. Technol.* **213,** 791–800 (2013).

44. Pyka, G., Burakowski, A., Kerckhofs, G., Moesen, M., Van Bael, S., Schrooten, J., and Wevers, M. “Surface modification of Ti6Al4V open porous structures produced by additive manufacturing”. *Adv. Eng. Mater.* **14,** 363–370 (2012).

45. Pyka, G., Kerckhofs, G., Papantoniou, I., Speirs, M., Schrooten, J., and Wevers, M. “Surface roughness and morphology customization of additive manufactured open porous Ti6Al4V structures”. *Materials.* **6,** 4737–4757 (2013).

46. Thompson, A., Maskery, I., and Leach, R. K. “X-ray computed tomography for additive manufacturing: a review”. *Meas. Sci. Technol.* **27,** 72001 (2016).

47. Kruth, J. P, Bartscher, M., Carmignato, S., Schmitt, R., De Chiffre, L., Weckenmann, A. “Computed tomography for dimensional metrology”. *CIRP Ann. - Manuf. Technol.* **60,** 821–842 (2011).

48. Townsend, A., Pagani, L., Scott, P., Blunt, L. “Areal surface texture data extraction from X-ray computed tomography reconstructions of metal additively manufactured parts”. *Precision Eng. J.* **48,** 254-264 (2014)

49. Jamiolahmadi, S., and Barari, A. “Surface Topography of Additive Manufacturing Parts Using a Finite Difference Approach”. *J. Manuf. Sci. Eng.* **136,** 61009 (2014).

50. Sood, A. K., Ohdar, R. K., and Mahapatra, S. S. “Improving dimensional accuracy of Fused Deposition Modelling processed part using grey Taguchi method”. *Mater. Des.* **30,** 4243–4252 (2009).

51. Kruth, J.-P., Leu, M. C., and Nakagawa, T. “Progress in Additive Manufacturing and Rapid Prototyping”. *CIRP Ann. - Manuf. Technol.* **47,** 525–540 (1998).

52. Wohlers, T. “Future potential of rapid prototyping and manufacturing around the world”. *Rapid Prototyp. J.* **1,** 4–10 (1995).

53. Mani, K., Kulkarni, P., and Dutta, D. “Region-based adaptive slicing”. *CAD Comput. Aided Des.* **31,** 317–333 (1999).

54. Ma, W., But, W. C., and He, P. “NURBS-based adaptive slicing for efficient rapid prototyping”. *CAD Comput. Aided Des.* **36,** 1309–1325 (2004).

55. Pandey, P. M., Reddy, N. V., and Dhande, S. G. “Real time adaptive slicing for fused deposition modelling”. *Int. J. Mach. Tools Manuf.* **43,** 61–71 (2003).

56. Huang, B., and Singamneni, S. B. “Curved Layer Adaptive Slicing (CLAS) for fused deposition modelling”. *Rapid Prototyp. J.* **21,** 354–367 (2015).

57. Sikder, S., Barari, A., and Kishawy, H. A. “Global adaptive slicing of NURBS based sculptured surface for minimum texture error in rapid prototyping”. *Rapid Prototyp. J.* **21,** 649–661 (2015).

58. Kim, H. C., and Lee, S. H. “Reduction of post-processing for stereolithography systems by fabrication-direction optimization”. *CAD Comput. Aided Des.* **37,** 711–725 (2005).

59. Ahn, D., Kim, H., and Lee, S. “Fabrication direction optimization to minimize post-machining in layered manufacturing”. *Int. J. Mach. Tools Manuf.* **47,** 593–606 (2007).

60. Duleba, B, Greskovic, F., and Sikora, J. “Materials and finishing methods of DMLS manufactured parts”. *Transf. inovácií*. **21,** 143–148 (2011).

61. Rossi, S., Deflorian, F., and Venturini, F. “Improvement of surface finishing and corrosion resistance of prototypes produced by direct metal laser sintering”. *J. Mater. Process. Technol.* **148,** 301–309 (2004).

62. Tay, F. E. H., and Haider, E. A. “Laser sintered rapid tools with improved surface finish and strength using plating technology”. *J. Mater. Process. Technol.* **121,** 318–322 (2002).

63. Zhang, B., Zhu, L., Liao, H., and Coddet, C. “Improvement of surface properties of SLM parts by atmospheric plasma spraying coating”. *Appl. Surf. Sci.* **263,** 777–782 (2012).

64. Atzeni, E., Barletta, M., Calignano, F., Iuliano, L., Rubino, G., and Tagliaferri, V. “Abrasive Fluidized Bed (AFB) finishing of AlSi10Mg substrates manufactured by Direct Metal Laser Sintering (DMLS)”. *Addit. Manuf.* **10,** 15–23 (2016).

65. Lamikiz, A., Sánchez, J. A., López de Lacalle, L. N., and Arana, J. L. “Laser polishing of parts built up by selective laser sintering”. *Int. J. Mach. Tools Manuf.* **47,** 2040–2050 (2007).

66. Marimuthu, S., Triantaphyllou, A., Antar, M. Wimpenny, D., Morton, H., and Beard, M. “Laser polishing of selective laser melted components”. *Int. J. Mach. Tools Manuf.* **95,** 97–104 (2015).

67. Ross, I., Kumstel, J., Bremen, S., and Willenborg, E. “Laser polishing of laser additive manufactured surfaces made from Inconel 718 and ASTM F75”. *Proc. - ASPE 2015 Spring Top. Meet. Achiev. Precis. Toler. Addit. Manuf.* **60,** 136–140 (2015).

68. Rosa, B., Mognol, P., and Hascoët, J. “Laser polishing of additive laser manufacturing surfaces”. *J. Laser Appl.* **27,** S29102 (2015).

69. Schanz, J., Hofele, M., Hitzler, L., and Merkel, M. “Laser Polishing of Additive Manufactured AlSi10Mg Parts with an Oscillating Laser Beam”. *Machining, Joining and Modifications of Advanced Materials, Volume 61 of the series Advanced Structured Materials.* 159–169 (2016).

70. Dadbakhsh, S., Hao, L., and Kong, C. Y. “finish improvement of LMD samples using laser polishing”. *Virtual Phys. Prototyp.* **5,** 215–221 (2010).

71. Rosa, B., Magnol, P., and Hascoet, J. “Laser polishing of additive laser manufacturing surfaces”. *J. Laser Appl.* **27,** 100 (2015). doi: 10.2351/1.4906385

72. Kulkarni, P., and Dutta, D. “On the Integration of Layered Manufacturing and Material Removal Processes”. *J. Manuf. Sci. Eng.* **122,** S29102 (2000).

73. Boschetto, A., Bottini, L., and Veniali, F. “Finishing of Fused Deposition Modeling parts by CNC machining”. *Robotics and Computer-Integrated Manufacturing.* **41,** 92–101 (2016).

74. Williams, E. R., and Melton, V. L. “Abrasive flow finishing of stereolithography prototypes”. *Rapid Prototyp. J.* **4,** 56-67 (1998).

75. Leong, F. K., Chua K. C., Chua, S. G., and Tan, H. C. “Abrasive jet deburring of jewellery models built by stereolithography apparatus (SLA)”. *J. Mater. Proc. Technol.* **83,** 36–47 (1998).

76. Boschetto, A., and Bottini, L. “Surface improvement of fused deposition modeling parts by barrel finishing”. *Rapid Prototyp. J.* 21, 686–696 (2015).

77. Barari, A. “Optimized Vapor Treatment Operation for Fused Deposition Modeling Process to Improve Surface Quality”, *Society of Manufacturing Engineering, Rapid,* JUNE 9-12, 2014, Cobo Center, Detroit, MI, (2014).

78. Galantucci, L.M., Lavecchia, F., and Percoco, G. “Experimental study aiming to

enhance the surface finish of fused deposition modeled parts". *CIRP Annals–Manufac. Technol.* **58,** 189–192 (2009).

79. Galantucci, L.M., Lavecchia, F., and Percoco, G. "Quantitative analysis of a chemical treatment to reduce roughness of parts fabricated using fused deposition modeling". *CIRP Annals–Manufac. Technol.* **59,** 247–250 (2010).

80. Kuo, C. C., and Mao, R. C. "Development of a Precision Surface Polishing System for Parts Fabricated by Fused Deposition Modeling". *Mater. & Manufac. Proc.* **0,** 1-6 (2016). DOI: 10.1080/10426914.2015.1090594

81. Garg, A., Bhattacharya, A., and Batish, A. "On Surface Finish and Dimensional Accuracy of FDM Parts after Cold Vapor Treatment". *Mater. & Manufac. Proc.* **31,** 522–529 (2016). DOI: 10.1080/10426914.2015.1070425

Appendix A

The reconstructed surfaces representing the 3D surface topography of each surface angle are presented here. The figures in the left and right are for 0.01 and 0.013 inch layer thicknesses, respectively.

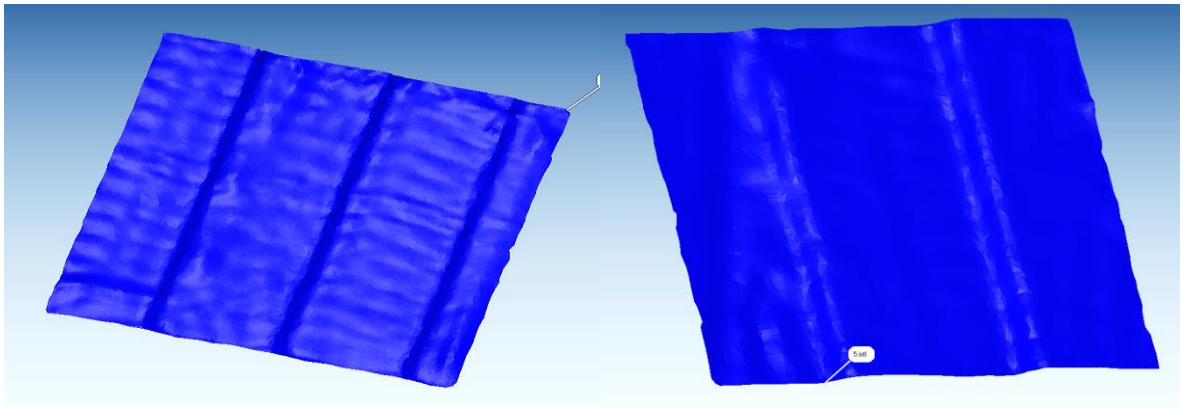

5° surface angle

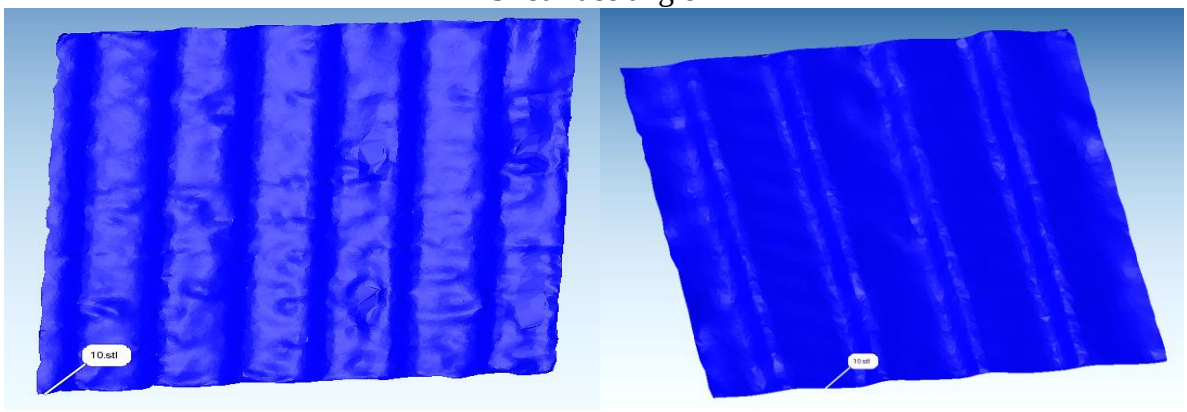

10° surface angle

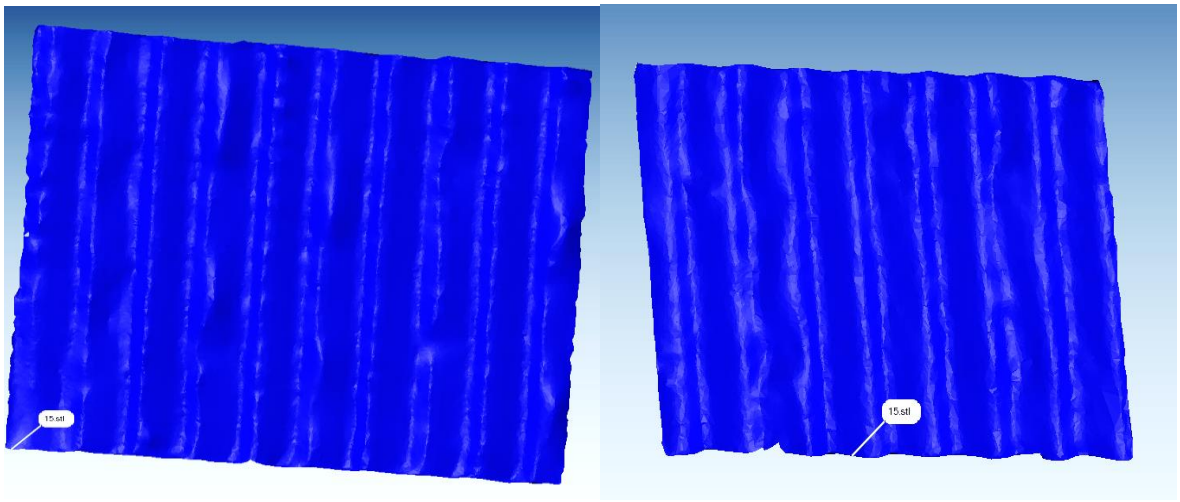

15° surface angle

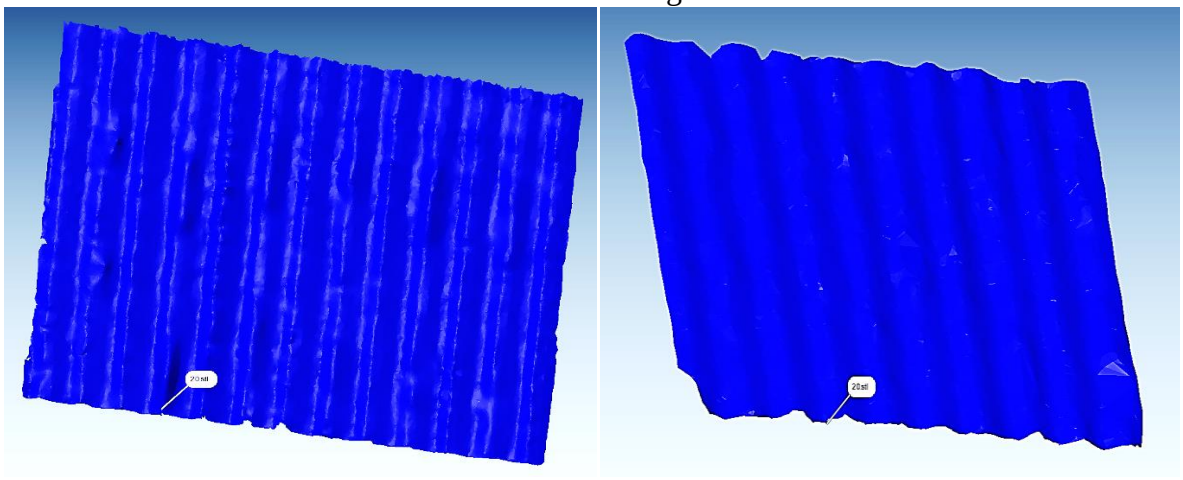

20° surface angle

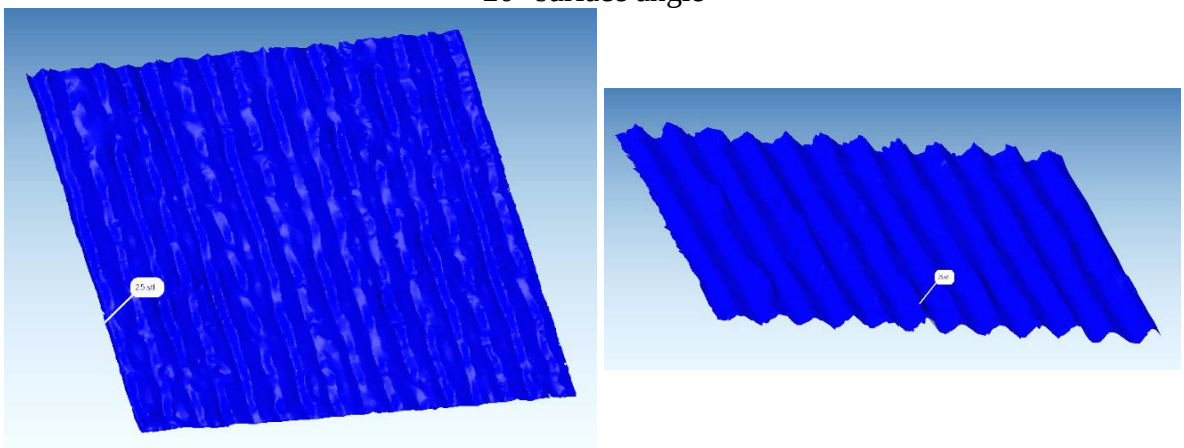

25° surface angle

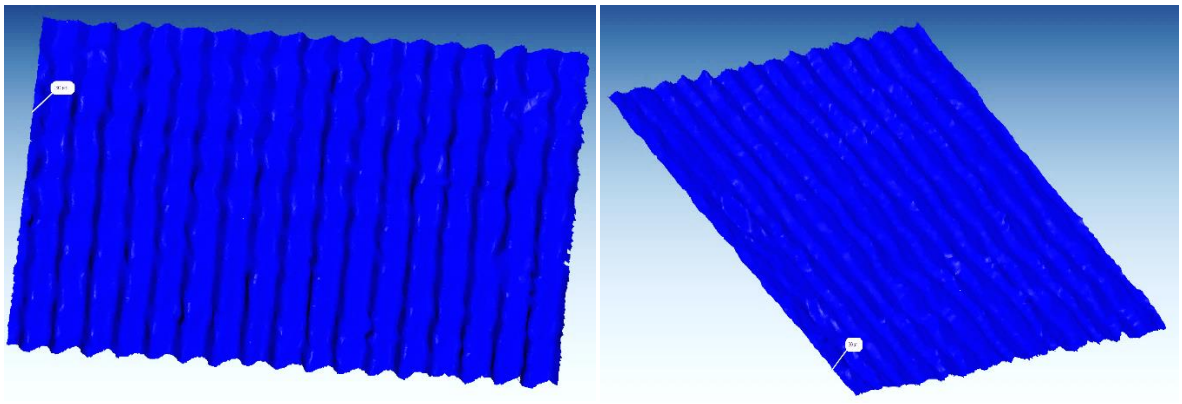

30° surface angle

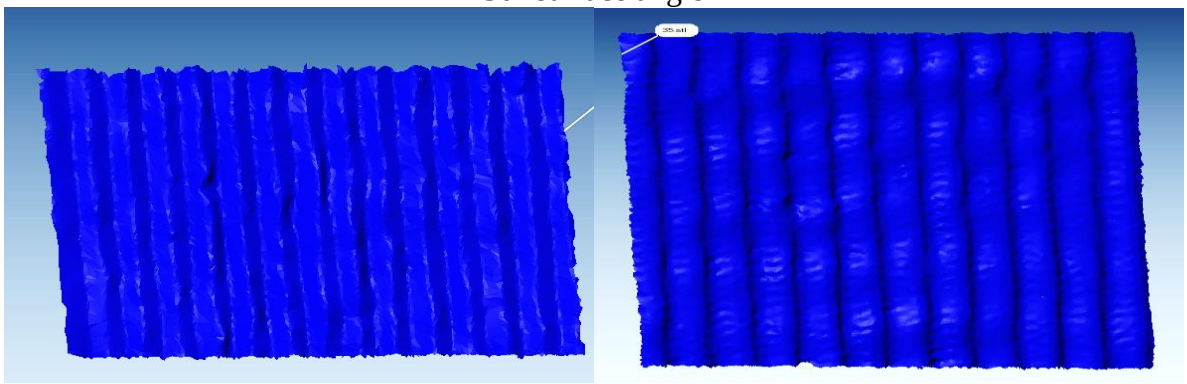

35° surface angle

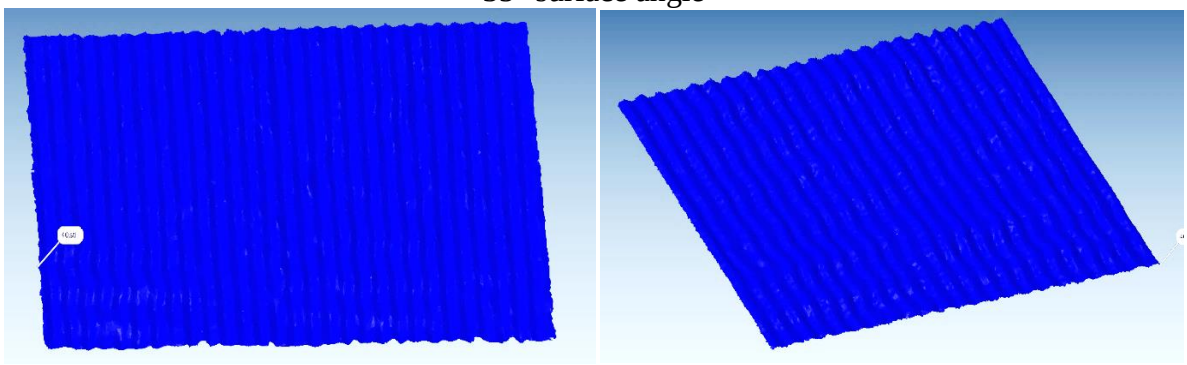

40° surface angle

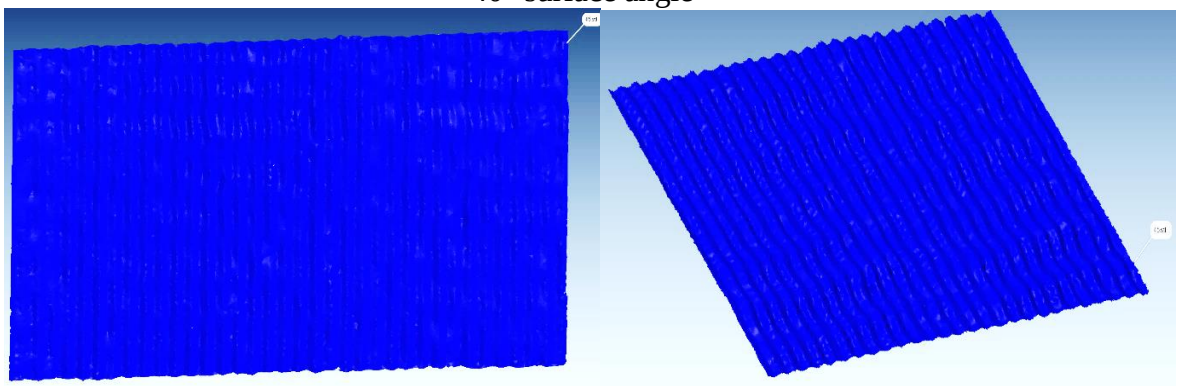

45° surface angle

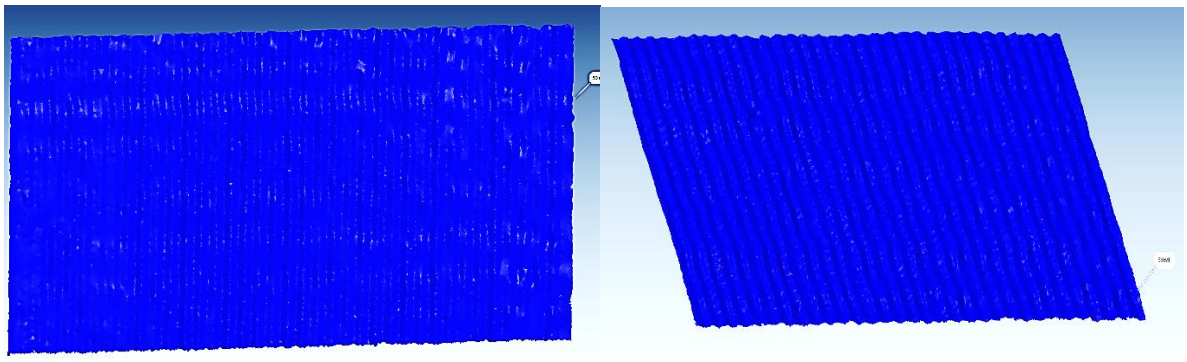

50° surface angle

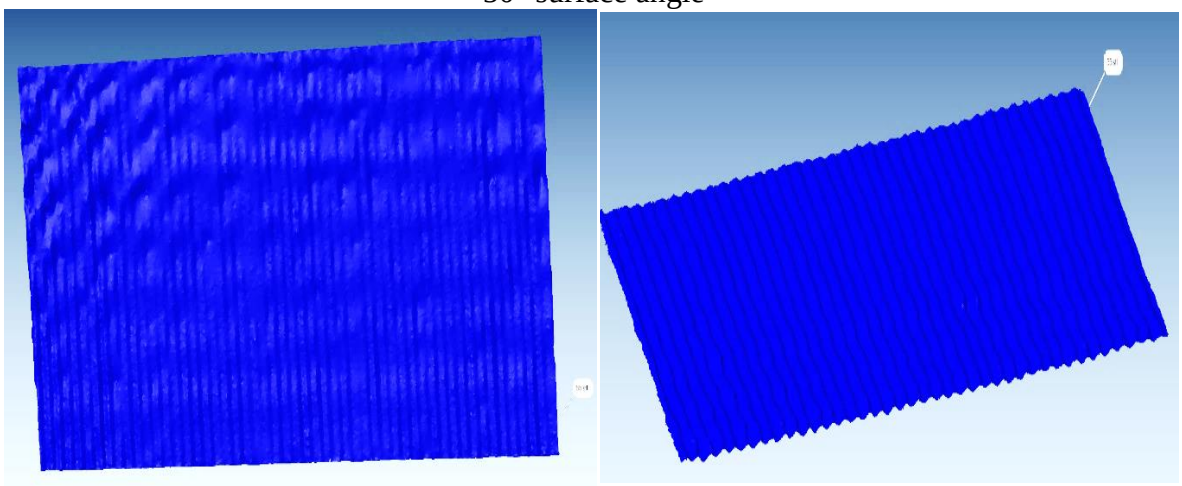

55° surface angle

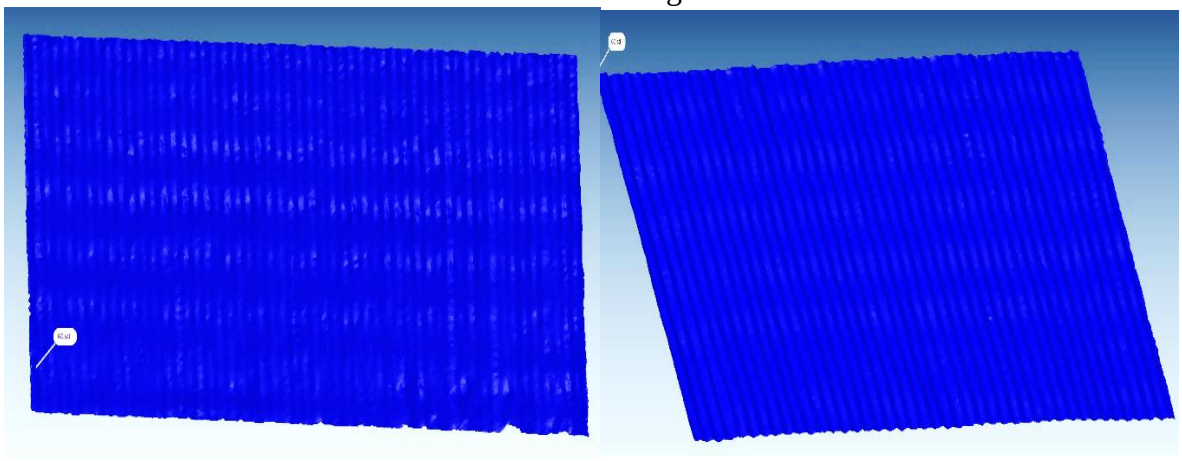

60° surface angle

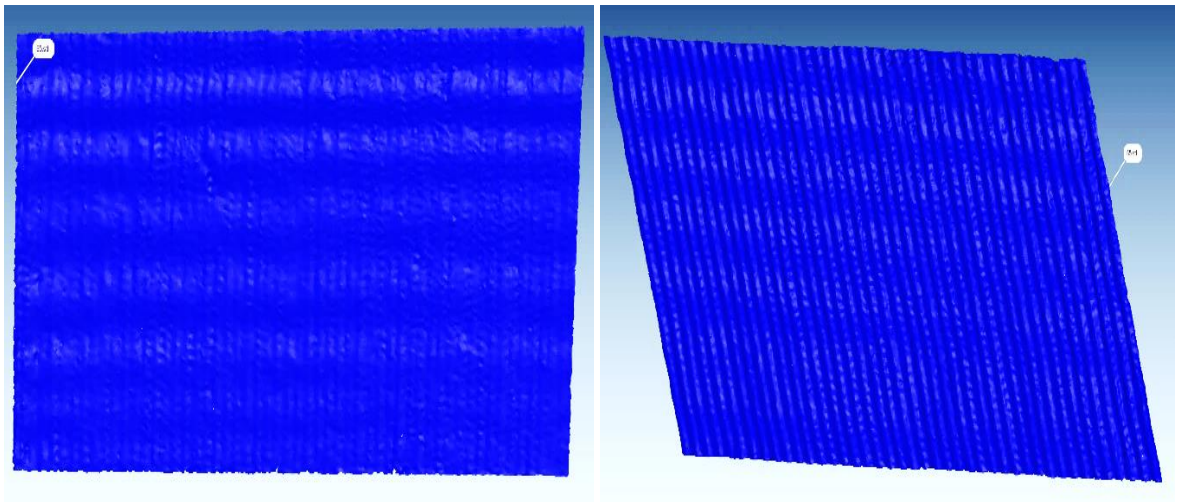

65° surface angle

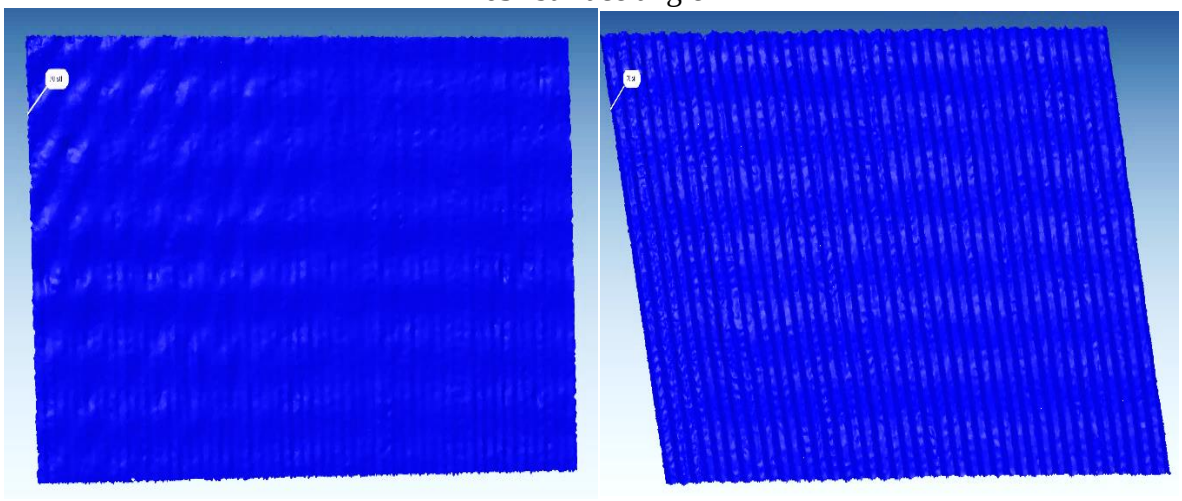

70° surface angle

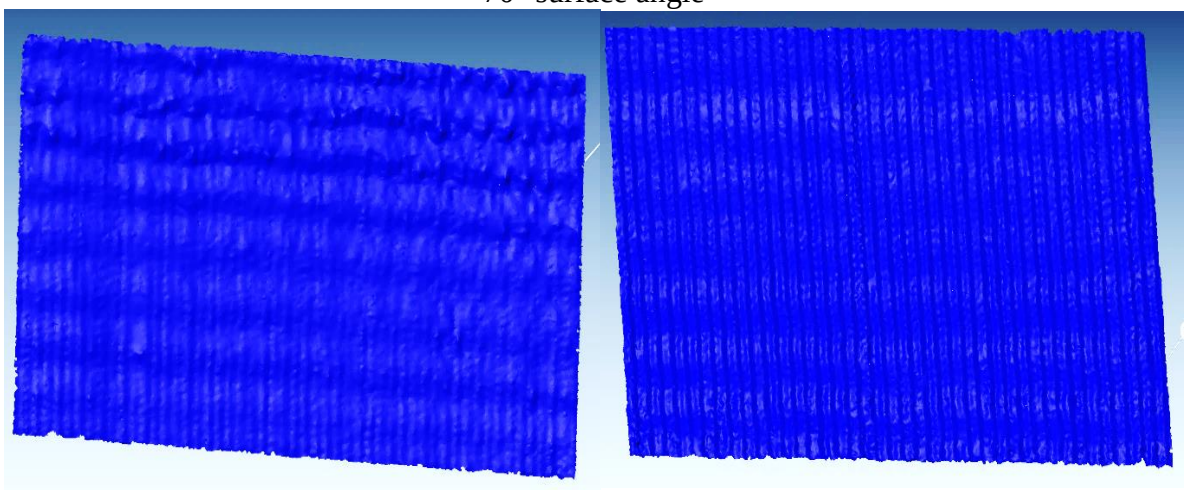

75° surface angle

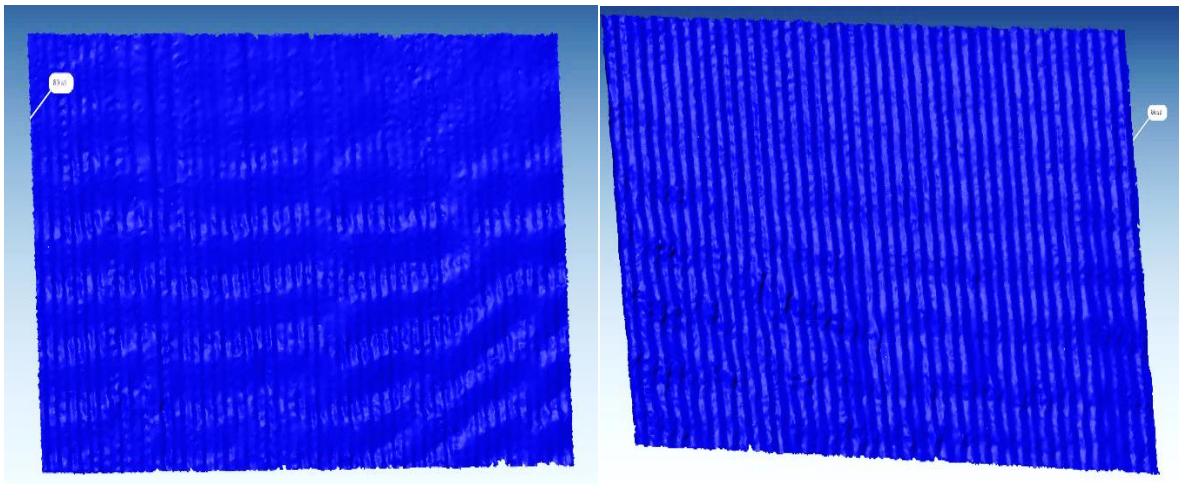

80° surface angle

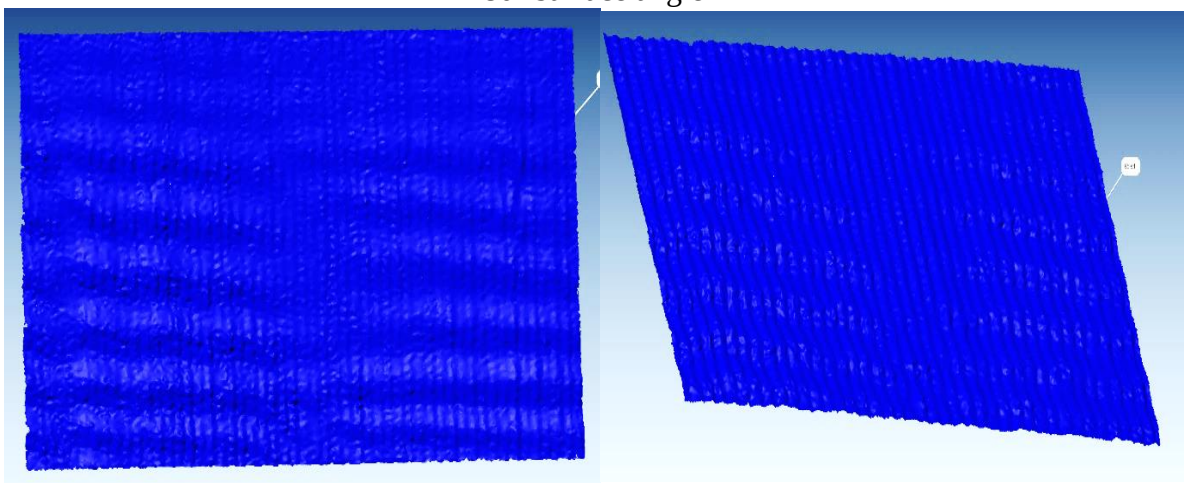

85° surface angle

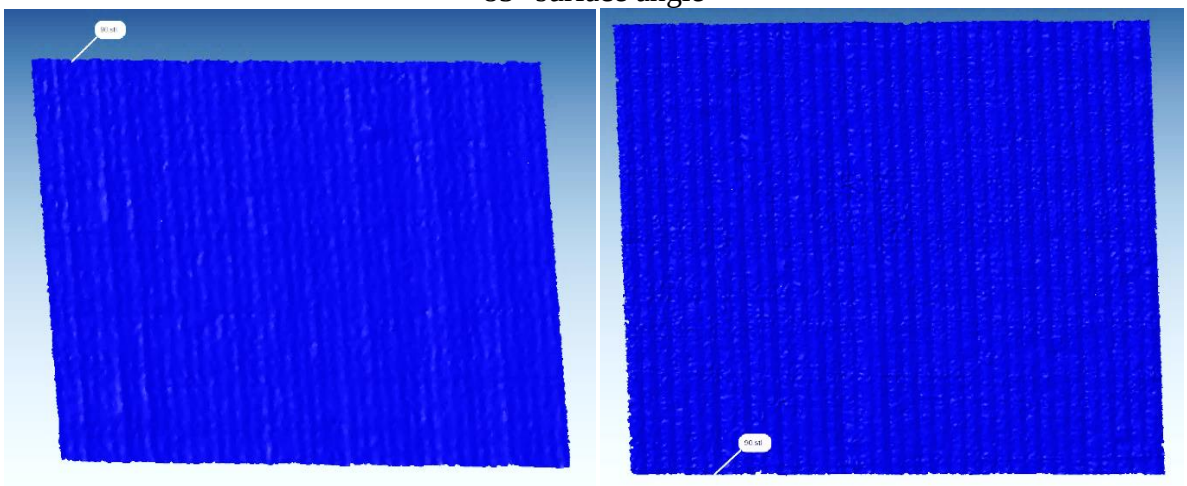

90° surface angle

Appendix B

The experimental quadratic models for surface angles from 5 to 90°, with 5° increments and both layer thicknesses are presented. Surface roughness vs. total exposure time models are given for each case.

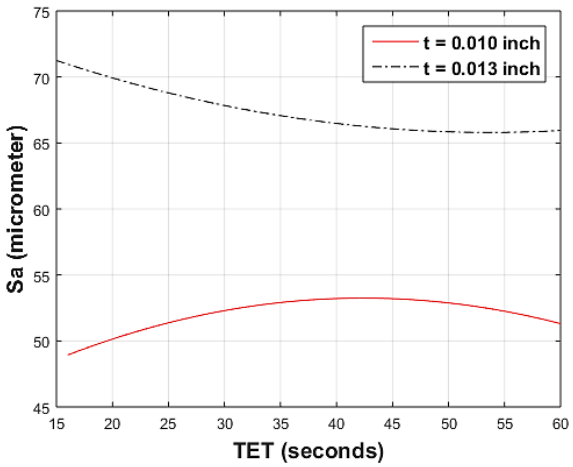

a) 5 degrees

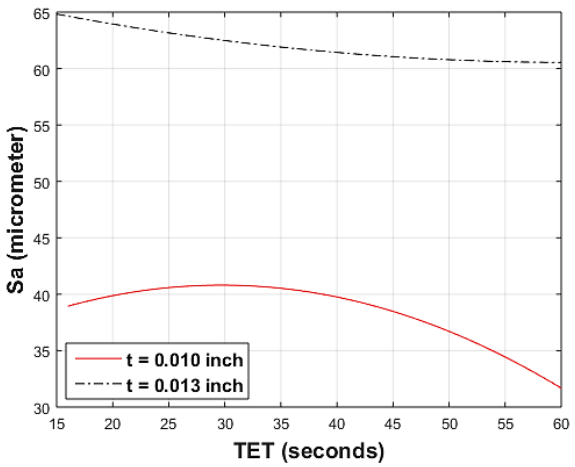

b) 10 degrees

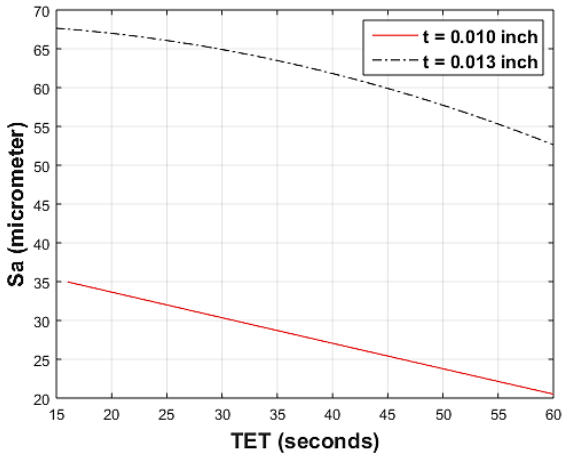

c) 15 degrees

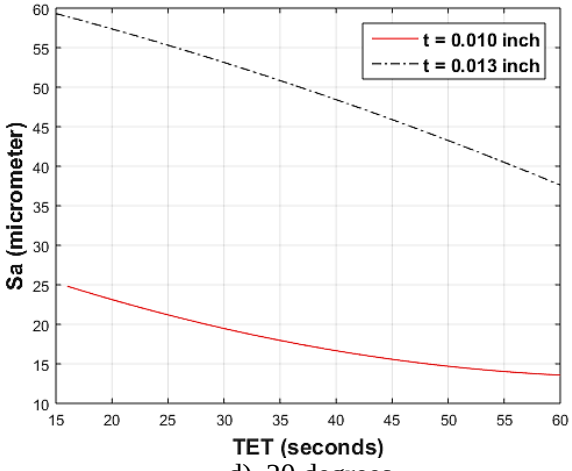

d) 20 degrees

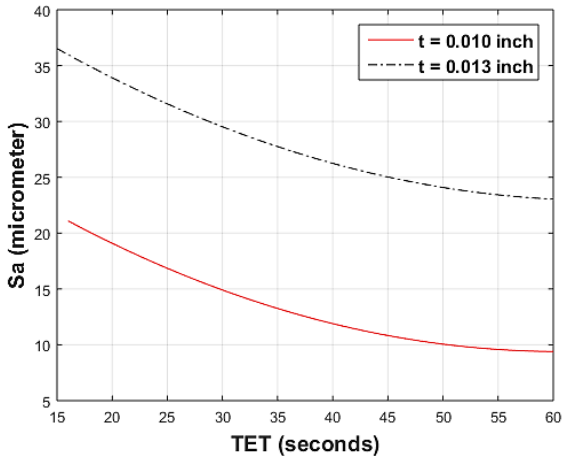

e) 25 degrees

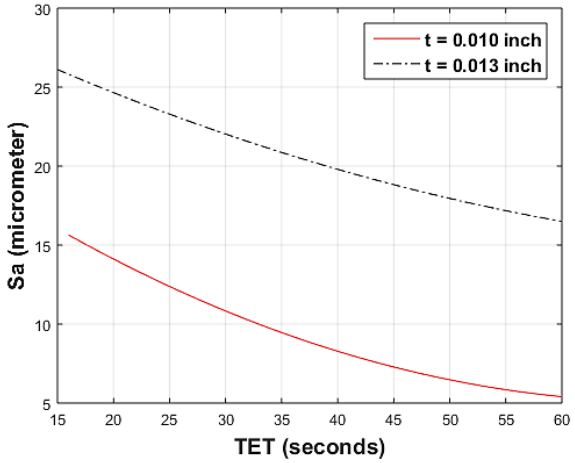

f) 30 degrees

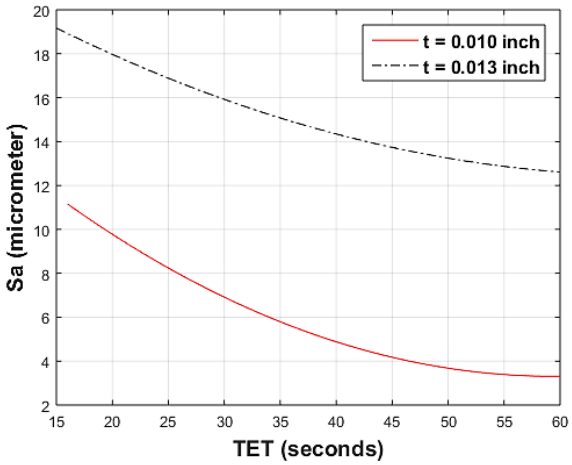

g) 35 degrees

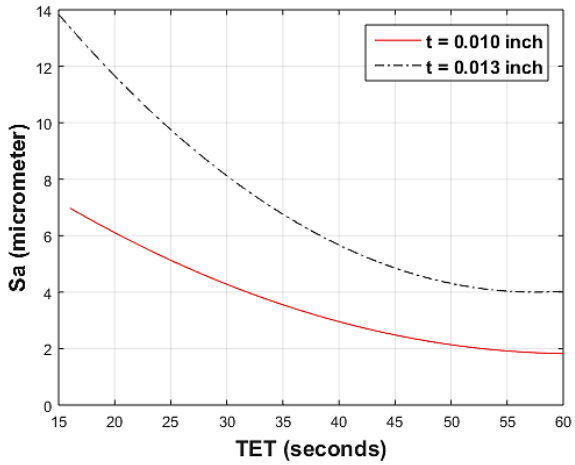

h) 40 degrees

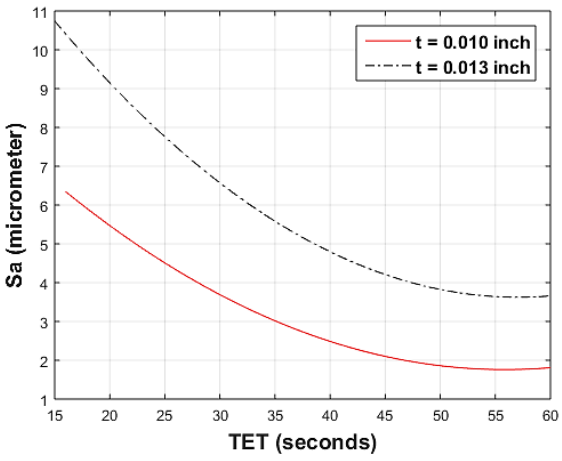

i) 45 degrees

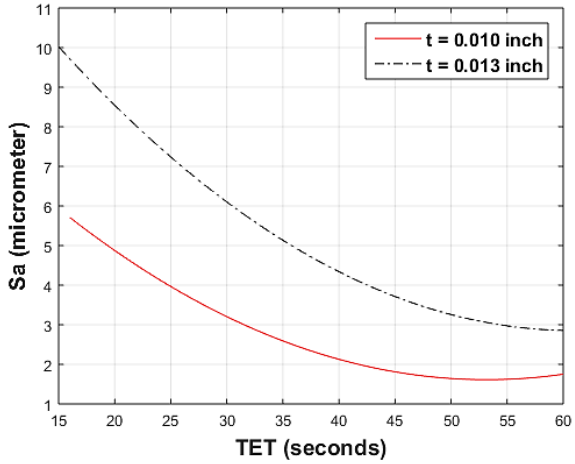

j) 50 degrees

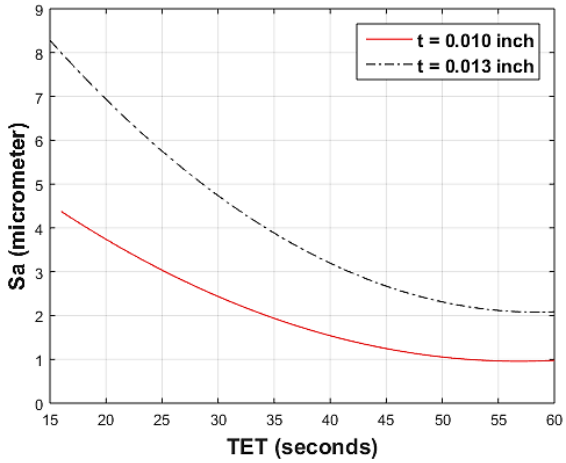

k) 55 degrees

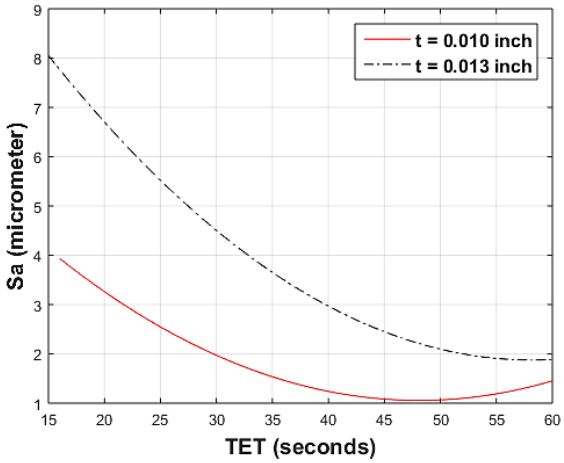

l) 60 degrees

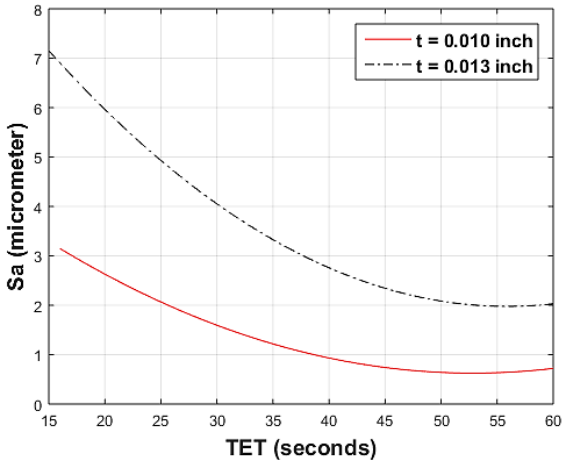

m) 65 degrees

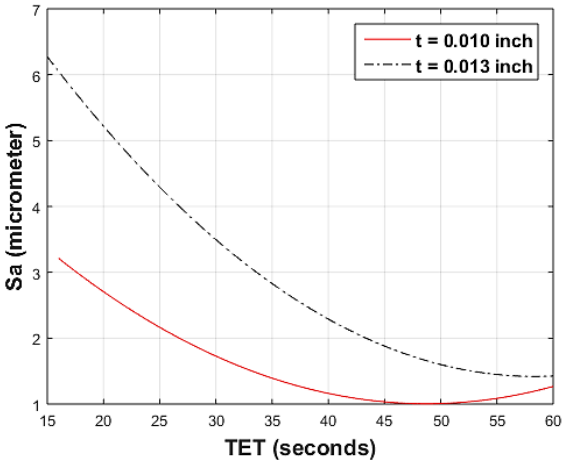

n) 70 degrees

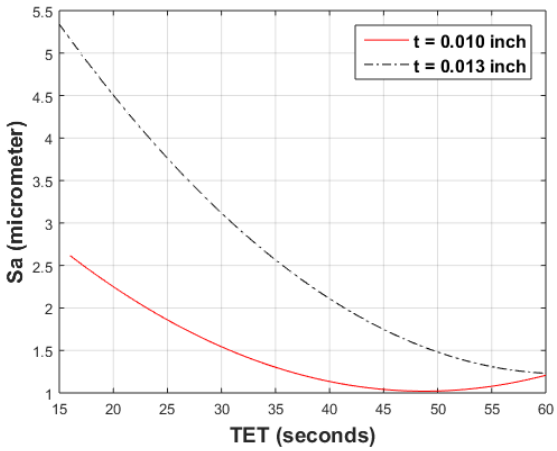

o) 75 degrees

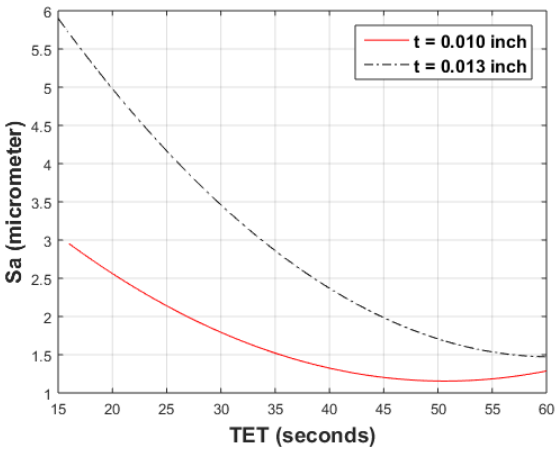

p) 80 degrees

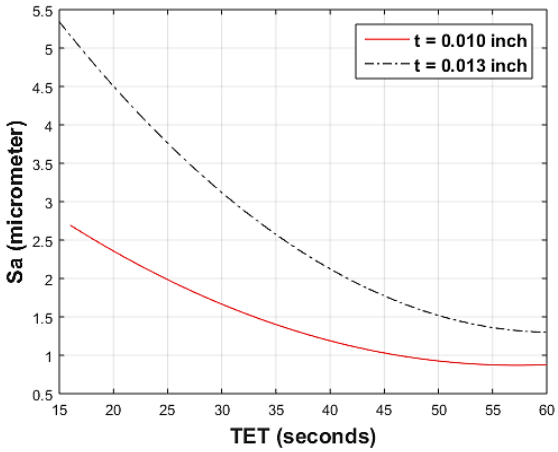

q) 85 degrees

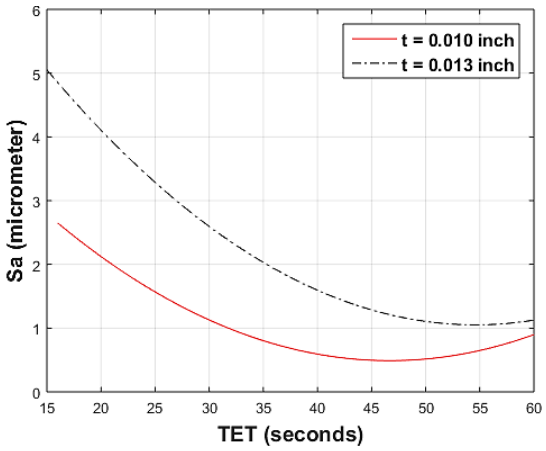

r) 90 degrees